Mechanics of Material/Cell/Tissue Interactions in vitro

Malgorzata Lewandowska-Szumiel

Department of Biophysics and Human Physiology, Medical University of Warsaw, Chalubinskiego 5, 02-004 Warsaw, Poland

INTRODUCTION: Our knowledge of the mechanical interactions between cells/tissues and materials is far from complete. However, it seems likely that an improved understanding will facilitate successful clinical intervention at all levels: repair, reconstruction and replacement.

This is the case especially with load-bearing tissues, and this lecture will focus mainly on bone tissue as an example. Artificial materials are playing a growing role in bone repair. This is due first to the fundamentally good and broad tolerance of bone cells and tissue towards many materials including a wide variety of metals, ceramics and polymers. This has led to new possibilities in bone reconstruction/regeneration, including so-called tissue engineered products, in which scaffold materials are enriched with living host cells.

Studies both reported by others in the literature and from our group in Warsaw will be presented. They will relate to three main topics:

METHODS: The difficulties to fully understand material/cell/tissue mechanical interactions are in great part a consequence of problems with finding adequate experimental systems. Thanks to recent developments in cell culture in vitro techniques, there are new and interesting possibilities. Some methods and resultant data will be shown, which indicate that elastic deformation of metallic implants may play a role in bone regeneration in contact with them, due to its influence on the osteogenic cell differentiation. Also, methods and results for exploring the role of other mechanical factors, such as shear stress will be briefly discussed in relation to their effect on the osteogenic potential of bone cells, which, in turn, is responsible for osteoconduction in vivo.

CONSEQUENCES: Relatively new findings suggest that attached cells are probably able to "feel" the supporting surface, i.e. their viability and function seems to be dependent, for example, on the surface stiffness of the support materials. Although this general concept is neither fully established nor understood, there are a growing number of reports, which describe such phenomena, including studies in our laboratory. The potential role of these observations in directing efforts to identify and develop new

biomaterials - including new scaffolds for tissue engineered products - will be discussed.

MECHANISMS: What are the means by which bone cells respond to mechanical stimulation? Recent scientific reports concerning bone cell mechanoreceptors will be presented.

The lecture is intended to not just cover scientific methods and phenomena. It is also intended to suggest the practical consequences of an improved understanding of the mechanics of material/cell/tissue interactions for further development of implant products and clinical treatment methods.

Cellular mechanosensing: Analysis of molecular interactions between fluorescent-tagged focal adhesion proteins talin and vinculin

Anne-Kathrin Born, Arie Bruinink, Katharina Maniura

Laboratory for Materials-Biology Interactions, Empa, Materials Science and Technolgy, Lerchenfeldstrasse 5, 9014 St. Gallen, Switzerland

INTRODUCTION: The development of new material concepts for medical applications as well as cell based sensors will be greatly by tools that allow on-line advanced monitoring of cellular processes. Processes depending on mechanosensing of cells such as cell spreading and generation of force on the extracellular matrix (ECM) play an important role for cell viability, migration, proliferation and differentiation. Primary sites of adhesion are formed between integrin receptors and the underlying substratum. These initial adhesions consist of a large number of linker proteins such as talin. The talin rod contains up to eleven vinculin binding sites (VBS) whereas five VBS are located within fragment H1-H12 [1]. Binding of the talin head to intracellular integrin domains cause activation of integrins followed by rapid accumulation of talin in focal contacts. Recruitment of vinculin to cell adhesion sites, however, is force dependent. Intramolecular interactions between the head and tail domains retain vinculin in an inactive closed conformation and prevent binding to talin and actin and hence focal adhesion formation. When mechanical forces are applied to adhesion complexes talin becomes stretched which leads to unfolding of talin rod into helix sub-bundles and activation of VBS. Vinculin switches to an open, activated conformation that can now interact with VBS within the talin rod. The number of exposed VBS is defined by applied forces and forceexposure time of talin [2]. FRET microscopy using the CFP-YFP pair is a powerful technique that enables the visualization of protein interactions, protein conformations and biochemical status inside living cells.

The goal of our study is to investigate the molecular interaction of talin and its binding partner vinculin in focal adhesions.

METHODS: For FRET measurements we generated several constructs in which yellow fluorescent protein is inserted in close

proximity to vinculin binding sites within the talin rod. As the binding sites for talin are located in the N-terminal vinculin head domain CFP was positioned in front of vinculin. These FRET constructs were used for nucleofection of human fibroblasts followed by confocal laser scanning microscopy to monitor the fluorescence localisation of fusion proteins.

RESULTS: Our first results showed that transfection of cells with the different fluorescently-labelled vinculin or talin variants is efficient and results in the expected accumulation of fluorescence signal at focal adhesion sites. The correct localisation of both proteins was individually confirmed by immunohistochemical staining against talin or vinculin, suggesting that both tagged proteins are correctly synthesized and localized. First cotransfection experiments of both fluorescently labelled proteins resulted in colocalisation promising **FRET** be observable.

DISCUSSION & CONCLUSIONS: Cell adhesion to surfaces is strongly influenced by substrate topography, chemical properties as well as mechanical cues. Therefore our FRET-based approach for online monitoring of cell adhesion state seems to be an attractive tool for studying newly developed biomaterials.

REFERENCES:

- 1. Gingras, A.R., et al., Mapping and Consensus Sequence Identification for Multiple Vinculin Binding Sites within the Talin Rod. J Biol Chem, 2005. **280**(44): p. 37217-37224.
- 2. Hytönen, V.P. and V. Vogel, *How Force Might Activate Talin's Vinculin Binding Sites:*SMD Reveals a Structural Mechanism.
 PLoS Computational Biology, 2008. **4**(2): p. e24.

Stretch Induced Cell Sheet Alignment

E. Thomasson¹, M. Aschwanden², R. Ilinca¹, R. Enning², A. Stemmer², J. Vörös¹, A. Franco-Obregón¹

¹Laboratory of Biosensors and Bioelectronics, ETH Zürich, Switzerland.

² Nanotechnology Group, ETH Zürich, Switzerland.

INTRODUCTION: Cell sheets are a promising new strategy in tissue engineering. For instance, primary corneal epithelial cells grown in vitro form sheets of tightly adhered cells possessing an ECM matrix that can then be successfully transplanted into hosts without any carrier substrate or sutures. [1] On the other hand, cardiac myocyte cell sheets can fail, since the myocytes often are not oriented properly with reference to cardiac contractility. [2] In order to create a better mimic of in vivo conditions the aim of this project is to create aligned cell sheets by applying well defined modalities of stretch. Moreover, cyclic stretch serves as a mitogenic stimulus to promote myoblast proliferation. Lastly, substrate stretch will be used to detach the myoblasts sheets from our actuators. This approach is simple and elegant since no exogenous substrates are required.

METHODS: A two-dimensional electroactive polymer (EAP) bioreactor has been developed. The technique relies on a new methodology to apply well-defined stresses onto differentiating muscle cells with a precision not imaginable with existing technologies. A frequency range of tens of mHz to Hz is possible to achieve. The spatial resolution of stretching, moreover, can approach the single cell The substrate facing level. the cells, Poly(dimethylsiloxane) (PDMS), is turned slightly hydrophilic by UV exposure and subsequently functionalized with weakly cell-adhesive Poly(Llysine). Proliferating myoblasts from C2C12 culture were plated at different densities onto the surface of the bioreactor and once adhered, different stretch frequencies during different time courses were tested in order to provoke alignment as well as the subsequent detachment.

RESULTS: Myoblast alignment perpendicular to the direction of the stretch vector was achieved reproducibly when cyclic stretch at 0.05 Hz was applied, see figure 1. The effect was visible after a few hours or after stretching over night. Once aligned, the cells remained aligned, regardless of stretching amplitude. Detachment was visible in the cultures plated with high cell density where a sheet left the surface spontaneously within a few hours after plating. As the cell density at the time of plating was decreased, sheets could be

mechanically detached in patches preferentially from the region of stretch at the substrate.

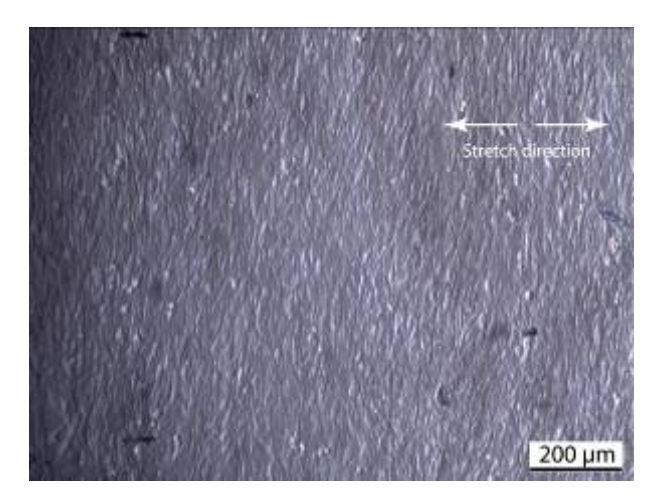


Fig. 1: Myoblasts aligned perpendicularly to the stretch vector.

DISCUSSION & CONCLUSIONS: These results indicate that a platform for the creation of aligned cell sheets is feasible. Alignment has been already achieved. The sheets detaching in patches preferentially on the stretching region indicates that mechanical stimuli can break the cell substrate interaction. Moreover, the cell-cell junctions are preserved in the presence of physiological levels of calcium. Furthermore, it would be interesting to investigate how stretch activated calcium channel blockers might alter the focal adhesions in the direction of detachment. With a functional detachment technique, fusion of layers of sheets would then be the next step towards a functional cell sheet under *in vivo* conditions.

REFERENCES: ¹ N. Matsuda, et al (2007) *Advanced Materials* **19**:3089-99. ² M. N. Giraud et al (2007) *Tissue Engineering* **13**: 1825-36.

ACKNOWLEDGEMENTS: This project is supported by a grant from the Swiss National Science Foundations, SNF K-32K1-116532.

Effects of Ridges on Spinal Cord Neuron Outgrowth

Arie Bruinink¹, Manuel Wiesli¹, Thomas Lehnert², Ursina Tobler¹, Thomas Osterwalder¹

MaTisMed, Materials-Biology Interactions Lab, EMPA, St. Gallen, Switzerland. ² Institute of Microsystems, EPF Lausanne, Switzerland

INTRODUCTION: One fundamental question in neurobiology is how neurites and neuronal connections can be localised with high precision. Control of neurite outgrowth and guidance of growth cones on material surfaces have become important topics in biomedically oriented material science. They have implications for the rational design of neuroimplants such as artificial nerve conduits or bioelectronic interfaces.

The aim of the present study was to investigate in how far ridges are able to affect neurite growth properties. For this, reaggregates of ventral spinal cord neurons of chicken embryos were cultured close to an array of ridges with different dimensions and surface chemistry

METHODS: Polyimid spin coated oxidized silicon wafers were patterned by photolithography. The resulting polyimide structure consists of parallel ridges with ridge width and interridge distances of 5μm to 100μm, and ridge height of 1.3 μm or 3.0 μm.

To obtain fluorescence, spinal cord neurons of chicken embryos were transfected *in ovo* with a modified RFP-plasmid vector pRFP-N1 of Clonetech (USA) after breeding the eggs for 70 hours at 37 °C. Motoneurons were isolated 74 hours after transfection. Single cell suspensions of spinal cord sections were obtained by trypsinisation. Reaggregates were prepared by gyratory shaking of cell suspensions for 1 day. Reaggregates were placed near the structures and pictures were taken every 5 min. for the following 16 hours. Cells were kept under cell culture conditions during the whole process (37°C and 5 % CO₂). Dislocation of marked growth cones was analysed using Visiometrics software as previously described [1].

RESULTS: Polyimide is very neurocompatible taking the neurite outgrowth into account. Furthermore, nerve cells behaved similarly on SiO₂, polyimide and on a-C:H coated surfaces.

Neurites changed their direction in parallel orientation to the ridges being trapped between 2 ridges forming a channel-like structure. The ridge-like structures also reduced neurite branching. The tendency of crossing the ridges was not only increased by reducing the ridge height from 3.0 to 1.3 μ m but also by decreasing the interridge distance from 100 to 5 μ m (Fig. 1). The velocities found for outgrowth (v+) were around 18 % higher than for retraction (v-). By increasing the period between the measurements the retraction of neurites increasingly affects the measured velocity. By measuring *net* velocity instead *mean* velocity (v_{mean}) measured every 5 minutes SiO₂-PI surfaces with 10 μ m width -10 μ m ridges were able to significantly promote

the outgrowth by a factor of two. However, no differences were found for v_{mean} .

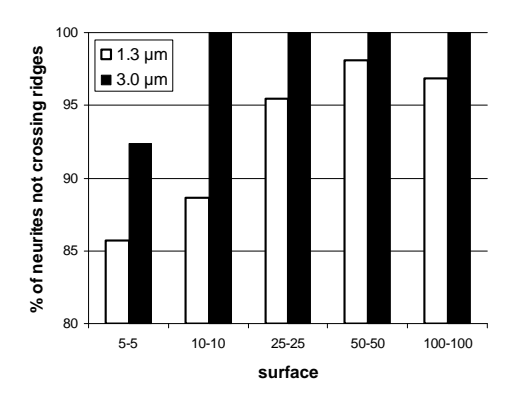


Fig. 1. Percentage of neurites crossing the ridges (data of SiO₂-PI and a-C:H coated surfaces pooled). Values are based on behaviour of 28-85 neurites.

DISCUSSION & CONCLUSIONS: We conclude that a-C:H and polyimide are neurocompatible coating materials. Furthermore, topographic structures in the low micrometer range have a strong influence on outgrowth behaviour of spinal cord neurons, and may therefore be used to optimise surfaces of neuroprostheses. The present study shows that topographical cues with dimension of around 3 μ m in height and 5-10 μ m interspacings are enough to result in a precise, stereotypical pathfinding and that these cues do not alter nerve functionality taking outgrowth and retraction velocity as indices.

REFERENCES: ¹ J.P. Kaiser, A. Reinmann, A. Bruinink (2006) *Biomaterial* **27**:5230-41.

ACKNOWLEDGEMENTS: We thank Dr. Ulrich Müller (EMPA, CH) for coating part of the surfaces with a-C:H and Dr. Stefan Weigel for the discussions.

Fibronectin unfolding plays a major role in fibrils formation and anastellin binding

Delphine Gourdon, Michael L. Smith, Sheila L. Morris, Radmila Vukmirovic, Kris E. Kubow, Viola Vogel

> Laboratory for Biologically Oriented Materials, Department of Materials Swiss Federal Institute of Technology, ETH Zurich, Switzerland

Smith *et al.* recently showed that a broad range of fibronectin (FN) conformations was present within the elastic FN fibrils forming the extracellular matrix (ECM), and that tension exerted by cells on their surrounding ECM induced the loss of both quaternary and tertiary structures of around half of the FN molecules forming the fibrillar network [1].

Here we investigate the physiological implications of such a broad range of FN conformations present within the matrix, in particular the crucial role of cellinduced unfolding of individual type III FN modules (in addition of quaternary changes) both in the assembly of new FN matrix by cells, i.e., fibrillogenesis and in the binding of cancer 'drugs' proteins such as anastellin (AN). We used a fluorescence resonance energy transfer (FRET)-based technique as an indirect indication of FN conformation to address whether newly incorporated FN and AN molecules were affected by the local conformation of the preexisting matrix. Cells were grown for 24 hours in the presence of FRET-labeled FN (double labeled with Alexa Fluor® 488 and Alexa Fluor® 546), and subsequently the media was exchanged to contain either new FN or AN labeled with a third color (Alexa Fluor® 633) to map the location of newly incorporated molecules of within the FRET-labeled pre-existing matrix.

Our findings reveal that cell-induced FN unfolding is required for FN fibrillogenesis as well as for anastellin binding which then affects irreversibly mechanotransduction processes involved in the matrix.

[1] Smith *et al.* PLoS Biology, 5, e268 (2007)

Experimental Characterization of Pressure Wave Generation and Propagation in Biological Tissues

M. Benoit¹, J. H. Giovanola¹, K. Agbeviade¹, M. Donnet²

¹ Swiss Fed. Institute of Technology, 1015 Lausanne, Switzerland ² E.M.S. Electro Medical Systems S.A., Switzerland

INTRODUCTION: This work develops a measurement technique for pressure waves in soft tissues. It aims at characterizing, understanding and modeling the generation and propagation of pressure waves in soft tissues, with a view towards medical applications for the treatment of various tissue pathologies.

METHODS AND RESULTS: First, Hopkinson bar techniques¹ have been adapted to measure the waves emitted by an impact generator, transmitted through the material and reflected at the interfaces. Simulation with an explicit FEM software reproduce the measured data well.

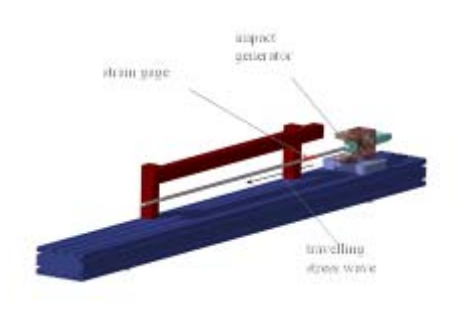


Fig. 1: Schematic of Hopkinson pressure bar and stress records at one location along the bar

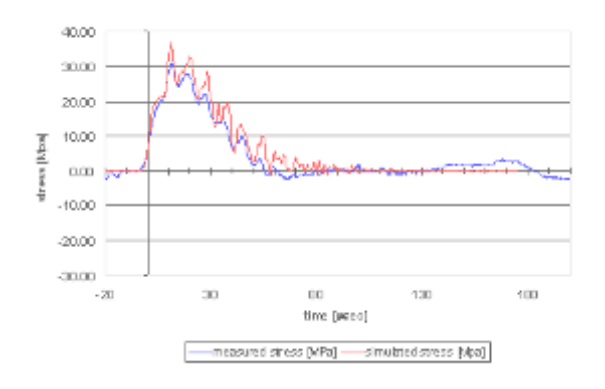


Fig. 2: measured and simulated record for an impact speed of 15m/sec

Secondly, flexible PVDF gages have been calibrated for measurement of wave propagation in soft tissues. Although PVDF gages have acoustic impedance similar to soft tissues, they act nevertheless as foreign inclusion and perturb the measurements. FEM simulation using a non linear hyper-elastic Ogden model (1) to represent soft

tissues can predict the behavior of wave propagation in biological material.

$$\phi = (2\mu/\alpha^2)(\lambda_1^{\alpha} + \lambda_2^{\alpha} + \lambda_3^{\alpha}) \tag{1}$$

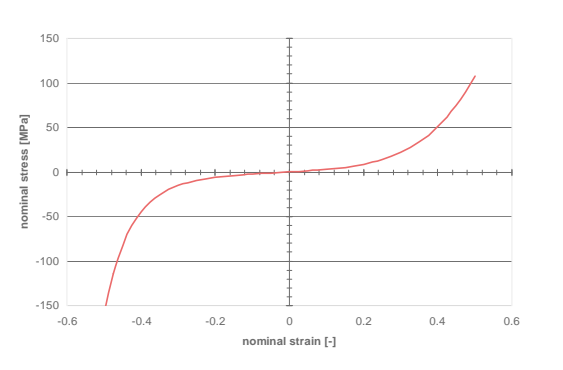


Fig. 4: Ogden model for an incompressible, isotropic, hyper-elastic solid and nominal stress-strain response

Comparison of results of simulations with and without the gage inclusion provides a method to evaluate the measured signals and extract reliable pressure data. Results are applied to the design of biomedical devices for the Extracorporeal Shock Wave Therapy (ESWT).

DISCUSSION & CONCLUSIONS: Adapted Hopkinson bar technique coupled with FEM simulation can predict pressure wave emitted, transmitted and reflected at the interfaces of an impact generator. PVDF flexible gages are a technique potential for measuring propagation in soft tissues and non linear hyperelastic Ogden model is a good candidate for FEM simulation of wave propagation in these tissues. This work contributes to improve the scientific knowledge of the healing effect of shockwaves for different pathologies by providing a well characterized mechanical wave input in the treated

REFERENCES: ¹ H. Kolsky (1963) *Stress waves in solids*, New York, Dover publications, Inc.

Dual-mode dynamic functional stiffness of articular cartilage

H. Ardura Garcia^{1,2}, A.U. Daniels¹, D. Wirz¹

¹ Lab. for Orthopedic Biomechanics, Faculty of Medicine, Univ. of Basel, Basel, Switzerland.
² Biomedical Engineering Dept., Universidad Iberoamericana, Mexico City, Mexico.

INTRODUCTION: Dynamic stiffness parameters (elastic modulus, loss angle, Poisson's ratio) determine how poroviscoelastic materials or structures (e.g. cartilage) distribute and dissipate loads. Also, these parameters are highly sensitive to structural changes and thus have diagnostic value. Nutrition processes in cartilage occur at slow loading rates which move water in and out of the tissue. In contrast, gait subjects hip, knee and ankle cartilage to impact loads which severely limit water movement, produce higher modulus values and lower loss angles, indicating energy storage. We hypothesize that evaluating cartilage in dual modes provides a more complete picture of functional stiffness. Also, indentation testing minimizes specimen preparation and is more functionally relevant ¹. This study provides initial results.

METHODS: The cartilage source was fresh, healthy cadaver knees from young pigs (9 months old). Specimens were 7.6mm diameter osteochondral plugs from the lateral condyles. Each specimen was evaluated in both test modes, using a steel spherical tip indenter.

"Nutritional" loading was accomplished with a Synergie 100 MTS® programmed to perform a series of single sinusoidal cycles at 1, 0.3 and 0.1 Hz under displacement control to a depth of ~0.1 mm, separated by 50s pauses--shown to be sufficient to allow dimensional recovery. "Gait" loading was accomplished with a single impact micro-indentation (SIMI) device ², mounted in a rigid load frame. The SIMI indenter pendulum falls freely, with impact force thus determined by mass and gravity. The mass and indenter dimensions used provided indentation depths of ~0.1 to 0.2 mm in healthy cartilage. (Actual depth depends on specimen stiffness.) An electromagnetic coil captures indenter motion data. The equivalent frequency of SIMI velocity at impact is ~350Hz.

All previous calculations of cartilage modulus from indentation data 1 are compromised by being based on a model which assumes cartilage is an "infinite elastic layer" 3 . In the resultant indentation equation, modulus values are inversely proportional to a correction factor, κ , which varies with both indenter-radius/cartilage-thickness ratio and Poisson's ratio. Instead, we used the approach of

Kren 2 which assumes viscoelasticity, does not require specimen thickness measurement and does not require κ . The modulus is calculated from

$$E_{dyn}=(1-\nu)[P_{Qmax}/(R^{1/2}\alpha_{max}^{3/2})]$$
 (1) Where $E_{dyn}=$ dynamic elastic modulus, $\nu=$ Poisson's ratio, $\alpha_{max}=$ maximum displacement, $P_{Qmax}=$ force at maximum displacement, and $R=$ indenter radius. Literature values of ν for cartilage vary widely 1 , and $\nu=0.44$ was assumed. This does not affect relative magnitudes of E_{dyn} calculated from (1). The loss angle ϕ was read directly from the differences between the sinusoidal force and displacement curves.

RESULTS: See Table 1 Table 1. Nutrition-mode (0.1Hz) and gait-mode stiffness, same specimen: n = 8 in each mode.

| | Indenter | Mean | S.D. | | S.D. |
|--------|----------|-----------|-----------|-------|------|
| | radius | E_{dyn} | E_{dyn} | Mean | ф |
| Method | [mm] | [MPa] | [MPa] | φ [°] | [°] |
| N-mode | 1 | 8.2 | 0.9 | 15.7 | 2.2 |
| G- | | | | | |
| mode | 0.5 | 14.9 | 0.8 | 7.7 | 0.6 |

DISCUSSION & CONCLUSIONS: Precision of both test modes was acceptable (worst S.D.=14%). Compared to N-mode, G-mode modulus was ~82% higher, and loss angle was ~51% lower. The data demonstrate the dependence of cartilage stiffness parameters on test mode, and support dual mode tests to evaluate two aspects of cartilage function.

REFERENCES: ¹ R.K. Korhonen, et al (2002) *J Biomech* **35**:909. ² A. P. Kren, et al *Determination of viscoelastic characteristics of biological materials by SIMI* (m.s. in preparation). ³ W. C. Hayes (1972) et al. *J Biomech* **5**:541.

ACKNOWLEDGEMENTS: Deutsche Arthrose Hilfe (Saarlouis DE), Hardy & Otto Frey-Zünd Stiftung (Basel CH).

Nano- versus Micron-sized Bioactive Glass Reinforcement of P(3HB) – Are Nano-fillers the Way Forward?

D. Mohn¹, S.K.Misra², T.J. Brunner¹, A.R. Boccaccini², W.J. Stark¹

¹Institute of Chemical and Bioengineering, Department of Chemistry and Applied Biosciences, ETH Zurich, 8093 Zurich, Switzerland

²Department of Materials, Imperial College London, London SW7 2BP, UK

INTRODUCTION: Composites of biodegradable polymers and bioactive ceramics in the form of biocompatible scaffolds have been proposed and used in the field of tissue engineering with emphasis towards hard tissue regeneration [1, 2]. Calcium phosphate-based ceramics or glasses can be incorporated into the polymer matrix in order to reinforce the polymer and add bioactive properties. A popular polymer within the family polyhydroxyalkanoates is poly(3hydroxybutyrate), known as P(3HB). In order to investigate the effect of particle size of the fillers we have introduced micron- or nano-sized bioactive glass particles [3] in different concentrations within the P(3HB) matrix and compared their mechanical and thermal properties, topography, protein adsorption, in vitro degradation behaviour and cell proliferation [4].

METHODS: Composite films of P(3HB) with 10, 20, or 30% micron-sized, conventional (m-BG) or nano-sized bioactive glass (n-BG) were prepared by solvent casting. The topography of the resulting materials was investigated using SEM and the thermal as well as the mechanical properties using DSC and tensile strength tests respectively. Further investigations included protein adsorption with foetal bovine serum, an *in vitro* bioactivity study in SBF and cell proliferation of MG-63 osteoblast-like cells.

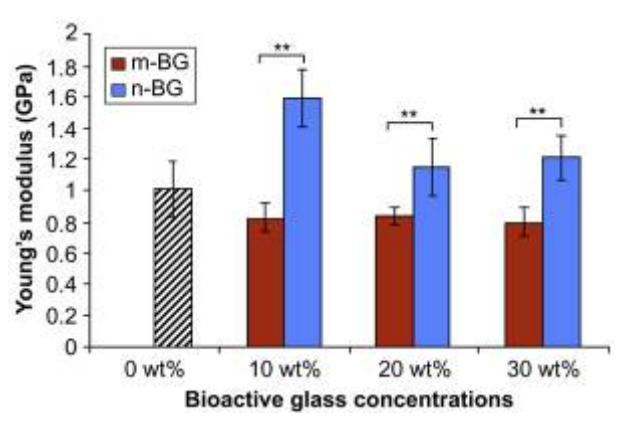


Fig. 1:Mechanical properties in dependence of the filler concentration and m- vs. n-BG.

RESULTS: The addition of n-BG particles induced a nano-structured topography on the surface of the composites not visible on m-BG composites. This surface containing observed for n-BG composites considerably protein increased the adsorption. interestingly, n-BG particles caused a significant stiffening of the composite (Fig. 1) but had no effect on the thermal properties. Immersion in SBF revealed a high level of in vitro bioactivity for P(3HB)/n-BG composites. Proliferation of MG-63 osteoblast-like cells on the various composites demonstrated a good biocompatibility of all composite materials.

DISCUSSION & CONCLUSIONS: The results of this study have confirmed that the addition of nanoparticulate bioactive glass has a more significant reinforcing effect on the mechanical and structural properties of a composite system than the corresponding micron-sized particles. Therefore such nanoparticles are a most interesting bioactive filler material for biodegradable polymers in order to prepare advanced composites for tissue engineering.

REFERENCES: ¹ Rezwan, K. et al, *Biomaterials*, **27**, 3413-31, 2006. ² Loher S. et al, *Nanotechnology*, **17**, 2054-61, 2006. ³ Brunner, T.J. et al, *Chem. Commun.*, **13**, 1384-6, 2006. ⁴ Misra, S.K., et al, *Biomaterials*, **29**, 1750-61, 2008.

ACKNOWLEDGEMENTS: Financial support by the Overseas Research Scholarship UK, IDEA league research grant and Gebert Rüf Foundation (grant nr. GRS-048/04) is kindly acknowledged.

Effects of silver nitrate and a silver nanoparticle biomaterial additive on *E. coli* growth, determined by isothermal micro-nano calorimetry (IMNC)

U.von Ah¹, D. Wirz¹, U. Pieles², A. U. Daniels¹

¹ Laboratory for Orthopaedic Biomechanics, Faculty of Medicine, University of Basel, Switzerland. ²Fachhochschule Nordwestschweiz, Muttenz, Switzerland.

INTRODUCTION: Silver has long been used as an antimicrobial; e.g. in disinfectant solutions and ointments for burns. Problems with antibiotic resistance have spurred renewed interest in silver, and in new forms, such as nanoparticles, to be added to or coated on medical materials. Using our isothermal micro-nano calorimetry (IMNC) method, we evaluated the effect of both silver nitrate solutions and silver nanoparticles (in an amorphous silica agglomerate carrier) on growth of *E. coli*.

METHODS: Heat is atomic-scale kinetic energy, transferred within liquids by mechanical interactions. Cultured cell metabolism and growth processes produce heat which is transferred to the medium. IMNC measures transfer rate changes as low as 22 nano J/sec--equivalent to an increase of only $\sim 10^4$ in the number of bacteria in a culture.

E. coli W3110 was cultured in LB broth at 37°C. An overnight culture was adjusted to an OD₆₀₀ of 0.01, and 1% of this solution was used as inoculum. Minimum inhibitory concentrations (MICs) were determined according to CLSI standards ¹ with one change: Instead of using a single twofold serial dilution row, a second was overlaid (Fig. 1). Both silver nitrate solutions and micron-range amorphous silica agglomerates with 5, 9 and 20 % (w/w) of 5-20 nm silver particles were studied.

Growth over 24 h at 37 °C was monitored in sterile sealed 4 ml microcalorimetry ampoules. Before sealing, ampoules were filled with 2.97 ml LB broth supplemented with dilutions of silver nitrate or silica/nanosilver plus the 30 µl *E. coli* inoculum. Before heat transfer measurement, ampoules were equilibrated for 45 minutes in the microcalorimeter chambers to eliminate transient heat phenomena.

To confirm calorimetry results, parallel ampoules were incubated at 37 $^{\circ}$ C and evaluated for growth both visually and by OD_{600} determinations.

RESULTS: For silver nitrate, a MIC (no growth at 24 hours) of 8 mg Γ^1 was determined using IMNC. This result was confirmed in parallel ampoules using traditional visual/optical (turbidity) methods. Calorimetry (Fig.1) also showed something new. Subinhibitory concentrations of silver nitrate did not alter the time history of heat production (corresponding to bacterial growth). Instead, the effect of silver nitrate was only to delay the start of

growth. For example 6 mg l⁻¹ AgNO₃ delayed growth for 600 min compared to the control (culture medium and *E. coli* alone).

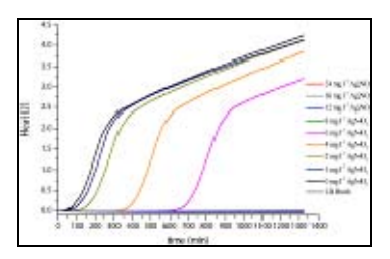


Fig. 1: IMNC change in total heat as f(t) & AgNO₃ concentration, E.coli growth in LB broth @37°C.

The MIC for the silica/nanosilver determined by IMNC was 1 mg ml⁻¹ for 5 % silver, 0.5 mg ml⁻¹ for 9 % silver and 0.25 mg ml⁻¹ for 20 % silver. The MIC for silica/nanosilver was thus inversely proportional to the percent silver. The effect of subinhibitory concentrations on *E. coli* growth was the same as for silver nitrate (data not shown).

DISCUSSION & CONCLUSIONS: Heat transfer in liquids is a nanomechanical process, and IMNC can measure rates as low as 22 nano J/sec. Here, it precisely determined the MIC of two forms of silver for *E. coli*. IMNC also measured something missed by traditional methods--the real time effects of subinhibitory concentrations of silver on bacterial growth. Subinhibitory concentrations of silver delay growth, but once it starts, initial concentration has no effect on the rate. Further IMNC studies will measure the effect of silver additives on energetics of bacterial adhesion. IMNC can also determine MICs of antibiotics ² and measure rate processes in other types of cultured cells, biomaterials and their interactions.

REFERENCES: ¹ Clinical & Laboratory Standards Institute (2006) *M07-A7*, CLSI, USA. ² von Ah, Wirz, Daniels, J Clinical Microbiology (accepted 04/2008).

ACKNOWLEDGEMENTS: Support - HeiQ AG (Bad Zurzach CH), Velux Stiftung (Zürich CH), Hardy & Otto Frey-Zünd Stiftung (Basel CH). Gratefully acknowledged: Use of Uni. Basel Dental Institute Microbiology Laboratory.

Optical Coherence Tomography: Applications in Dentistry

C.Sinescu¹, M. Negrutiu¹, M.Hughes², A.Bradu², M.Rominu¹, P.Laissue³, G.Dobre², A.Podoleanu²

Department of Dental Materials and Dental Prostheses Technology, "Victor Babeş" University of Medicine and Pharmacy of Timişoara, Romania. Applied Optics Group, University of Kent, Canterbury, UK. Kent Institute of Medicine and Health Sciences, University of Kent, Canterbury, UK.

INTRODUCTION: In dental restoration, a prosthetic is prepared to replace one or more missing teeth. Fixed partial prostheses as integral ceramics, integral polymers, metal-ceramics or metal-polymers bridges, are mainly used in the frontal part of the dental arch (especially the integral bridges). They have to satisfy high stress requirements as well as esthetic. The masticatory stress may induce fractures of the bridges. These may be triggered by initial materials defects or by alterations of the technological process. The fractures of these bridges lead to functional, esthetic and phonetic disturbances which finally render the prosthetic treatment inefficient. One from the purposes of this study is to evaluate the capability of OCT in detection and analysis of possible fractures in several fixed partial dentures. Bone implants insertion implies the necessity of a important primary stability. The quality of the implant insertion could be investigated by implant bone interface analysis. There are several methods for evaluating the micro leakage in composite restorations such as bacterial penetration, fluid transport, clarification, and penetration radioisotopes, electrochemical methods and gas chromatography. Dye penetration tests; however, seem to be the most widely used.

METHODS: The optical configuration uses two single mode directional couplers superluminiscent diode as the source at 1300 nm. The scanning procedure is similar to that used in any confocal microscope, where the fast scanning is en-face (line rate) and the depth scanning is much slower (at the frame rate) (1). The en-face scans provide an instant comparison to the familiar sight provided by direct view or via a conventional microscope. Features seen with the naked eye could easily be compared with features hidden in depth. Sequential and rapid switching between the en-face regime and the cross section regime. specific for the en-face OCT systems developed by us, represents a significant advantage in the noninvasive imaging. **Images** with orientations and 3D OCT imaging can be obtained using the same system.

RESULTS: The detected defects have a large volume and therefore are highly capable to generate fracture lines in the proximal or almost

superficial on the occlusal area, leading to the failure of the prosthetic treatment. The detection of these defects before inserting the prostheses allows all the corrections in order to avoid the fracture of the ceramic component. The all ceramic prostheses entered the field of prosthetics as a maximum esthetic alternative. The fractures that occur within the structure of these prostheses were motivated by the elasticity module of the ceramics and by the defects within the ceramic layers. Early detection of substance defects within these layers allows for optimal corrections before inserting them into the mouth and applying masticatory stress together with reduction of fractures. In this study, we demonstrate that en-face optical coherence tomography can be used to evaluate these interfaces. We have collected both C-scans OCT images (en-face) as well as B scan OCT images (cross section). 3D analysis was possible by acquiring 30-100 C-scans which were used post acquisition to explore the volume of the tissue around the interface. The images show gaps of different sizes and shapes between the implant and the bone at different depths.

DISCUSSION & CONCLUSIONS: OCT could act as a valuable tool in dentistry as a noninvasive method. Utilisation of OCT will save time and resources by eliminating prostheses with defects before being mounted in the patient's oral cavity and to identify the gaps in direct composite restorations.

REFERENCES: ¹ A. Gh. Podoleanu, J. A. Rogers, D. A. Jackson, S. Dunne (2000) *Three dimensional OCT images from retina and skin* Opt.Express, Vol. 7, No. 9, p. 292-298, (2000). ² I. Bratu D., R. Nussbaum (2001) *Bazele clinice și tehnice ale protezării fixe*, Editura Signata. ³ C.Sinescu, M.Negruțiu, C.Todea, A.Gh. Podoleanu, M.Hughes, P. Laissue, C. Clonda (2007) *Coherente Tomography as a non invasive method used in ceramic material defects identification in fixed partial dentures*, Dental Target, nr. 5, year II.

Polyelectrolyte multilayers on Nitinol

S.Schweizer¹, A. Taubert², G. Siekmeyer³

1Departement of Chemistry, University of Basel, Klingelbergstrasse 80, 4056 Basel, Switzerland 2Institute of Chemistry, University of Potsdam, 14476 Golm, Germany 3 Admedes Schuessler GmbH, Pforzheim, Germany.

INTRODUCTION: Surface treatment plays an important role for increasing the overall biocompatibility of devices as stents or implants. Unlike restenosis, which is fairly common, stent thrombosis is a rare but much more dangerous complication after coronary stent placement. It usually occurs before endothelialisation has been completed. To improve the risk of stent trombosis fast endothelialisation is necessary. For that reason, we deposited and mineralized Calcium Phosphate on Nitinol stent devices in a polyelectrolyte multilayer film from Chitosan and Heparin.

METHODS: Nitinol (an acronym for <u>Ni</u>ckel <u>Ti</u>tanium <u>Naval Ordnance Laboratory</u>) is a shape memory alloy and is already used for stents and implants.

The multilayer films are constructed by using the layer-by-layer (LbL) technique as shown in figure 1 [1, 2]. During LbL deposition, Nitinol, a solid substrate bearing negative charges on the surface, initially immersed into a cationic polyelectrolyte solution. The substrate containing the cationic layer was subsequently immersed in the anionic polyelectrolyte solution. We used the two natural polysaccharides Chitosan and Heparin as polycation and polyanion respectively. Chitosan is a linear polysaccharide produced commercially by deacetylation of chitin. Heparin, also a linear polysaccharide, is widely used as an injectable anticoagulant.

After LbL deposition Calcium Phosphate was mineralized on the new surface. Hydroxyapatite may have advantageous effects for endothelialisation.

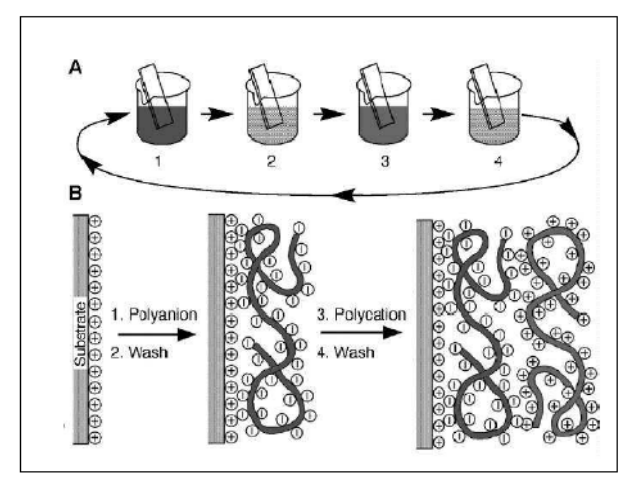


Fig. 1: Layer-by-Layer (LbL) deposition technique. Step 1 and 3 represent the adsoption of a polyanion and polycation, respectively, step 2 and 4 are washing steps [1].

RESULTS: The deposition of Calcium Phosphate on Nitinol substrate in general is possible even without a polymer. With the use of the polymer matrix, however, Calcium Phosphates deposits faster. On SEM images we can see explicitly more Calcium Phosphate crystals.

Secondly we investigated the concept of using the polymer multilayer as matrix and porous membrane for drug deposition. For this reason we did some LbL depositions adding Rhodamine and/or Oxonol as model for drug molecules. UV/Vis experiments show linear release of these chromophors over a time period of several weeks.

REFERENCES: ¹ G. Decher, *Science* 1997, 227, 1232. ² F. N. Crespilho, *Int. J. Electrochem. Sci.* 2006, 1, 194.

Control of Human Osteoblast adhesion on polymers after ion beam irradiation

G.Guibert¹, T.Rossel², G. Weder², S. Mikhailov¹, C. Meunier³, B. Betschart².

¹ IMA-Arc La Chaux-de-Fonds Switzerland, ² Institut de Biologie Université de Neuchâtel Switzerland, ³ Institut FEMTO-ST Montbéliard France

INTRODUCTION: when a biomaterial is inserted in the body, the biological responses are associated with their surface properties. Surface treatments are developed to create some mimetic polymer or biomaterials with high performances, preserving the bulk properties and creating some specific interaction between the designed surfaces and the bio molecules or the cells. Some applications require the control of the cell behaviour: protein adsorption, cell proliferation, cell differentiation, cell mobility, spreading etc. The field of polymers application is vast and the surface treatment must be adapted: biosensors, tissue engineering, tissue regeneration, neural probes, drug delivery, bioactuators etc.

METHODS: The surface treatment of organic materials by ion beam offers some advantages [1-3]: the depth of treatment is well controlled, the treatment could be local or total without mask (at the scale cell), surface modifications (scission, cross-linking, grafting, topography etc.) depend on the parameters of irradiation, and the treatment process is clean and realised in high vacuum. Polymers samples (PTFE, PMMA, PEEK, PET. HDPE, Parylene) are irradiated with a 900 keV Helium beam produced by a Van de Graaf Accelerator. The Polymers are cut out by a water jet at 13 mm diameter to be easily put in the cellular culture box. Three lines of irradiation are realized on each sample (line: 500 µm width, 6 mm length).

Cell cultures are done with an Osteoblast hFOB 1.19 lines from ATCC. After the treatment, samples are sterilized. Then they are immerged in a PBS medium culture heated at 37 °C. 10 000 Osteoblast cells are introduced with a pipetman and let incubated during 96 hours at 37° C with 5% of CO2. The cells are fixed with formol and after rinsing the cells are coloured with a blue Toluidine solution, then they are cleaned and let dried. Observations were performed with an Olympus® microscope.

RESULTS: No cell adhesion was observed on the PS, PTFE and PEEK material without any treatment. For the majority of the treated polymers, the cell adhesion depends on a threshold doses (number of atoms/cm²): 5.10¹¹ at/cm² for the PS and 5.10¹³ at/cm² for PTFE and PEEK. To induce some significant modifications which facilitate the

cell adhesion on PEEK and PTFE polymers, it is necessary to multiply the dose by a factor 100 compared to the PS. In some particular case, a local treatment allows the cells to colonize the whole surface.

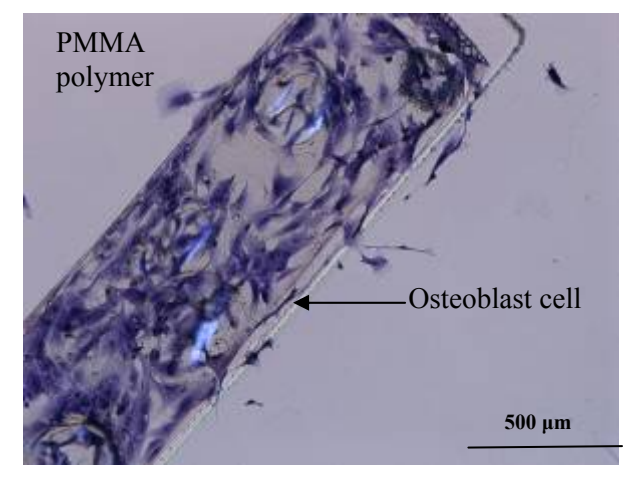


Fig. 1: Control of the adhesion of the Human Osteoblast cell on PMMA polymer. In this case cells adhere directly on the line of irradiation (900 keV He beam, .Dose 5.10¹⁴ at/cm²).

possible. Theses parameters (dose, time of treatment) have to be adapted according the kind of polymer. Some chemical and topographical modifications are induced on the surface without affecting the bulk properties at the micrometer scale cell. Irradiation by He beam do not bring any pollution during the treatment nor toxicity.

REFERENCES: ¹M. Iwaki (2001) *Ion Surface Treatments on organic materials* in Nucl. Instr. and Method B 175:368:374. ² Y. Suzuki (2003) *Ion beam modification of polymers for the application of medical devices* in Nucl. Instr. Method. B 206:501-506. ³J.M Colwell et al. (2003) A *studies of the chemical and physical effects of ion implantation of micro-porous and non porous PTFE* in Surface and coatings technology 168:216-222.

ACKNOWLEDGEMENTS: This research was supported by Haute Ecole Arc and MaCHop network in Collaboration with CSEM and Neuchatel University.

A bioactive biodegradable guided bone regeneration membrane: from the bench to the dental practice

FE Weber^{1,2}, McKenzie G², B. Hardwick²B San Miguel^{1,2}, C Ghayor¹, M Ehrbar¹ KW Grätz ¹ University Hospital Zurich, Bioengineering, Department for Cranio-Maxillofacial Surgery, Frauenklinikstrasse 24, 8091 Zurich, Switzerland; ²Inion Ltd, Cambridge UK

INTRODUCTION: Bone morphogenetic proteins (BMPs) are the key cytokines in bone formation and repair. A possible strategy to utilize BMP activity in clinical applications is to enhancer the activity of autologous BMP. Here we show that NMP (N-methyl-pyrrolidone) is an enhancer of BMP activity and can be used to generate a guided bone regeneration (GBR) membranes of the 3rd generation, where biocompatibility, biodegradability and bioactivity are combined. To identify possible other pro osteogenic pathways induced by NMP we, then, applied micro array techniques and found that in addition to the BMP signalling, the natriuretic hormone system is also tuned into a pro osteogenic state.

METHODS: MC3T3-E1 pre-osteoblastic cells were tested for different cell maturation responses: ALP (Alkaline phosphatase activity) and Alizarin Red mineralization assay. Micro array experiments were performed with C2C12 cells. The effect of NMP was determined *in vivo* in a guided bone regeneration model. Histological and histomorphometric analysis of bone repair *in vivo*: non critical size 6 mm defects were created in rabbit calvarias and subsequently treated with three different membranes, namely PLGA, and NMP-PLGA, or left untreated (control).

RESULTS: In preosteoblastic cells, NMP increases ALP and mineralization concentration dependent. NMP action depends on extracellular BMP, because it is sensitive to BMP antagonist Noggin. In combination with rhBMP-2, NMP shows a synergistic effect on ALP activity, mineralization and Smad 1,5,7 phosphorylation. Although BMP activity depends on proteinkinase D, the synergistic effect is proteinkinase C dependent. The in vivo results in a GBR model show that at 4 weeks in the presence of NMP healing of the defect is 79.17% complete compared to 49.31 % without NMP.

Micro array experiments performed with the multi potent mesenchymal stem cell revealed that 4 h exposure of C2C12 cells to 5mM of NMP halved the expression of natriuretic peptide receptor type 3 (npr3) and increase in the expression of the natriuretic peptide precursor type B (BNP) 1.5 fold. These results were confirmed by low density arrays and RT-pcr.

DISCUSSION & CONCLUSIONS: The results suggest that NMP improves the biological activity of BMP in vitro and in vivo by enhancing the kinase activity of the BMP-BMP-receptor complex in a proteinkinase C dependent way. The in vivo results show that the content of autologous BMP in bone is sufficient for NMP to enhance bone healing. Since NMP can be delivered by PLGAbased materials the combination of PLGA and NMP generates a 3rd generation GBR membrane, membrane since this GBR biocompatibiliy, biodegra-dability, and bioactivity. Interestingly, NMP shows also effect in the absence of BMP. The plasticizer NMP decreases npr-3 expression and increases BNP expression, mimicking the knock-out and over-expression of those genes in mice which is manifested in formation of longer bones and increased bone formation¹. Therefore, the direct effect of NMP on the transcription of 2 elements of the natriuretic peptide hormone system in a pro osteogenic way could at least partially account for the accelerated bone healing seen under the influence of NMP in vivo.

REFERENCES: ¹Bartels CF, Bükülmez H, Padayatti P, et al .Mutations in the transmembrane natriuretic peptide receptor NPR-B impair skeletal growth and cause acromesomelic dysplasia, type Maroteaux. Am J Hum Genet. 2004 75(1):27-34

ACKNOWLEDGEMENTS: This study was in part supported by Inion OY, Tampere Finland and by a grant from the AO Foundation (Davos, Switzerland) through the Biotechnology Advisory Board.

Neurotrophic factors release from nerve conduits for peripheral axonal regeneration

Srinivas Madduri¹, Michaël Papaloïzos², Bruno Gander¹

Institute of Pharmaceutical Sciences, ETH Zurich, 8093 Zurich, Switzerland

²Center for Hand Surgery and Therapy, CH8, 1205 Geneva, Switzerland

INTRODUCTION: Axonal regeneration after peripheral nerve injury is insufficient for functional recovery and is therefore a significant clinical problem. Neurotrophic factors (NTFs) play crucial role in neuronal survival and axonal regeneration, and nerve conduits (NC) provides support and protection to the regenerating axons. combined with NTFs have been used in several studies to improve nerve regeneration, but the clinical outcome remained unsatisfactory¹. This may be attributed to several poorly known or understood parameters such as NTF dose, temporal and spatial requirements (i. e., release kinetics), and need for multiple factors rather than single factor mostly applied so far. In the present study, we have developed collagen nerve conduits for the co-delivery of glial cell line-derived neurotrophic factor (GDNF) and nerve growth factor (NGF) to exploit the synergistic effects of these two factors on axonal regeneration. The release kinetics was controlled by physical cross-linking of collagen and by an integrated delivery system.

METHODS: Collagen NCs were produced by spinning mandrel technology. NTFs were loaded into NC and the tubes were coated with poly (lactide-co-glycolide). *In vitro* release of GDNF and NGF was determined by incubating the NC in citrate buffer (pH 5.0); the released NTFs were assayed by ELISA and a bioassay. For the latter, DRGs were isolated from E9-chicken embryos (9 days old), and the explants were cultured as described previously².

RESULTS: The *in vitro* release of GDNF and NGF from the NC was sustained over 30 days. The main parameter that influenced the NTFs release was the dehydro-thermal (DHT) treatment of the NC. During the initial 2-3 days of release, the DHT-treated NCs released the NTFs at significantly lower rates, whereas this difference vanished after 3 days. The total release of NGF and GDNF amounted to, respectively, 56 and 68% of the total dose for DHT-treated NC; for not DHT-treated NC, these values were 83 and 78%, respectively. In both NC types, the total amount of each growth factor was 80 ng.

The bioactivity of released GDNF and NGF was assessed in an *in vitro* bioassay. Incubation of

DRG explants with release medium containing NGF and GDNF released from NCs resulted in axonal outgrowth (Fig. 1). These results show combined release of biologically active GDNF and NGF from collagen nerve conduits over 30 days.

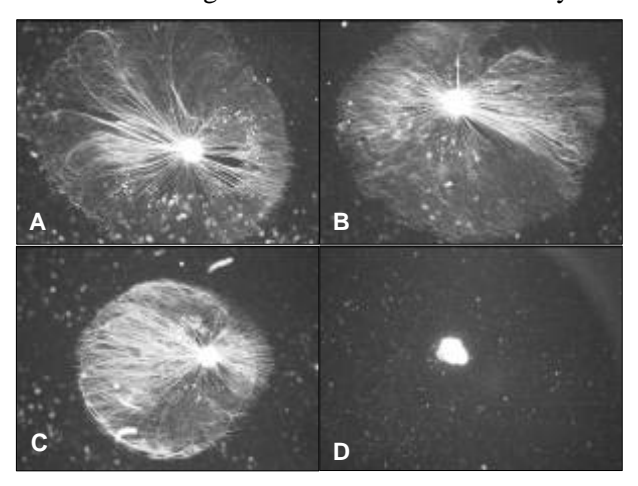


Fig. 1: Bioactivity of neurotrophic factors released from nerve conduits, as determined using DRG explants culture. (A) GDNF+NGF; total concentration: 1 ng/ml (positive control); (B) 1st day release medium with GDNF+NGF released from DHT-NC; (C) 30th day release medium with GDNF+NGF released from DHT-NC; (D) DRG treated with buffer (negative control).

DISCUSSION&CONCLUSIONS: Collagen nerve conduits were successfully developed with integrated delivery system for combined release of GDNF and NGF. Our results prove the feasibility of developing nerve conduits for co-delivery of NTFs. Future studies will assess the potential benefit of combined GDNF+NGF over single factor delivery in a nerve gap model in the rat.

REFERENCES: ¹L. B. Moran, et al (2004) *Brain Res Rev* **44**:154-78. ²E. Stoeckli et al (1991) *J Cell Biol* **112**:449-55

ACKNOWLEDGEMENTS: We acknowledge the enabling financial support by GEBERT RÜF FOUNDATION (Basel).

Fine-tuning of Bioactive Glass for Root Canal Disinfection

T. Waltimo¹, D. Mohn², F. Paqué³, T. J. Brunner², W. J. Stark², T. Imfeld³, M. Schätzle⁴, M. Zehnder³

¹Institute of Oral Microbiology and Preventive Dentistry, University of Basel Center of Dental Medicine. ²Institute for Chemical and Bioengineering, Department of Chemistry and Applied Biosciences, ETH Zurich. ³Department of Preventive Dentistry, Periodontology, and Cariology, University of Zürich Center of Dental Medicine. ⁴Department of Orthodontics and Pedodontics, University of Zürich Center of Dental Medicine, Switzerland.

INTRODUCTION: Bioactive glasses of the SiO₂-Na₂O-CaO-P₂O₅ type have recently been suggested as topical root canal disinfectants¹. Similarly to calcium hydroxide, the gold standard material for that purpose, bioactive glasses disinfect their environment via continuous release of alkaline species in a wet environment². Antibacterial effect of bioactive glasses could be greatly enhanced by lowering their particle size and thus their immediate release of alkaline species³. On the other hand, the antimicrobial effect is also related to the capacity of these materials to continuously maintain an alkaline environment over time⁴. In the restricted volume of a root canal system, this effect might be related to the mass of bioactive glass material per total volume of the applied suspension. The hypothesis of this study was that more material per volume of bioactive glass slurry is obtained with a superfine (<2 µm) micrometric material or a micrometric/nanometric hybrid rather than a solely nanometric counterpart. This should correlate with alkaline capacity and antimicrobial effectiveness.

METHODS: Conventional bioactive glass 45S5 (45 wt% SiO₂, 6 wt% P₂O₅, 24.5 wt% CaO, and 24.5 % Na₂O) with a mean particle size of $< 5 \mu m$ (NovaminTM, US Biomaterials Corp., Alachua, FL) was obtained from a commercial source. Bioactive glass 45S5 of nanometric size was prepared from suitable anion precursors as described earlier³. A hybrid material with 50/50 wt% of nanometric and micrometric bioactive glass, respectively, was mixed. Calcium hydroxide (Stoke Canon, Devon, UK) served as control. Defined slurries with known specific surface areas and masses were prepared in physiological saline solution. Continuous titration of the slurries with hydrochloric acid was performed, and their antimicrobial effectiveness was tested in extracted human premolars mono-infected with E. faecalis ATTC 29212 (N = 12 per material). Dentin samplings from layers of different depths were conventionally cultivated. The number specimens showing residual growth of E. faecalis per sampled dentin layer was compared between groups applying Fisher's exact test with Bonferroni's correction. The alpha-type error was set at 0.05.

RESULTS: While the nanometric slurry had a 12-fold higher specific surface than the micrometric counterpart, the latter had a considerably higher alkaline capacity and a significantly better disinfecting capacity (Fisher's exact test, Bonferroni, P < 0.05). The hybrid slurry behaved similar to the micrometric one (Table 1).

Table 1. Residual growth ratio (sample-positive specimens/total specimens) in sampled dentin layers of human premolars infected with E. faecalis ATTC 29212 after 10 days of test and control treatments. Identical superscript letters indicate that there was no significant difference between respective treatments within a sampling layer.

| Material | Layer 1 | Layer 2 | Layer 3 |
|---------------------|-------------|-------------|-------------|
| Nano | $11/12^{A}$ | $12/12^{A}$ | $12/12^{A}$ |
| Micro | $1/12^{B}$ | $1/12^{B}$ | $1/12^{B}$ |
| Nano-Micro | $3/12^{B}$ | $3/12^{B}$ | $3/12^{B}$ |
| Ca(OH) ₂ | $0/12^{B}$ | $0/12^{B}$ | $0/12^{B}$ |

DISCUSSION & CONCLUSIONS: Based on the current and previous results, it may be concluded that a combination of nano- and micrometric bioactive glass could be useful for root canal disinfection, as this system shows an early-onset effect and long-lasting antimicrobial effect.

REFERENCES: ¹ Zehnder et al., 2004, J Endod, 30, 220-4; ² Allan et al., 2001, Biomaterials, 22, 1683-7; ³ Waltimo et al., 2007, J Dent Res, 86, 754-7; ⁴Gubler et al., Int Endod J (in press).

ACKNOWLEDGEMENTS: This research was supported by funds of the Department of Preventive Dentistry, Periodontology, and Cariology, University of Zürich and Grant number GRS-048/04 by the Gebert Rüf Foundation.

Comparison of two different **B-TCP** composites for reconstruction of ovine mandibular continuity defects.

M.C.Nolff^{1,2}, H. Kokemüller¹, G. Hauschild^{2,3}, M. Fehr², A Kampmann¹, K.Rohn², S. Spalthoff¹, J.–H. Bormann¹, M. Rücker¹, N.-C. Gellrich¹

Department of Oro- Maxillofacial Surgery, Hannover Medical School. ² Small Animal Clinic, University of Veterinary Medicine Hannover, Foundation. ³ Department of Orthopedics, University of Münster.

INTRODUCTION: The reconstruction of large mandibular bone defects after traumatic bone loss or tumor resection is challenging surgeons around the world. Among the various investigated materials, ceramic scaffolds proved to be biocompatible and osteoconductive $^{1-3}$. The aim of the study was to compare osseointegration and degradation of a blood-loaded β -TCP composite (β -TCP_B) with a similar composite that had been additionally loaded with autologous bone marrow and cancellous bone (β -TCP_{B/BM/CB}) after reconstruction of critical size mandibular defects.

METHODS: Twelve German Black-Headed Sheep with an average weight of 72.5 +/- 10 kg underwent segmental resection of the right hemimandible. Animals assigned to group A (n=6) were reconstructed using blood-loaded B-TCPB while sheep assigned to group B received β-TCP_{B/BM/CB} grafts with a central through-bore-hole that was filled with bone marrow and milled autologous cancellous bone, both obtained from core biopsies taken from the iliac crest during the same surgery session. After a maintenance time of twelve weeks all sheep were sacrificed. Tissue quality was histologically assessed and bone-, scaffold-, cartilage- and fibrous-tissue area were estimated semiautomated histomorphometrical using software. The impact of the different graft types (TCP_B vs. TCP_{B/BM/CB}) and slide position (surface, intermediate, central) was examined using twoway analysis of variance with post hoc t-test for five pair wise comparisons between corresponding slides.

RESULTS: All animals underwent clinical uneventful healing. Two sheep presented inflammation of the graft side associated with graft dislocation at sacrifice and were excluded from further evaluation. Fracture of the reconstruction plates occurred in two animals of each group leaving three sheep per group that underwent bone healing under stable conditions. Statistical analysis revealed no significant difference specimens retrieved from stable and unstable defects, thus affected animals were not separated and five specimens per group were included in further evaluation. New deposited bone within group A was immature and none of the specimens showed defect union. The defect center was still occupied by a ceramic core. Direct bone—ß-TCP contact was rare due to an intervening soft tissue layer. Animals assigned to group B achieved defect union and a high grade of bone maturation. Residual ceramic remnants were rare, disconnected and integrated within newly formed bone (Fig. 1).

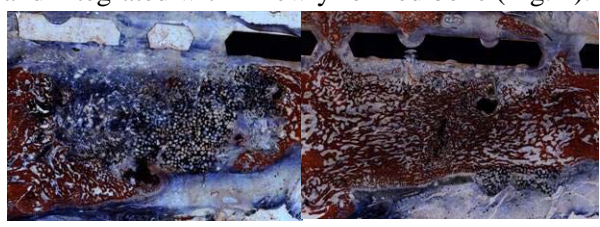


Fig. 1: Histological overview sections of defects grafted with β -TCP_B (left) and β -TCP_{B/BM/CB} (right) Alizarin-red Methylene-blue stain

Composites in group B exhibited significant (p<0.01) higher amounts of bone formation and ß-TCP degradation than composites used in group A. Cartilage- and soft tissue area did not significantly differ between the two groups.

DISCUSSION & CONCLUSIONS: The described method offers the advantage of manufacturing an efficient bone graft substitute table-side during surgery using the patient's own cells, circumventing the need of cell culture, expansion, and preservation. The osteoregenerative capabilities of the TCP_{B/BM/CB} composite indicate a promising potential for mandibular reconstruction.

REFERENCES: [1] Blokhuis TJ, Termaat MF, den Boer FC, Patka P, Bakker FC, Haarman HJ. Properties of calcium phosphate ceramics in relation to their in vivo behavior. J Trauma 2000;48(1):179-86. [2] Bauer TW, Muschler GF. Bone graft materials. An overview of the basic science. Clin Orthop Relat Res 2000: 10-27. [3] Bloemers FW, Patka, P, Bakker, FC, Haarman, HJTM. The use of calcium phosphates as a bone substitute material in trauma surgery. Osteo Trauma Care 2002: 10:33-37

BIOREACTOR-BASED TISSUE ENGINEERING STRATEGIES

Ivan Martin, Stefania Riboldi, Marcel Jakob, David Wendt Departments of Surgery and Biomedicine, University Hospital Basel, CH

INTRODUCTION

Lately we have witnessed an increased recognition of the importance of 3D culture models to study various aspects of cell physiology and pathology, as well as to engineer implantable tissues. Bioreactor systems may provide the technical tools to address challenging scientific questions and to allow the successful translation of Tissue Engineering processes from bench to bedside.

TECHNICAL BACKGROUND

Bioreactor systems have proved to be crucial to establish and maintain 3D cell/tissue cultures, and have the potential to provide such cultures with a controlled chemico-physical environment. In particular, bioreactors may offer the following features: 1) Efficient and uniform cell seeding on 3D scaffolds, especially when relying on perfusion techniques; 2) Improved mass transfer in 3D hydrodynamic cultures, mostly using patterns; 3) Physical conditioning of developing physical constructs, since forces hydrodynamic, mechanical and electrical) play a key role in tissue development and remodeling; 4) Automation of medium and gas exchange procedures, with consequent smoother variations in the concentration of key metabolites.

SCIENTIFIC CHANCE AND CHALLENGE

Bioreactor systems offer the possibility to investigate cell function, cell interactions and tissue development within controlled 3D models, which may be designed to recapitulate specific aspects of the actual in vivo milieu. In particular, the application of defined environmental factors will be key to gain a deep insight into the mechanobiology of tissue development, and the consequent capability to drive and actively modulate the in vitro generation of engineered grafts. In order to achieve these goals, critical challenges lie in the integration of bioreactor technologies with 1) model-based design (e.g., computational fluid dynamics modeling to predict actual fluid velocity and shear profiles) and 2) sensing and control techniques (e.g., online, noninvasive monitoring of the constructs functional and morphological properties, and implementation of feedback-based strategies of system control).

CLINICAL PROSPECTIVE

Even the most clinically successful products will need to demonstrate: (a) cost-effectiveness and cost-benefits over existing therapies, (b) absolute

safety for patients, manufacturers and environment, and (c) compliance to the evolving regulatory framework in terms of QC and GMP. In this context, the following bioreactor-based features and strategies will be reviewed. 1) Automating tissue culture processes: Closed and minimally operator-dependent systems automation and control of the entire tissue manufacturing process possess great benefits in terms of safety and regulatory compliance. Such systems, despite high initial development costs, would have great potential to improve the costeffectiveness of tissue engineering approaches and facilitate large-scale production in the long-term. Streamlining conventional cell culture alternative to systems techniques: As an automating established manual culture procedures, novel concepts and techniques that streamline the conventional engineering processes (e.g., cell expansion directly in 3D scaffolds) will likely have the greatest impact on tissue manufacturing. 3) Manufacturing in centralized vs de-centralized facilities: Manufacturing at central locations allows close supervision over the entire production process, but is associated with complicated logistical issues. De-centralized production systems, located within the confines of hospitals, would simplify logistics but would involve the greatest upfront risks in terms of development time and costs. 4) "Intraoperative engineering" approaches: In spite of a paradigm shift (i.e., towards a regenerative medicine approach), in vitro bioreactor systems will continue to play a critical role. In fact, they will be necessary to streamline and automate biopsy processing and cell isolation/seeding, as well as to generate the knowledge of environmental factors required in vivo for predictable tissue development.

CONCLUSIONS

Progress made in the *in vitro* generation of 3D tissues starting from isolated cells is slowed down by the complexity of the process. By providing a comprehensive level of monitoring and control over specific environmental factors, bioreactors can provide the technological means to identify which specific chemico-physical parameter plays which function in engineering a defined tissue. At this stage, implementing the defined bioprocesses in bioreactor systems will support safe, standardized, scaleable, traceable and possibly cost-effective manufacturing processes for clinical use.

Microscopy analysis of total knee prosthesis failure caused by polyethylene wear

Antoniac Iulian¹, D.Laptoiu², F.Miculescu¹, R.Istrate³, C.Trisca-Rusu⁴

¹University "Politehnica" of Bucharest, Faculty of Materials Science and Engineering; ²Colentina Clinical Hospital, ³Med4Med Group Ltd, Bucharest, ⁴IMT Bucharest, Romania

INTRODUCTION: For the longevity of total knee arthroplasty it is very important to predict the polyethylene wear and optimize the prosthetic design [1]. Polyethylene wear is affected by contact stress, sliding motion and kinematics of the knee prosthesis. The most important factors which cause long-term failure of a prosthetic joint are: macroscopic fracture of the metallic components, wear of implant, corrosion process and osteolysis. Retrieval studies of components of knee prosthesis should help to answer some of these questions.

METHODS: The aim of this study was to study the wear characteristics of retrieved total knee implants. We examined 36 tibial components of knee prosthesis retrieved at revision between 3 and 5 years after implantation.

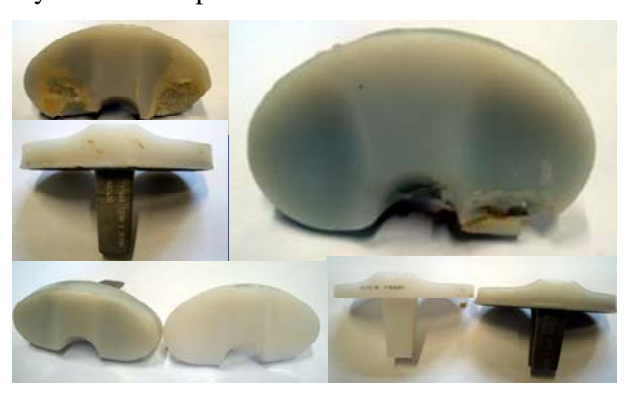


Fig.1: Example of some retrieved polyethylene components from knee prosthesis

The damage of the polyethylene was analysed by scanning electron microscopy. Also, the macroscopical aspects of retrieval polyethylene components were revealed using 10x light stereomicroscopy; Hood's scoring system was used.

RESULTS: Different modes of surface degradation were identified: burnishing; pitting: depressions in the articulating surface; surface deformation (caused by cold flow and/or creep); abrasion caused by direct contact with bone-cement debris; scratching; delamination. In our retrieved specimens, both longitudinal and transverse wear patterns "ripples' were observed consistent with the "natural" sliding and rolling movement of the knee. Another observation is related to the surface delamination of the surface observed by SEM, with a low uniformity of it,

possibly related to a shelf aging phenomenon. This may also explain the relative agglomeration of revision cases in one year time interval.



Fig.2: Macroscopic aspects of polyethylene components (left); stereomicroscopic image from failure zone (right)

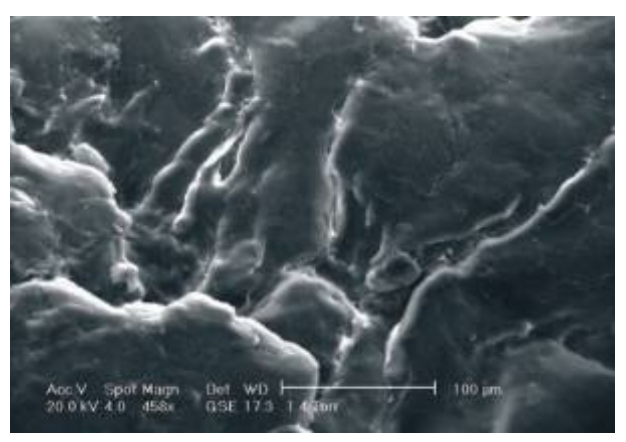


Fig.3: Scanning electron micrographs of retrieved polyethylene components (successive delamination was observed)

DISCUSSION & CONCLUSIONS: Some knee implants are more "forgiving" versus the surgical technique; generally, small rotational errors $(\pm 5^{\circ})$ are consistent with surface damage of the tibial insert. Burnishing, scratching and abrasion are the mechanisms mainly involved in these failures; most damage was seen at the posteromedial area. Delamination and surface deformation are connected to shelf or service life wear. The damage mechanisms of polyethylene components are dependent on the component geometry, the sliding conditions, and the shelf to service lifetime of the implant.

REFERENCES: ¹Hood RW, Wright TW Burstein AH., "Retrieval analysis of total knee prostheses - a method and its application to 48 total condylar prostheses", J.Biomed.Mater.Res., 1983.

Behavior of Mandible-Implant Interface under Stress and Temperature

F. Baciu¹, D. Vlăsceanu¹, M. Târcolea¹, D. Slăvescu², R.M. Târcolea², C.M. Cotrut¹, R.Bololoi¹

**Iniversity POLITEHNICA of Bucharest, ² University «Titu Maiorescu», Bucharest, Romania

INTRODUCTION: Dental implants function is to transfer load to surrounding biological tissues. Thus the primary functional design objective is to manage (dissipate and distribute) biomechanical loads in order to optimize the implant-supported prosthesis function.

METHOD: FEM study has been made by a numerical code, using the Finite Element Method. There was studied a new type dental implant in order to determine its peculiarity. The structure was blocked in the inferior side and the temperature variation was considered between 0 and 70 °C. The thermal load was applied in the screw head as well as the concentrated force.

RESULTS: Several graphs corresponding to an implant load with mastication force of about 717N and a temperature variation according with the oral cavity temperature. Evolution of stresses developed by temperature variation (0 and 70 °C – fig.1-2) and mastication force (fig.3-4) is presented for the main parts of the implant. Maximum stresses appear in the blunt superior side. This could be a problem for implant lifetime.

DISCUSSION & CONCLUSIONS: Temperature variations determine supplemental efforts that can be considered also in the study of optimum design for implants in order to eliminate the potential unwished effects induced by the temperature variations. This should be the initial phase that practicing dentist will use in order to identify the best implant type.

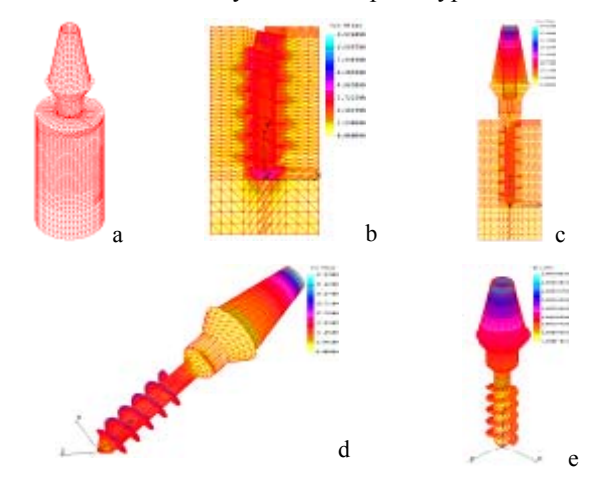


Fig. 1: The model (a) analyzed with temperature. The tension on mandible bone(b), mandible bone – implant (c) and screw assembly (d) at 0° C and displacement of screw assembly (e)

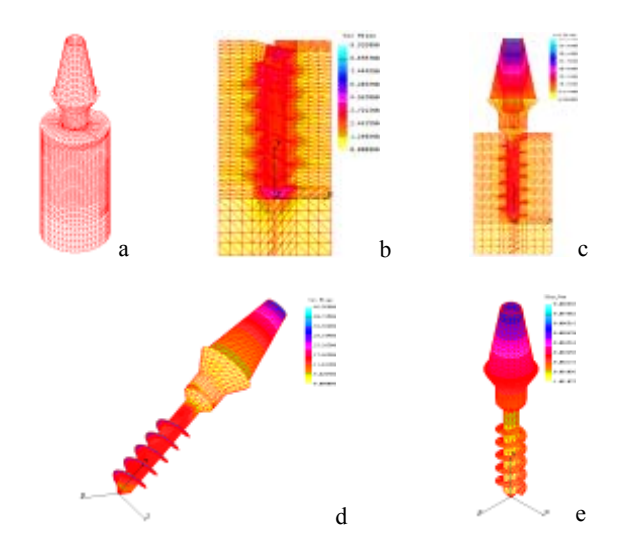


Fig. 2: The model (a) analyzed with temperature. The tension on the mandible bone(b), mandible bone – implant (c) and screw assembly (d) at 70°C and displacement of screw assembly (e)

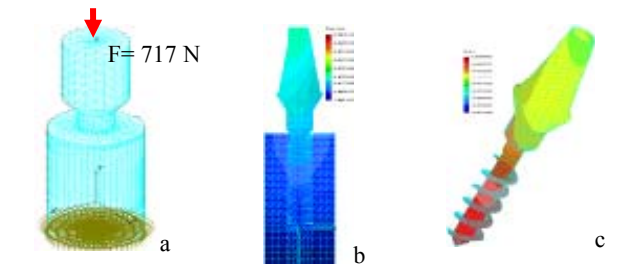


Fig. 3: Load and constrains of the model(a)
Displacements on the mandible bone – implant (b)
and screw assembly (c)

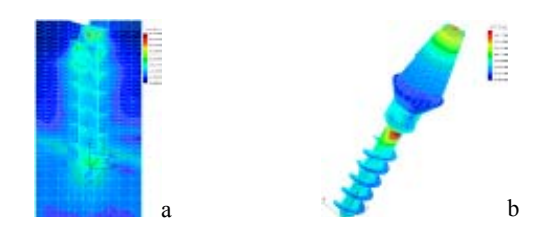


Fig. 3: Von Mises equivalent stress in bone(a) and screw assembly(b)

REFERENCES: ¹Ş. Sorohan, I.N. Constantinescu (2003), *Practica modelării şi analiza cu element finit*, Editura POLITEHNICA Press, Bucureşti, ²***. USER GUIDE, COSMOS/M, ³D. Slăvescu, D.D. Slăvescu, V. Rogojinaru (2006), *Implant dentar tip şurub, metodă de implantare şi trusă instrumentar*, Romanian Patent no 120379B1, ⁴C.E. Misch (2005), *Dental Implant Prosthetics*. ELSEVIER MOSBY.

Measuring Dynamic Stiffness of Human Teeth by Single-Impact Micro-Indentation (SIMI): a feasibility study

W. Baschong¹, F. Schmidli², M. Imholz¹, B. Goepfert³, A.U. Daniels³, D. Wirz³

¹Klinik für zahnärztliche Chirurgie und ²Institut für Werkstoffkunde, Universitätskliniken für Zahnmedizin. ³Labor für orthopädische Biomechanik am Universitätsspital.Universität Basel, Basel, Switzerland.

INTRODUCTION: Teeth must bear a wide range of loads and retain their shapes during contactinduced static and dynamic stresses. In vivo, the critical contact area between opposing teeth ranges from $0.4 - 2.2 \text{ mm}^2$ with a maximal biting force of up to ~1000 N, i.e. conditions inducing contact stresses of 0.45 - 2.5 GPa [1] which can precipitate damage. Since damaged teeth do not heal like other mineralized tissue, functional integrity is restored by repairing lesions with xenobiotic materials such as gold, alloys (e.g. Ni-Cr-Mo alloy Remanium CS[®]), amalgam or polymer-ceramic composites (e.g. Filtek® Supreme). Material determines load distribution. Quasi-static stiffness (elastic Young's modulus E_Y) is the parameter usually reported in order to describe stiffness of mineralized tooth constituents (cementum, dentin, enamel) as well as dental repair materials. However, tissues and materials containing polymeric components and water are viscoelastic and have no elastic Young's modulus. Their stiffness depends on the conditions measurement; especially loading rate. Therefore, to better emulate functional dental conditions, we measured stiffness in a non-destructive, dynamic impact mode. We used a Single-Impact Micro-Indentation (SIMI) instrument, developed from a handheld computer-assisted device for polymer quality control [2] and used by some of the authors to evaluate cartilage [3]. The response of viscoelastic materials to a non-destructive impact is characterised by the complex dynamic Young's modulus or aggregate modulus, E*, and its components--the storage modulus E' and the loss modulus E''. The latter two are usually expressed as the loss angle ϕ =arctan(E'/E''). The loss angle describes the damping behaviour of viscoelastic structures.

METHODS: The SIMI device [3] with a 1 mm \emptyset spherical steel tip was further equipped with a sliding cross table and laser for positioning the indenter with sub-millimeter precision. 3^{rd} molars were embedded in PMMA, then cut longitudinally in 2-3 mm thick sections and ground parallel. Sections were placed on a stainless steel block and stabilized laterally by enclosing them with wax. E* and ϕ average values (n = 10) were obtained.

RESULTS: See Table 1.

Table 1: E^* and loss angle ϕ (brackets) of dental structures and repair materials by SIMI.

| Results [GPa, °] | Root dentin | Crown dentin | Enamel | Filtek® | Remanium® |
|---------------------|----------------|----------------------|-----------|---------------------|-----------|
| Tooth 1 | 0.0025± | 4.3±0.4 | 3.5±5 | | |
| | 0.003 | (19±0.7°) | (20±2°) | | |
| | (19±3°) | | | | |
| Tooth 2 | | 7±0.1 | 8.5±30.2 | | |
| | | $(18\pm0.7^{\circ})$ | (17±0.8°) | | |
| Repair | | | | 4.2±0.1 | 56.5±15 |
| material | | | | $(12.\pm4^{\circ})$ | 7.2±0.1° |

DISCUSSION & CONCLUSIONS: In this first set of measurements on sectioned teeth, SIMI modulus (E*) data were not strictly analogous to reported E_Y values [1]. However, micro-dynamic and quasi-static nano-indentation data rarely agree. Factors contributing to observed discrepancies: (i) Viscoelastic material moduli are highly dependent on loading geometry and rates. (ii) Most reported E_v values are based on micro- or nano-indentation which employs much higher stresses than SIMI. (iii) The contact surface of SIMI is > 1000x larger than that of nano-indenters. For enamel's anisotropic structures, measured stiffness is inversely related to indenter size [1]. (iv) The indenter tip used was steel (E~200 GPa) which may deform when used on materials approaching this stiffness. SIMI is a simple method for quantitative functional characterisation of load-bearing tissues. To our knowledge SIMI provided here, for teeth, the first combined measurements of E* and ϕ . In the future, measurement of site-specific variations in dynamic impact stiffness (E* and \$\phi\$) may better describe how dental structures distribute and absorb impact This may substantially improve our understanding of tooth function and the structural changes caused by disease.

REFERENCES: ¹L.H. He & M.V. Swain (2008) *J. Mech Behavior Biomed Mater* **1**: 18-29. ²M. Vriend & A.P. Kren (2004) Polymer Testing **23**: 369-375. ³D. Wirz, et al. (2008) Abstract, *Proceedings 16th Congress Eur Soc Biomech*.

ACKNOWLEDGEMENTS: We thank A. Filippi, G. Krastl, J.T. Lambrecht and B. Müller (University Clinics for Dentistry, Basel) for their encouragement and suggestions.

Controlled Surface Functionalisation of Orthopaedic Titanium Implants: In-vitro Osteogenic Bioactivity.

Malak Bitar, 1 Philipp Imprund², Astrid Rota², Stefanie Lischer¹, and Arie Bruinink 1

¹EMPA Materials Science & Technology, Lerchenfeldstrasse 5, 9014 St. Gallen Switzerland

²Fraunhofer Institute for Manufacturing and Advanced Materials (IFAM), Wiener Str. 12, 28359 Bremen,

Germany

INTRODUCTION: Controlled surface topography may induce favourable cell reactions upon implantation and, at a later stage, increase bone-implant contact (BIC) thus leading to greater stability¹. The latter is especially important in areas of low bone density. Variations of surface topography produced using the current methods produce extremely randomised surface patterns in terms of shape, spacing and distribution. This may negate potentially controllable, reproducible and possibly predictable post-implantation responses of cells contacting the implant surface.

We report on the in-vitro bioactivity of surface topography produced using a novel patented method for orthopaedic implant structuring. This method produces micro-nano surface patterns in an easy to apply, industrial scale, setting.

METHODS: Sample preparation Samples were produced from grade 316L stainless steel alloy. The patterned surface consisted of 50 and 30 μm diameter hemispheres and 20 μm distance between adjacent hemisphere circumferences (samples codes 50_20 and 30_20).

Cell culture Human bone marrow stromal cells (HBMC's) cultivated in α-MEM (Invitrogen, supplemented 10% FCS, 1% PSN , 50 μM Ascorbate-2-phosphate, 10 nM Dexametasone, 2 mM β-Glycero phosphate and 50 μM Vitamin D3. Cultures were maintained in a humidified atmosphere, at 37° C and 5% CO2. Cells were seeded at $\sim 2.5 \times 10^3$ cells/ cm².

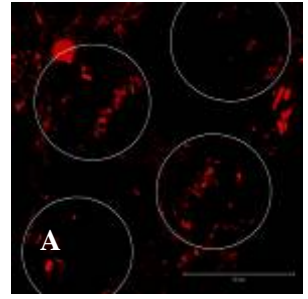
Immunocytochemistry At various time points, the cell actin microfilaments labelled using Phalloidin (Alexa Fluor 488, 1:40, Invitrogen). Cells were also labelled using α -vinculin mouse monoclonal IgG (clone HVIN-1, 1:300, Sigma) followed by secondary goat α -mouse IgG (Alexa Fluor 546, 1:100, Molecular Probes).

Polymerase chain reaction At day 14 in culture, cells were lysed and total RNA purified using Quiagen RNeasy kit (Quiagen). The RNA was reverse transcribed into cDNA using iScript cDNA Synthesis kit (BioRad) and osteoblastic gene regulation was assessed using a BioRad iCycler.

RESULTS: The cell-substrate interaction was mediated by the formation and clustering of thick patches of focal adhesions related to the

hemisphere structure (Figure 1A). This particular pattern was not seen on non-structured controls surfaces. The seeded cells also exhibited morphology associated with 3 dimensional matrices (Figure 1B).

PCR experiments revealed an enhanced osteogenic differentiation in cells seeded on the structured surfaces compared to cell culture control surfaces (results not shown). The genes (ALP, Osteocalcin) investigated are directly related to formation and maintenance of a mineralised bone matrix.



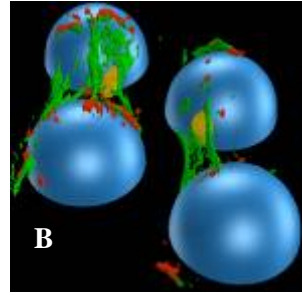


Fig1. Confocal laser microscope images of HBMC cells seeded on 50_20 structured 316L surfaces at day 7 in-culture. The labelled cellular components are actin (green), vinculin (red) and nuclei (yellow). A: Focal adhesion formation and an outline of the hemisphere bases. B: 3D reconstruction of confocal laser microscope image stack showing cells attaching to the hemispheres.

DISCUSSION & CONCLUSIONS: Defined, positive hemispheric, exhibited significant bioactive properties in influencing osteogenic differentiation. Further studies are currently underway to investigate cell migration, proliferation and expression of phenotype as a function of this particular surface topography.

REFERENCES: ¹ A. Bruinink, J.P. Kaiser, C. Meyer (2005) *Adv Eng Mater.* **7**, 411-8. ,.

ACKNOWLEDGEMENTS: This study was supported by the VW-Foundation grant I/82 297.

Modification of PMMA using NMP in a stiffness-adapted bone cement for vertebroplasty

A.Boger, K.Wheeler, A.Montali, E. Gruskin

Synthes Inc., R&D Biomaterials, Oberdorf, Switzerland

INTRODUCTION: Percutaneous Vertebroplasty with polymethylmethacrylate (PMMA) achieves effective pain relief in 80% to 90% of cases. Because of PMMA's high stiffness, an increased fracture risk has been found for the adjacent vertebral bodies [1]. It seems reasonable to assume that the optimal stiffness of a cement is close to native cancellous bone (100-700 MPa). Using an additive which acts as a plasticizer on the PMMA may decrease stiffness. 1-methyl-2pyrrolidone (NMP) is an organic solvent which is miscible with the liquid component of PMMA. NMP's miscibility with water allows for a full exchange of NMP with body fluids after implantation. NMP has previously shown to have potentially favourable properties on bone growth [2]. A new cement design must also take viscosity [3] into account. The goals of this study were to determine the mechanical properties of the new PMMA as a function measure the viscosity during hardening.

METHODS: The modification of the PMMA cement to less stiff material was performed by partly substituting the fluid MMA by NMP (Fluka AG, Switzerland). Cement preparation was done by manual mixing. 21 g of PMMA powder were mixed with 10 ml of liquid component. The liquid component consisted of 100% MMA in the control group and of 80%, 70%, 50% and 40% MMA with the rest substituted by NMP in the test groups. Cement samples were produced according to ISO 5833. For each material composition, 24 samples were produced for the mechanical investigations. Materials were hardened in the mould for 2 h and removed. Subsequently, the samples were stored in PBS at 37±1°C for 48 h. Young's modulus and yield strength were then measured on all samples.

Mechanical testing was carried out in compression by means of a 10kN load cell and a crosshead speed of 5mm/min. The determination of the Young's modulus and yield strength was made according to ISO 5833. The viscosity of the cement during hardening was measured using a rheometer (Rheolab QC, Anton Paar, Austria) equipped with a double gap measurement system. Viscosity measurement as well as cement preparation was conducted at 22 ± 2 °C.

RESULTS: Measurements of the viscosity vs. time showed that NMP leads to a substantial reduction of the speed of the curing reaction. The time needed to reach a viscosity of 1100 Pas is approximately doubled when 60% of the MMA are substituted by NMP.

Characterization of the stiffness and yield strength of the material with and without substitution of MMA by NMP give further insight into possible effects of the NMP on the material. Both the stiffness and the yield strength are reduced by the addition of NMP. Young's modulus ranged from 2.3 ± 0.023 GPa to 320 ± 29 MPa and yield strength from 78 ± 0.8 MPa to 24 ± 4 MPa, when the amount of NMP was increased from 0 to 60%.

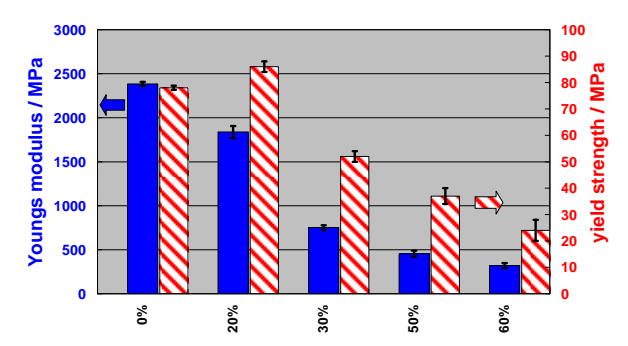


Fig. 2: Young's modulus and yield strength of NMP-modified PMMA cement.

DISCUSSION & CONCLUSIONS: Adjustment of the mechanical properties of PMMA is expected to reduce the fracture risk of adjacent vertebral bodies. This study shows that adding NMP to regular PMMA bone cement provides a possible solution: substitution of around 40% of the MMA content by NMP was able to yield a cement stiffness comparable to that of cancellous bone. The viscosity measurements showed a reduced speed in the curing reaction. This is an advantage in that it gives a clinician more time for injecting the cement, as opposed to the standard cement formulation without NMP. The fatigue properties will be analyzed in the future.

REFERENCES: ¹ F. Grados F et.al. (2000) *Rheumatology (Oxford)*, 39:1410-1414. ² FE. Weber FE et.al. (2006) *Proceeding, AO Biotechnology Symposium (Lausanne)*, p. 37. ³ G. Baroud G et. al,(2003) *Medical Engineering & Physics* 25(4), 283-288.

ACKNOWLEDGEMENTS: Authors thank aap Biomaterials, Germany, for valuable discussions and input.

Finite Element Analysis for Stress Distribution in Welded Zones Used In RPD Technology

C.Bortun¹, N. Faur², A. Cernescu³, S. Porojan⁴, O. Gombos⁵, L. Sandu⁶, B. Ghiban⁷

^{1,4,5,6} "Victor Babes" University of Medicine and Pharmacy Timisoara, Romania; ^{2,3} Polytechnic University Timisoara, Romania, ⁷ Polytechnic University Bucuresti, Romania.

INTRODUCTION: By applying finite element analysis we can make experiments regarding the efficiency of welded joints, used for the repair of removable partial dentures components.

METHODS: For testing it was used "C" alloy, (Vaskut Kohàszati Kft–, Hungary), which has the following chemical composition: Co-85%, Cr-29%, Mo-5% and mechanic parameters: R_m=760MPa, R_{p0,2}=560MPa, E=219000MPa. XXS Laser (Orotig, Italy) welding equipment was used. The welding method was in butt joint configuration with filling material on two surfaces (fig.1).





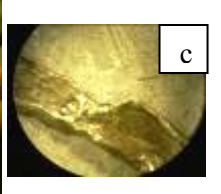


Fig. 1: Welding in Dental laboratory: a. Welding equipment; b. welding a removable partial denture major connector; c. welded area aspect.

It was used a geometrical three-dimensional cast, which was meshed into solid elements (65960 elements, 294623 junctions), using Solid Works 2007 program. The analysis consists of tension state simulation evaluation for a welding procedure, applied to "C" alloy parameters. There was made a static analysis of tension state (resulted after welding) regarding temperature and heat flux distribution. The thermal parameters used for estimation were: coefficient of linear expansion- β =3,36·10⁵ W/mm².°C, coefficient of heat conductivity- λ =6,05·10⁻²W/mm·°C; Specific heat—C=434 J/Kg·°C.

RESULTS: Figure 2 presents the meshed geometrical model and the welding afferent to stress areas.



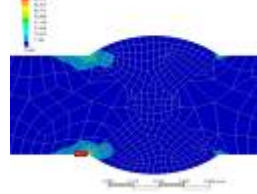


Fig. 2: Welding with filling material on two surfaces: a. meshed geometrical model, b. stress areas, pointed out through numerical analysis.

The results of the analysis consist in temperature distribution on a period of 1-5s (a,b), total heat flux distribution of the fusion zones (c,d) and equivalent tension at 1s (e) and 5s (f) after application of welding arch.

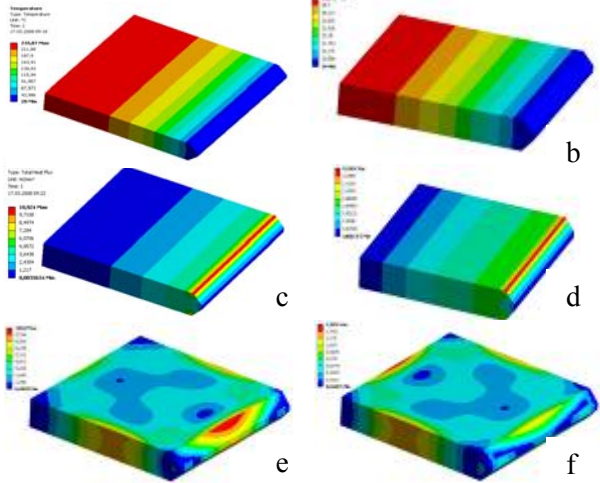


Fig. 3: a,b. Temperature fields for 1-5 s; c,d. Total heat flux distribution for 1s and 5s.; e,f. Equivalent von-Misses stress distribution for 1s and 5s.

DISCUSSIONS & CONCLUSIONS: The welded area has the peak tensile residual stresses longitudinal to weld direction and perpendicularly to welding arch. Study results reveal that around the fusion zone there is a stress gradient and this is the one that forms cracks in the fusion zone in steel [1,2]. Welding is a useful method in metallic prostheses repairs, and the decrease of alloys hardness in the welded zone is a priority. So, it is important to control welding heat input, in order to reduce welding stress and avoid cracks.

REFERENCES: ¹ Li. Yajiang, Wang Juan, Chen Maoai, Shen Xiaoqin (2004), *Finite element analysis of residual stress in the welded zone of a high strength steel.* Bull. Mater. Sci., Vol. 27, No. 2, pp. 127–132. ² J.D.Francis (2002), *Welding Simulations of Aluminum Alloy Joints by Finite Element Analysis*, Thesis-Faculty of the Virginia Polytechnic Institute and State University.

ACKNOWLEDGEMENTS: This study was supported by CNCSIS grant type A, no 744 from the Ministry of Education and Research of Romania.

Contamination of bonding sites and its influence on conventional etching and conditioning with a self-etching primer. An in vitro study.

L. Brauchli, M. Eichenberger, A. Wichelhaus

Clinic for Orthodontics and Pedodontic Dentistry, University of Basel, Switzerland.

INTRODUCTION: Adhesive technologies in orthodontics have rapidly developed over the last decades. However, contamination of the bonding site with blood or saliva still leads to a drastical decline in bond strength, and thus to bracket failure in the orthodontic patient¹⁻³. It was the aim of this study to evaluate the influence of contamination on bond strengths and to investigate possible decontamination procedures.

METHODS: Four different bonding systems were evaluated for their shear bond strengths under five different bonding situations: control (without contamination and decontamination), contamination with blood/saliva, decontamination with water, air and repriming following the above mentioned contaminations. The 25 specimens of each group consisted of composite blocks bonded to bovine teeth. Shear forces were measured with an Instron 4444 after thermo-cycling.

RESULTS: The 3 composite primers showed a similar behaviour. With the exception of Transbond SEP with saliva contamination, all contaminations resulted in strongly reduced shear forces. The controls as well as the decontaminated groups showed shear forces of around 20 MPa. The resin modified glass ionomer however did not reach clinically sufficient bond strengths in either setup.

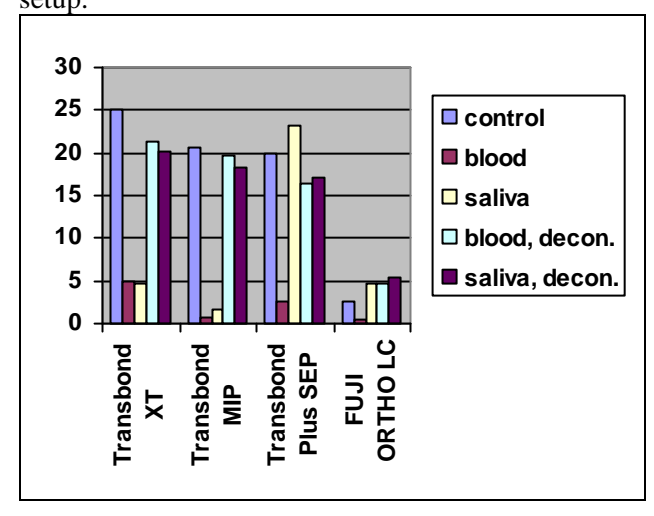


Fig. 1: Diagram showing mean shear force values (MPa) for five different bonding situations: control, contamination with blood or saliva, decontamination after contamination with blood or saliva.

DISCUSSION & CONCLUSIONS: The present investigation showed that a decontamination procedure consisting of thorough rinsing with water, drying with air and repriming can successfully be administered to surfaces contaminated with blood or saliva after priming. A contamination with blood without decontamination however results in strongly reduced bond strengths for all tested adhesives. Interestingly the selfetching primer Transbond SEP was not affected by a saliva contamination, whereas the other groups all showed strongly reduced bond strengths. The clinical management of contaminated bonding surfaces can be recommended as follows: renewed etching is not necessary. A simple decontamination with water, air and repriming gives sufficient bond strength for all tested adhesives. In the case of Transbond SEP and saliva contamination even repriming only leads to adequate adhesion.

REFERENCES: ¹V. Cacciafesta, MF. Sfondrini, A. Scribante, et al. (2004) *Am J Orthod Dentofacial Orthop* **126**: 207-12. ²MJ Webster, RS Nanda, MG Duncanson, et al. (2001) *Am J Orthod Dentofacial Orthop* **119**: 54-8. ³SE Bishara, C Oonsombat, R Ajlouni, G Denehy (2002) *Angle Orthod* **72**: 554-7.

ACKNOWLEDGEMENTS: We would like to thank those manufacturers who supplied materials for this study.

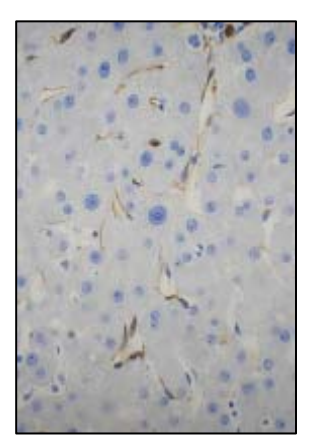
The intermediate filament Nestin is not a specific marker for proliferating endothelium – its expression *in situ* and *in vitro*

C. Brochhausen, C. B. Wiedenroth, V. H. Schmitt, S. Halstenberg, C. J. Kirkpatrick REPAIR-lab, Institute of Pathology, Johannes Gutenberg-University, Mainz, Germany

INTRODUCTION: For several Tissue Engineering strategies the determination proliferating endothelial cells is of special interest. In this context, the intermediate filament nestin is expressed by endothelial cells (ECs) regenerative tissues and malignant tumours. It is widely believed that nestin is a marker for proliferative endothelium only. In the present study, we documented the in situ expression of nestin in the endothelium of the human cardiovascular tree as well as in human haemangiomata and human lymphangiomata. Furthermore, we investigated the in vitro expression of nestin by cultured ECs of different origin.

METHODS: Human aorta (n=5), vena cava (n=5), arteria et vena renalis (n=5), capillaries in liver and lung (n=5),haemangiomata (n=5)lymphangiomata (n=5)were analyzed immunohistochemically using the peroxidase method. We used the panendothelial marker CD31 and the lymphatic marker D2-40. Nestin was detected with a monoclonal antibody. Proliferating cells were visualized using antibodies against Ki67. For in vitro analyses, we cultured human umbilical vein ECs (HUVECs), human pulmonary microvascular **ECs** (HPMECs), immortalized HPMEC cell line (HPMEC-ST1). In subconfluent and confluent populations the cells analyzed by immunofluorescence expression of CD31 and nestin.

RESULTS: In all specimens of aorta, vena cava, arteria et vena renalis, the capillaries of liver and lung ECs were positive for nestin. *In situ* all EC reacted negatively with antibodies against Ki67. All haemangiomata were strongly positive for nestin and negative for D2-40. In contrast, the endothelium of the lymphangiomata showed a homogeneous expression of D2-40 and showed no reaction with monoclonal anti-nestin antibodies. In vitro, HUVEC, HPMEC and HPMEC-ST.1 showed no expression of CD31 in subconfluent cultures. When confluent, strong CD31 expression could be demonstrated at the intercellular contacts. In the subconfluent as well as in the confluent status, cultured ECs expressed nestin.



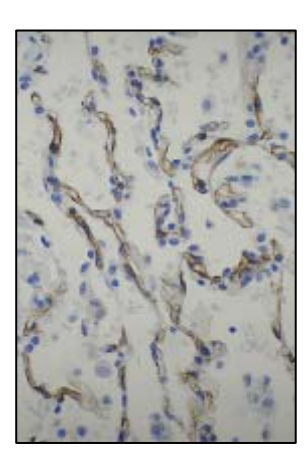


Figure 1, 2: Nestin expression in human liver (left) and lung capillaries (right).

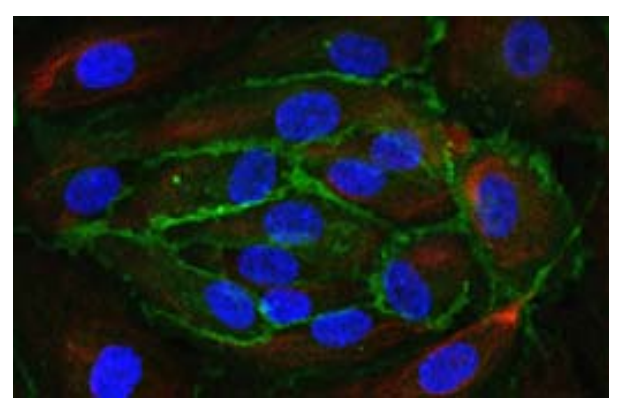


Figure 3: Nestin expression (red) in a confluent HUVEC monolayer with CD31 (green) and Hoechst (blue).

DISCUSSION & CONCLUSIONS: Nestin is expressed in endothelial cells of arteries, veins and capillaries within the cardio-vascular tree as well as in confluent EC cultures of different tissue origins. The differential expression of nestin in haemangiomata and lymphangiomata indicates the specifity of nestin for the endothelium of blood vessels. Our findings contradict the current view, which defines nestin as a marker for proliferative endothelium. In conclusion, nestin is not a specific marker proliferating endothelial Therefore, it appears that widely held beliefs about the functional role of nestin in ECs have to be reevaluated and re-defined in further studies.

Remesothelialization of a polylactide-based membrane for the prevention of peritoneal adhesions

C. Brochhausen¹, V. H. Schmitt¹, C. B. Wiedenroth¹, B. Krämer², T. K. Rajab², M. Wallwiener², C. Wallwiener², D. Wallwiener², H. Planck³, C. J. Kirkpatrick¹

¹REPAIR-Lab, Institute of Pathology, Johannes Gutenberg University, Mainz, Germany ² Department of Gynaecology and Obstetrics, University Tuebingen, Germany ³ITV Centre of Excellence on Biomaterials and Organ Replacement, Denkendorf, Germany

INTRODUCTION: Intraperitoneal adhesions represent a major problem after abdominal surgery and intraabdominal inflammation with relevant clinical complications such as bowel or vessel obstruction respectively. Therefore, great efforts are being made to understand the pathogenesis of adhesion formation and strategies for its prevention. In the peritoneal cavity mesothelial cells play a crucial role in prevention of adhesion formation, due to the maintenance of a smooth and gliding surface. Any damage to the mesothelial cell layer leads to fibrin exudation, micro-bleeding and adhesion formation. To prevent these processes several barriers have been developed. SupraSeal® is a synthetic Lactide-caprolactone-trimethylenecarbonate copolymer (Fig 1a, fig. 2a).

METHODS: Female, virgin Wistar rats with a weight range of 220–280 g were treated with a polylactide-based membrane (SupraSeal®) after bipolar electrocoagulation and induced ischemia (1). After 14 days the experiments were terminated and the peritoneal wall with the barrier-membrane including surrounding peritoneum was explanted. The barrier material and the interface with intact peritoneum were analysed histomorphologically by standard histological methods and SEM.

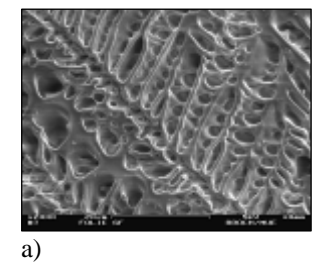
RESULTS: Immediately after implantation the experimental defect was completely covered by the membrane (fig.1a). 14 days after implantation at the second look SupraSeal® was still attached on the side of the peritoneal defect with marked shrinking and folding (fig 1b). Focally at the suture site minor smooth adhesive strands could be observed.

Histologically, a minor inflammatory reaction with multinucleated giant cells could occasionally be observed. The surface of the barrier material was completely covered by a single layer of almost flat mesothelial cells, which only rarely showed minimal activation (Fig 2b). The mesothelial cells in the surrounding tissue were typically flat without any signs of activation.





a) b)
Figure 1: SupraSeal® in native form (a)
immediately after implantation and (b) after 14
days implantation in the rat model.



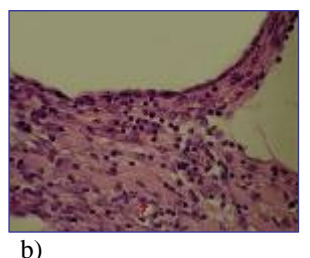


Figure 2: SupraSeal® in native form (SEM x1000) (a). Defect covered by SupraSeal® with a complete monolayer of flat mesothelial cells at the surface of the barrier material (HE x100).

DISCUSSION & **CONCLUSIONS:** In SupraSeal® conclusion, revealed good antiadhesive effects. The fact of a rapid remesothelialization within 14 days and the minor inflammatory reaction implies good biocompatibility of this material in application. The minor adhesions found in these first results had close contact to the suture material, which indicates the relevance of the suture or the suture material for the adhesion formation.

REFERENCES:

1. Wallwiener et al. (2006) Fertil Steril 86:1266-1276

Multidye coculture methodology to study fibroblast-osteoblast interactions

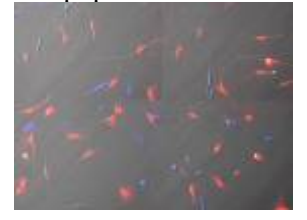
E.F. Burguera, J.P. Kaiser, M. Bitar, S. Lischer, A. Bruinink

MaTisMed, Materials-Biology Interactions Lab EMPA – Swiss Laboratory of Material Testing and Research, St Gallen, Switzerland

INTRODUCTION: Current bone related implant surfaces are optimized empirically with respect to their *in vivo* performance. The performance of such implants is defined by the velocity and degree of osteointegration and their long-term performance. Integration of an implant depends on: 1) attraction, 2)proliferation of the appropriate cells and , 3) their differentiation the into bone forming osteoblast cells. Current in vitro work to describe cell reactions in order to optimise implant surfaces is performed using one cell type. However, at the implant surface a variety of cell types are in competition with the capability to contact and colonize the implant surface, the most important of which are fibroblasts and cells of the osteoblast lineage. Furthermore, each of these cell types mutually affects the state of differentiation and functionality of the other cell types and these interactions play a defining role in the fate of the implant [1]. The aim of the present study is to establish a methodology to describe and monitor interactions between fibroblasts osteoblastic cells in coculture.

METHODS: Primary human fibroblasts (NHDF) were purchased from Cambrex and primary adult human bone cells (HBC) were obtained by cultivating spongiosa bone pieces from patients receiving hip prosthesis after washing under microscopic observation in culture flasks in proliferation medium. Cells growing out of the bone pieces were defined as HBC. Only HBC cells of the first passage were used for the experiments. To distinguish the two types, cells were labeled prior to seeding. NHDF fibroblasts were vitally labeled with VybrantTM DiD solution at 16 µl/ml and the HBC were vitally labeled with VybrantTM DiI solution at 16 µl/ml [2]. In addition, in order to recognize single cells both cell types were treated with DAPI (Sigma Aldrich) for visualization. Petri dishes (3.5 mm) inoculated with 2 ml of modified aMEM (10% foetal calf serum, 1% penicillin/streptomycin, 50 ascorbic acid phosphate, 2 mM βand glycerophosphate 10nM dihydroxyvitamine D3) containing NHDF and HBC. Cell clustering and proliferation were monitored with fluorescence microscopy at days 1, 4 and 7. Two different locations were scanned for each well and three wells were seeded for time point. Controls were used containing only fibroblasts or osteoblasts. After 7 days of coculture, cells were fixed with 2% paraformaldehyde containing 0.3% Tween 20 and immunostained for alkaline phosphatase.

RESULTS & DISCUSSION: A multidye coculture system was developed that allowed monitoring of individual cells over time. Membrane-bound dyes DiI and DiD permitted identification of fibroblasts and bone cells (Figure 1A). In addition all cells were stained with DAPI at day 4. With this dye combination we could account for all the cells and to assign them to one of the two populations at all times.



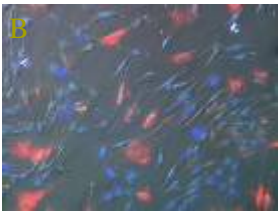


Fig. 1: Fluorescence image of NHDF fibroblast (DiD stained, blue) and human bone cells (DiI, red) after (A) 1 day and (B) 4 days in coculture.

The developed methodology is being used in ongoing experiments to investigate the cell-cell interactions of fibroblasts and human bone cells and how both cell types affect the proliferation and differentiation of the other.

REFERENCES: ¹B. Ogiso, F.J. Hughes, A.H. Melcher et al (1991) *J Cell Physiol* **146**:442-50. ²J.P. Kaiser and A. Bruinink (2004) *J Mater Sci: Mater Med* **15**:429-35.

ACKNOWLEDGEMENTS: EF Burguera gratefully acknowledges financial support through a postdoctoral fellowship from the Spanish Ministerio de Educación y Ciencia. We thank Prof. M. Kuster of the KSSG for providing us with human tissue samples.

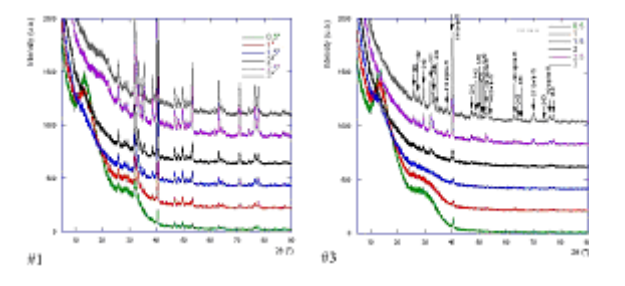
Bioceramic Coatings Obtained by Physical and Chemical Techniques

S. Ciuca¹, G. Cosmeleata¹, R. Borsa¹, M.Tarcolea¹, F. Miculescu¹, B. Ghiban¹, Adele Carrado², Eniko Gyorgy³, I.N. Mihailescu³

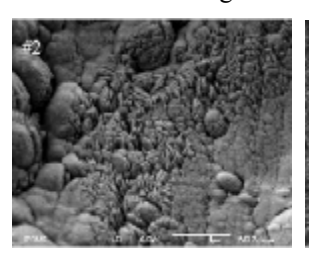
¹ University POLITEHNICA of Bucharest, ² IPCMS Strasbourg, ³ INFLPR Bucuresti

INTRODUCTION: Hydroxyapatite-based $Ca_{10}(PO_4)_6(OH)_2$ are largely biocompatible coatings on metallic components of prostheses for inducing osteoblasts apposition and subsequent re-growth. Nevertheless, the ceramics-metal interfaces are often the seat of residual stresses with amplitude primarily depending on the deposition technique and the coating conditions. HA layers are grown by pulsed laser deposition on either chemicallyetched or mechanically-polished G4 titanium samples. Usually the layers are deposited in the presence of water vapours or in oxygen with partial pressures of several tens of Pa. In our first investigations, depositions were carried out in a vacuum of about 10⁻⁴ Pa in order to preserve the memory of the physicochemical state of the expelled material from the target under the laser beam impact. Thin films of HA were also produced by spincoating sol-gel solution on chemically-etched Ti substrate. Calcium nitrate and triethyl phosphite were then used as precursors. We investigated the morphology, the structure and the composition of the deposited material by various techniques.

METHODS: All depositions have been performed with UV pulses generated by a KrF* laser source (λ = 248 nm and τ = 7 ns), following the PLD technique. After deposition, the samples were allowed to cool down to ambient temperature inside the irradiation chamber. Some of the samples were heat treated at 400°C for 6 hours in an atmosphere enriched in water vapours in order to improve the HA crystallinity status and to restore the loss of OH groups from the HA molecule. These samples are further noted #1 and #2. The obtained sol-gel (#3) was spin-coated onto a chemically-etched Ti disk at a speed of 2000 rpm for 5 s in ambient atmosphere. The films were dried at 80°C for 30 min. Five consecutive depositions were performed according to this protocol prior to a final heat treatment to 500°C for 30 min in air.



RESULTS: Coatings have been analyzed using grazing incidence X-ray diffraction in order to get in-depth phase distribution. Depth penetration of Cu-K_{α} X-ray depends on the incidence angle chosen between 0.5° and 3° .



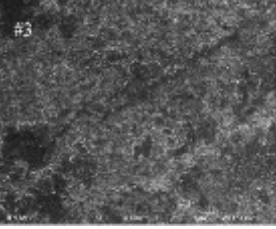


Fig. 2. SEM image of sample #1 and #3

DISCUSSION & CONCLUSIONS: PLD films exhibit irregular morphology: it presents nanometric aggregates of different sizes (< 100 nm) and crystalline orientations, as well as droplets of different micrometer sizes (0.1-3 µm). Such particulates have been previously observed on the surface and in the bulk of HA PLD films. The HA films of the sol-gel sample shows a porous and coral-like structure. PLD coatings present nanometric particles and micrometric droplets. Post treatment in water vapour involves a recrystallization of the HA coating. The sample elaborated by sol-gel process shows a porous and coral-like structure. In both cases, the HA layers are well crystallised but the PLD deposited HA layer is expected to be more susceptible to the natural remodelling processes when it is implanted in a living body due to its better adhesion on titanium.

REFERENCES: ¹M.Iliescu, V.Nelea, J.Werck-mann, I.N. Mihailescu (2004) *Surf. Coat. Technol. 187*, pp 131-140, ²H-W. Kim, J.C. Knowles, V. Salih, H-E. Kim (2004) *J. of Biom., Mater. Research Part B: Applied Biomaterials*, 71B, pp 66 - 76.

Fig. 1: X-ray diffraction phase analyses for samples #1 and #3

Microstructural and cytotoxicity evaluation for different surface treatments of TA6V4 alloy

A.Colceriu¹, C.Fratila², I.Roman³, M.Moldovan¹, M.Trif¹, C.Prejmerean¹, C.Tamas¹

Babes - Bolyai University, Raluca Ripan Chemistry Research Institute, Cluj-Napoca, Romania

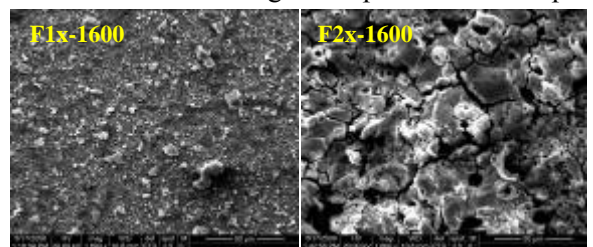
²R&D Institute for Nonferrous and Rare Metals, Bucharest, Romania

³ METAV Research and Development, Bucharest, Romania

INTRODUCTION: Titanium, the currently material used for dental implants manufacturing presents proper osteointegration characteristics, but from physological point of wiev is practical bioinert. Today, there are a permanent preocupation for improving the osteointegration characteristics of the dental implantable devices. The biomaterial surface is the only face which is in directly contact with the biological medium, so that it play a decisive role in the biological interactions. The performed researches showed that the preparation methods of the implants surface is able to have significaly impinge upon the resulting properties of the surfaces and implicitly the biological responses which take place on the surface. In this study it was evaluated the microstructure and the cytotoxicity of the titanium alloys with different surface treatments.

METHODS: The oxide layers on experimental alloy samples TA6V4 (F1, F2, AF4, AF5 and TEG) were realized at normal temperature by electrochemical proceedings and specific thermal treatments. The preparation of the surfaces was realized by abrasive cleaning (sandblast) with Al₂O₃ 240μ; polishing with metallographic paper 150-400 followed by degreasing and washing; warm air dries and acid pickling HF (6%)+HNO₃ (26%). For all samples, the oxide layer was deposing by anodization in different conditions; for F1 and F2 samples were applied a thermal treatment at 700°C, 60°. The structural and morphological aspects of superficial layers of titanium alloy were investigated through optical microscopy in polarized light (Axio Imager A1m, Carl Zeiss) and SEM (FEI system). The cytotoxicity test, according to ISO 10993 standards, was effectuated after the electrochemical deposition samples, in vitro, on fibroblast culture. The samples used for cytotoxicity test (2x2x8 mm) were sterilized by UV radiation exposed and put directly in contact with normal human fibroblasts, in culture medium for 72 hours. The adherent cells on the surface of culture were count, used a Neubauer counted camera. The viability was appreciated using trepan blue coloration.

RESULTS: The accomplished surface treatments have lead to the obtaining of the titanium oxide layers with different morphology. Certain electrochemical treatments assure the obtaining of some proper microstructure for penetration and attachment of the biological cells to the implant surface in the biointegration process. The aspects



of the obtained samples are showed in below figures.

The SEM micrographs of the studied implantable systems was compared with the images obtained in polarized light using an optically microscope. It was determinates thickness of oxide layers greater than 1μ . For the TEG sample, the TiO_2 thickness was about 22,5 μ . The cytotoxicity test results, respectively the values obtained for the human fibroblasts viability in 24 hours and 48 hours are showed in figure 1.

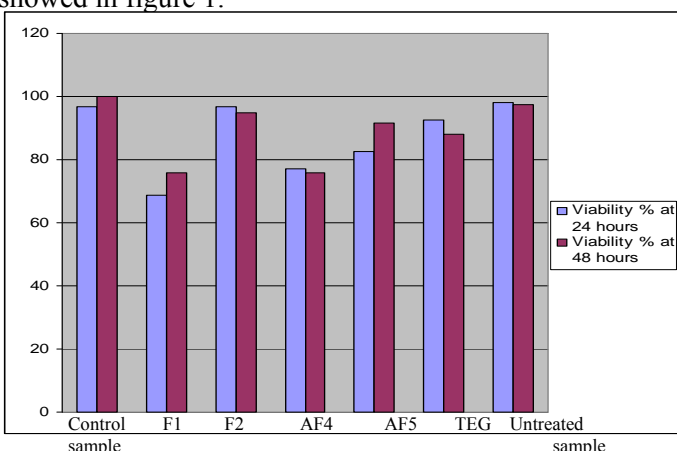


Figure 1.The human fibroblasts viability after 24 hours and 48 hours

DISCUSSION&CONCLUSIONS: microstructure analysis through SEM and microanalysis proved the presence of a compact, uniform and adherent layer of titanium oxide, with lower conductivity properties from electrical point of wiev. The oxide layer has a scaliness aspect, in our opinion, that thing contribute at the better tissue grown on the implant and anchorage of them. We established methods for treatment of implant surfaces TA6V4 to improve the biocorrosion strength, to create diffusion barrier to obstruct the release of the toxic ion in organism and to favor the growing and interaction between bone tissues and implant alloy.

REFERENCES: ¹F.J.Gil, E.Solano, J.Pena, E.Engel, A.Mendoza, (2004), *Journal of Materials Science: Materials in Medicine* 15:1181–1185; ²C.Libenson, F.J.Gil, J.A.Planell, (1993) *J. Mater. Sci: Mim.* 9:281; ³F.J.Gil, E.Fernandez, J.M.Manero, et all, (1996), *Biomed. Mat. and Eng.* 6(3) 153

ACKNOWLEDGEMENTS: This work has been supported by the Romanian Ministry for Education and Research; AMCSIT Program, (Project CEEX no: 2/2005)

Structural, mechanical and anti-corrosive properties of biocompatible Zr/ZrCN coatings

C.M.Cotrut¹, C.N.Zoita², A.Kiss², M.Braic², M.Balaceanu², V.Braic², A. Vladescu², I. Antoniac¹

¹ University Politehnica of Bucharest, Romania. ² National Institute for Optoelectronics, Romania.

INTRODUCTION: Multilayer coatings have been shown to outperform single layer films in terms of thermal stability, wear, abrasion and resistance to oxidation [1]. In recent years, nanometer-scale multilayers composed of two different alternating layers have been extensively developed due to their high hardness and excellent wear-corrosion behavior [2].

This work aims to investigate the properties of Zr/ZrCN coatings, with bilayer periods ranging from 4.4 to 190 nm, deposited on 316L stainless steel substrates. ZrCN single layer coatings were also prepared, as reference samples.

METHODS: Zr/ZrCN multilayers were deposited by the cathodic arc technique [3]. The elemental and phase composition, texture, microhardness, adhesion, surface roughness and residual stress were investigated by AES, XRD, Vickers microhardness and scratch adhesion measurements and surface profilometry. The bilayer period values were estimated from the rate and the deposition time of the individual layers. The corrosion resistance of the coated samples was evaluated using electrochemical tests in artificial physiological solution, by measuring the corrosion current and the critical current for passivation.

RESULTS: For the ZrCN monolayers and the ZrCN sub-layer in the multilayer structure, the elemental compositions were: Zr – 34.8 at.%, C – 44.5 at.%, N - 17.3 at.%, O - 3.4 at.%. The C/(C+N) and (C+N)/Zr ratios were found to be of 0.72 and 1.8, respectively. X-ray diffraction patterns revealed that the multilayers with Λ higher than about 20 nm exhibited a (111) orientation (similar to that of the ZrCN monolayers), which gradually changed to no preferred orientation with decreasing Λ . The peaks became broader with the decrease of the bilayer period, indicating a decrease of both the grain size and the stress. The results of the measurements of the main mechanical characteristics (bilayer period Λ , Vickers microhardness HV and critical load L_c, roughness R_a, residual stress σ) of the mono and multilayered coatings are summarized in Table 1.

The decrease of the corrosion current for the coated samples as compared with the uncoated ones indicated that the corrosion resistance of the 316 L steel improved by deposition of both mono

and multilayer coatings (Fig. 1). The best corrosion resistance was measured for the multilayer with $\Lambda \approx 6$ nm.

Table 1. Mechanical characteristics of the coatings.

| Coating | Λ | HV | L_{c} | Ra | σ |
|---------|------|-------|---------|------|-------|
| type | (nm) | (GPa) | (N) | (nm) | (MPa) |
| ZrCN | - | 28.0 | 44 | 490 | 1260 |
| Zr/ZrCN | 190 | 5.2 | 63 | 910 | 1030 |
| Zr/ZrCN | 25 | 15.5 | 61 | 780 | 810 |
| Zr/ZrCN | 6.3 | 28.7 | 39 | 510 | 720 |
| Zr/ZrCN | 4.4 | 17.3 | 41 | 350 | 920 |

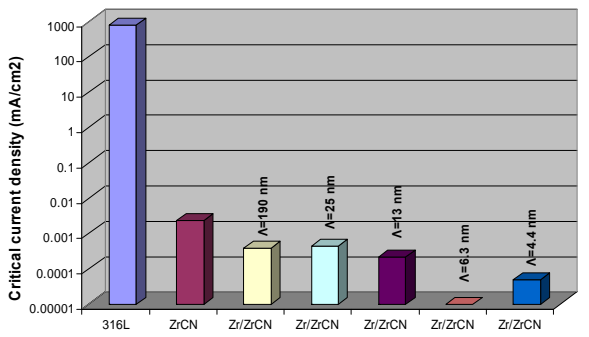


Fig. 1: Critical current densities of the coated and uncoated 316L steel samples

DISCUSSION & **CONCLUSIONS:** The investigations showed that the coating properties depended both on the values of the modulation period Λ . The mechanical and corrosion properties of the multilayers, for certain deposition parameters, were superior to those of the ZrCN monolayers. The highest microhardnesses of the multilayers, found for $\Lambda=6.3$ nm, was slightly higher than that for the ZrCN monolayers, while a better adhesion was measured for the coatings with relatively large Λ (>13 nm). The corrosion resistance of the multilayers was superior to those of the ZrCN single layer coatings. The multilayers with $\Lambda\approx 6$ nm exhibited the best corrosion behavior.

REFERENCES: ¹ J.N.Ding, Y.G.Meng, S.Z.Wen (2000) *Thin Solid Films* **371**: 178-82. ² J. Musil (2000) *Surf. Coat. Technol.* **125**: 322-30. ³A.Vladescu, A.Kiss, A.Popescu et al (2008) *J.Nanosci. Nanotechno.* **8**: 717–21.

ACKNOWLEDGEMENTS: The work was supported under the Project Osteosurf-235/2006.

Morphology of Metal-Coated Silicone Films

Hans Deyhle¹, Franziska Zuber², Martina Hirayama² and Bert Müller¹

¹ Biomaterials Science Center, University of Basel, c/o University Hospital Basel, Switzerland.

² IMPE, Zürcher Hochschule Winterthur

INTRODUCTION: Electrically activated polymer (EAP) thin film structures are promising alternatives to the currently used, mechanically driven artificial urinary sphincters. In order to reach clinically relevant voltages (below 42 V) the thickness of the EAP has to be reduced to around 1 μ m or even below. The thickness homogeneity of the films should be better than 2% to guarantee a constant electrical field in the polymer. State-of-the-art spin coating of biocompatible silicone can provide such precision over 2-inch wafers.

METHODS: The first contact layer of the EAP structure, i.e. Au, Au/Cr or Ti each 50 nm thin, was deposited onto a 30 μm-thick part of 4"-Si(100) by sputtering or thermal vapour deposition (Nordiko Ltd. NS 2550 and Pfeiffer ONF 010, respectively). Subsequently, the micrometer-thick silicone film was fabricated using spin coating (Laurell WS-400A 6NPP). The EAP structure, which is asymmetrically positioned on one side of the wafer piece, was finalized forming the second contact like the first one. The morphology of the EAP structures was characterized by means of optical and atomic force microscopy (Leica DMRM and Nanosurf Mobile S, respectively).

RESULTS: The physical vapour deposition onto the silicone film, i.e. sputtering or thermal techniques, did not result in homogeneous and flat EAP structures but in more or less regular ripple morphologies. Although the orientation was arbitrary and only directed at defects such as cracks (see Fig. 1), the periodicity of the corrugation was constant for each sample. The wavelength of the pattern formed only depends on the choice of metal coating and thickness. Based on Fourier transforms it has been found that 50 nm Au leads to 2.5 μm periodicity, 50 nm Ti to 4.0 μm and 50 nm Cr to 6.0 µm. The ripples align perpendicular to frequently detected defects in the silicone film, such as cracks, dust particles and sample edges. In defect-free regions no preferential orientation occurs. For the specimens sputtered with Ti, however, a remarkable amount of cracks in the silicone film was observed. Parallel cracks with distances varying between 0.2 and 10 mm run across the whole specimen. While the height variation of the ripples corresponds up to 10% of the silicone film thickness, the cracks were more than 30% of the film thickness deep as shown by the AFM image in the inset of Fig. 1. The ripple and crack structures were not present before the metal deposition.

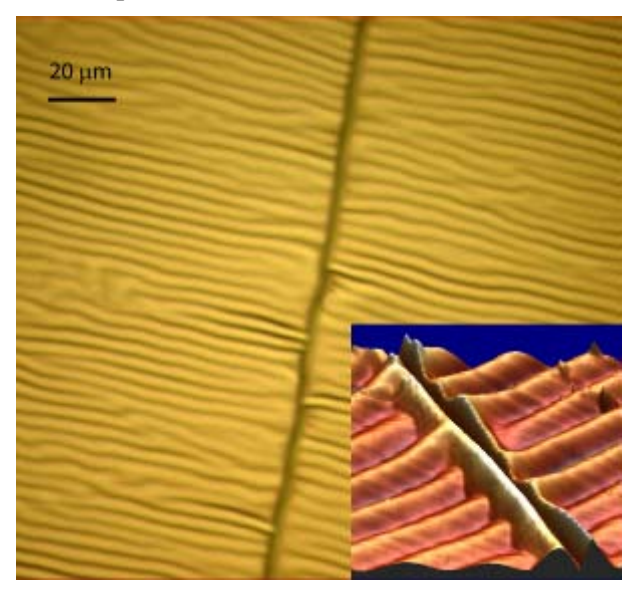


Fig. 1: The optical micrograph shows the regular corrugation of the Ti-coated silicone film oriented perpendicular to the crack. A related AFM image is given in the inset.

DISCUSSION & CONCLUSIONS: The ripples originate from the different thermal expansions of the silicone and the deposited metals. The periodicity of the corrugation depends on the thickness and the Young's modulus of the deposited metal. Higher Young's moduli and thicker films result in larger periodicities. Regular pattern of desired periodicity can be manufactured selecting the suitable metal and film thickness. The crack formation is associated with local charges that are generated during the sputtering process but not by thermal deposition.

REFERENCES: ¹ N. Bowden, S. Brittain, A.G. Evans, J.W. Hutchinson and G.M. Whitesides (1998) *Nature* **393**:146-9. ² M. Watanabe (2005), *Inc. J Polym Sci Part B: Polym Phys* **43**:1532-7.

ACKNOWLEDGEMENTS: The valuable support of J. Gobrecht and T. Vogel (PSI Villigen) for sputtering and of T. Glatzel, V. Thomen and F. Schmidli (University of Basel) for imaging is gratefully acknowledged.

OXIDATION OF VITAMIN-E STABILIZED CROSSLINKED UHMWPE AFTER 7 YEARS AGEING

Y. Dirix¹., A. Becker¹, L. Brunner¹, H. Schmotzer¹
Smith &Nephew Orthopaedics AG, Schachenallee 29, 5001 Aarau, Switzerland.

INTRODUCTION: Oxidation and wear of UHMWPE are two major factors that might affect the long term clinical survivorship of total joint replacements [1]. In the past, Vitamin E (Vit-E) has been suggested as an additive for UHMWPE to tackle the problem of oxidation [2]. The oxidative stability was tested using accelerated ageing protocols to simulate real time ageing. From these ageing studies, the Vit-E stabilized polyethylene can have a superior oxidative stability. However, no real-time ageing data are available. Therefore, the goal is to compare the oxidation after 7 years of real-time ageing of a gamma-sterilized highly crosslinked UHMWPE with- and without Vit-E addition.

METHODS: The UHMWPE (GUR 1020) blocks containing 0 and 0.2% w/w Vitamin E were prepared at PolyHiSolidur. Crosslinking was done by E-beam irradiation in air (10 MeV) to a total dose of 100 KGy followed by remelting. Pins according to DIN31680 were machined and used for a pin-on disc test at a speed of 0.5 m/s under dry conditions (TRM 200/Wazau Berlin; 9 MPa pressure). A polished stainless steel ring was used as a counterpart (INA, $R_z = 3.57 \mu m$). The linear wear of the pins (n=3/mat) was measured after 40 km sliding distance [3]. For the ageing experiment, the crosslinked pins were packaged in a single peel pouch consisting of a first generation barrier film. The packaging was flushed with nitrogen before gamma sterilization with a dose of 30.5 KGy. The packaged pins were stored in the dark at room temperature and were removed from their peel pouch after 86 months. The oxidation index was measured after ASTM F2102-06. Thin (150 µm) cross sections were cut from the pins and used for FTIR measurements to measure the oxidation index.

RESULTS: The wear rate for the crosslinked materials is significantly lower compared to the non-crosslinked reference polyethylene (p=0.020). The wear rate for the stabilized and crosslinked material is higher compared to the non-stabilized counterpart and almost at the level of the non-crosslinked reference (p=0.570). Ageing: The xlinked and gamma-sterilized material without a stabilizer shows a typical subsurface oxidation maximum and a high (>3) bulk oxidation (Fig 2) suggesting that the material has degraded. The stabilized polyethylene has only a relatively low surface oxidation (0.38).

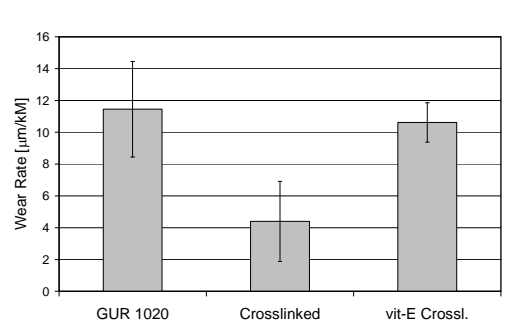


Figure 1: Wear rates for the UHMWPE pins before ageing (non-sterile).

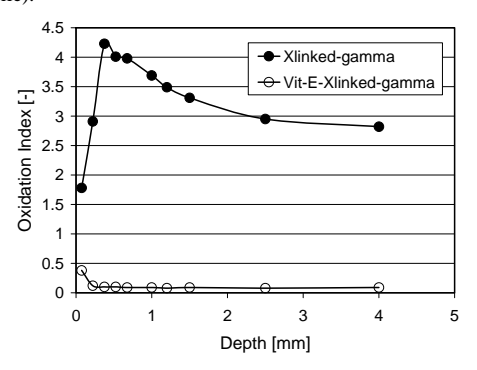


Figure 2: Oxidation index vs. depth for the gamma sterilized materials after 7 years of real time shelf ageing.

CONCLUSIONS: The crosslinking efficiency for UHMWPE was shown to be reduced by the presence of Vitamin E [4]; these results are confirmed by our tests. Although both materials received identical irradiation doses, the stabilized material had only marginal improved wear resistance. Therefore, the optimum balance between crosslinking and stabilization might be found at lower additive amounts [5]. The maximum oxidation for the crosslinked and sterilized pins was high (OI=4). Although packaged under nitrogen, the packaging used is of generation with moderate barrier performance, still enabling air penetration and therewith oxidation. However, the Vitamin E stabilized and crosslinked material, packaged and stored under identical conditions has virtually no oxidation, showing the protective power of this additive in a real-time ageing experiment.

REFERENCES: ¹Currier B. et al., Trans ORS 51, 1182, 2005. ²Wolf C. et al., J. Mat. Sci. Mat. Med, 17, 1333, 2006. ³A. Becker, KTI 3211.1, 2000. ⁴Oral E. et al., Biomaterials, 26, 6657, 2005. ⁵Kurtz S. et al., Trans ORS 53, 20, 2007.

ACKNOWLEDGEMENTS: We acknowledge KATZ Aarau for experimental help and KTI (Grant 3211) for financial support.

En-face optical coherence tomography scanning of amalgam-hard dental tissues interface

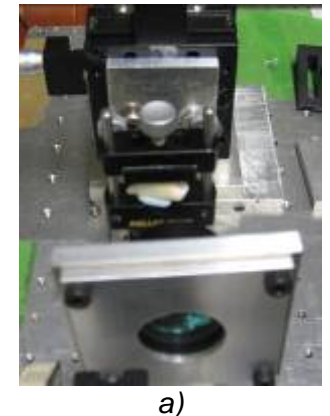
ZA Florița¹, DM Pop¹, CD Haiduc¹, AE Stoia¹, RO Romînu¹, ML Negruțiu¹, C Sinescu¹, C Clonda¹, Gh Dobre², A Gh Podoleanu²

University of Medicine and Pharmacy "Victor Babeş", România¹, University of Kent, United Kingdom²

INTRODUCTION: Many methods of investigation of the restoration - hard dental tissues interfaces are in use today, some of them being already classical. New methods are emerging, several of them focusing on the non-destructive characteristics of the investigation, thus allowing a dynamic evaluation of the samples. One of them, the optical coherence tomography (OCT), is used in the present study.

METHODS: Amalgam fillings were inserted in cavities prepared in the buccal fossae of extracted mandibular first molars. They were allowed to set completely and then were subjected to OCT examination. The optical configuration uses two mode directional couplers single with a superluminiscent diode as the source at 1300 nm. The scanning procedure is similar to that used in any confocal microscope, where the fast scanning is en-face (line rate) and the depth scanning is much slower (at the frame rate). The en-face scans provide an instant comparison to the familiar sight provided by direct view or via a conventional microscope. Features seen with the naked eye could easily be compared with features hidden in depth. Sequential and rapid switching between the en-face regime and the cross section regime, specific for the en-face OCT systems developed by us¹, represents a significant advantage in the noninvasive imaging. **Images** with different orientations and 3D OCT imaging can be obtained using the same system. C-scans are made from many T-scans along either of X, Y, repeated for different values of the other transverse coordinate, Y, X respectively in the transverse plane. The repetition of T-scans along the other transverse coordinate is performed at a slower rate than that of the T-scans, which determines the frame rate. In this way, a complete raster is generated. Different transversal slices are collected for different depths Z, either by advancing the optical path difference in the OCT in steps after each complete transverse (XY) scan, or continuously at a much slower speed than the frame rate. The depth scanning is the slowest in this case. It is more difficult to generate en-face OCT images than longitudinal OCT images as the reference mirror is fixed and no carrier is produced. Therefore, in order to generate T-scans and T-scan based OCT images, a phase modulator is needed in order to create a carrier for the image bandwidth.

RESULTS: The defect discovered inside the structure were identified at 0.286 mm. The defect volume can be computed using 3D reconstruction softwares, allowing the structure behavior during mastication and the fracture or microleakage hazards at this level.



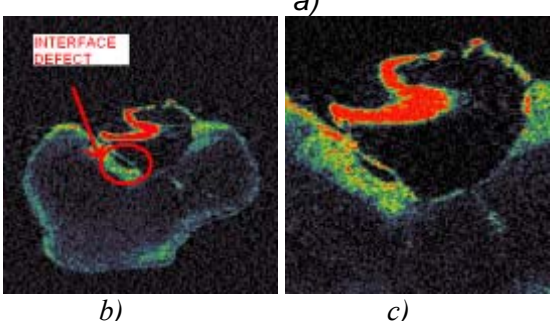


Fig. 1: Material defect at the amalgam-tooth structure interface investigated with en face OCT (a); slide 8 from 23, 18 degrees in air (b) and slide 5 from 23, 8 degrees in air (c).

DISCUSSION & CONCLUSIONS: This method allowed us to evaluate, in a non-invasive manner, the presence of the inner gaps at the amalgamtooth structure interface. In conclusion, OCT could act as a valuable tool in analyzing the restorations as a noninvasive method.

REFERENCES: ¹ A. Gh. Podoleanu, J. A. Rogers, D. A. Jackson, S. Dunne (2000) *Three dimensional OCT images from retina and skin* Opt.Express, Vol. 7, No. 9, p. 292-298, (2000).

Osseointegration of zirconia dental implants with a new rough surface. A biomechanical and histological study in mini pig.

M.Gahlert¹, S.Röhling², C.M.Sprecher², S.Eichhorn³, E.Steinhäuser³, M.Wieland⁴, H.Kniha¹, S.Milz²

¹ Private Dental Clinic, Munich, Germany. ² AO Research Institute, Davos, Switzerland. ³ Klinik für Orthopädie und Sportorthopädie der TUM, Munich, Germany. ⁴ Institut Straumann AG, Basel, Switzerland

INTRODUCTION: Mechanical properties and tooth like colour let zirconia ceramics appear as an interesting alternative for dental implants. The purpose of the present study was to investigate the osseointegration of zirconia implants with a new rough surface topography in comparison to the clinically¹ and experimentally² well documented titanium implants with a sandblasted and acidetched surface (SLA).

METHODS: Cylindrical zirconia implants 4.1 mm in diameter and 10.0 mm in length were produced by using a new low pressure injection molding technique. After that the implants were acid etched. Ti-SLA implants of the exact shape served as controls.

The incisors 2 and 3 were extracted from both sides of the maxilla. After a healing period of at least 6 months, 16 adult miniature pigs received a total of 96 implants in their maxillae. The animals were euthanized after 4, 8 and 12 weeks. 59 implants were subjected to removal torque testing (RTQ) directly after the euthanasia. 28 implants were removed with the surrounding bone and histologically investigated. 9 implants were lost due to wound healing problems. The origin of these problems was the use of PEEK healing caps.

RESULTS: Both materials showed similar RTQ results. The average mean value for zirconia was 60.4 Ncm (42.4 - 69.6 Ncm) and 63.4 Ncm for Ti-SLA (42.1 - 75 Ncm).

Histological evaluation showed direct osseous integration for both materials (Fig. 1, 2). Zirconia implants revealed mean peri-implant bone density values of 42.3% at 4 weeks, 52.6% at 8 weeks, and 54.6% at 12 weeks after implantation, whereas Ti-SLA implants demonstrated mean values of 29%, 44.1% and 51.6% at corresponding time intervals. Concerning bone interface contact ratio the mean values for zirconia ranged between 27.1% and 51.1% and for Ti-SLA between 23.5% and 58.5%. RTQ and histological evaluation revealed no significant differences between both materials at any given time point.

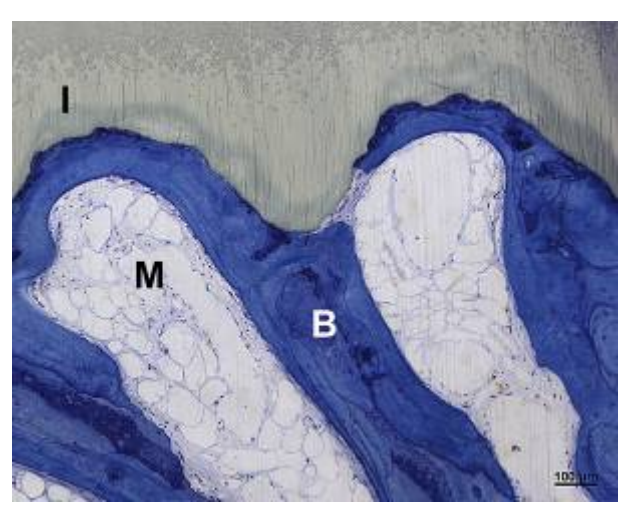


Fig. 1: Direct osseous integration of a zirconia implant (I); B: bone; M: bone marrow. Note that there is basically no difference in appearance when compared to Fig. 2.

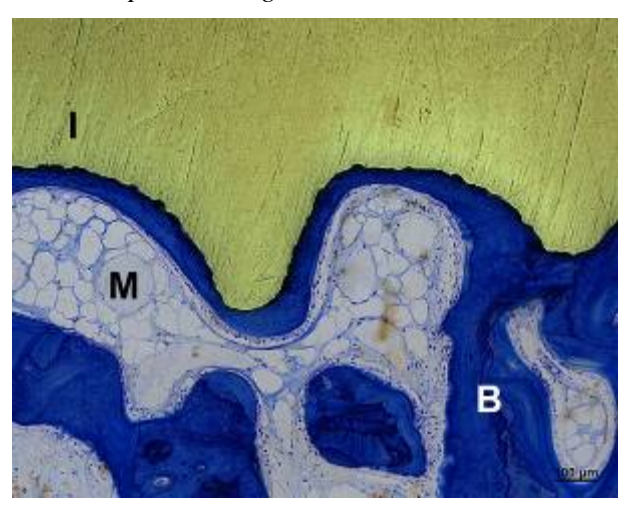


Fig. 2: Direct integration of a Ti-SLA implant (I); B: bone; M: bone marrow.

DISCUSSION & CONCLUSIONS: The biomechanical and histological results clearly indicate that zirconia implants have a comparable capacity for osseous integration as the titanium implants from the control group.

REFERENCES: ¹M. Bornstein et al. (2005) Clin. Oral Impl. Res. 16, 631-638. ²D. Buser et al. (1999) *J Biomed Mater Res.* 45, 75-83.

Structural Characteristics of Some Cobalt Dental Alloys After Heat Treatments

B. GHIBAN, C. BORIUN, G. COSMELEATA, S. CIUCA, N. GHIBAN, I. CARCEANU,

¹University Politehnica of Bucharest, Romania, "V. Babeş" University of Medicine and Pharmacy Timișoara, Romania, "Metallurgical research Institute", Bucharest, Romania

Introduction : Cobalt based superalloys continuous to be used with great interest in dentistry due to simultaneously properties, such as: high mechanical characteristics (vielding strength, ultimate strength, hardness). biocompatibility, or wear resistance [1,2,3,4,5]. In dentistry cobalt is still used for realizing of partial or total prosthesis. The problems which are met during casting of prosthesis are connected to cracks susceptibility and brittle behaviour after a rather short time of prosthesis working. Present paper is focused on structural modification analysis on different cobalt alloys used for denture prosthesis.

Methods: In present paper there are presented results of investigations on samples of partial removable denture made of cobalt base alloys (Co-Cr-Mo) regarding specific structural analysis: structural phases (by X-Rays diffraction was made on DRON 3 device), qualitative and qualitative microstructural analysis (on REICHERT microscope equipped with IMAGE -Pro software for analysis), microhardness determinations versus different casting parameters [1,2,3,4].

3. Results: Chemical composition of the experimental alloy is in accordance with ISO 5832 /4/, respectively: 0,29%C, 26,5%Cr; 5,35%Mo; 0,60%Ni; 0,64%Fe and Co rest. X-Rays diffraction (figure 1) put in evidence the specific phases in a cobalt alloy.

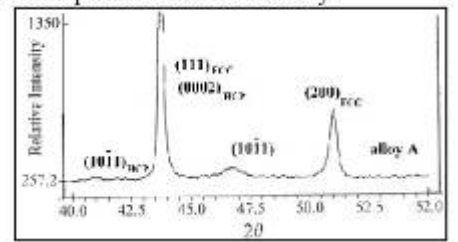
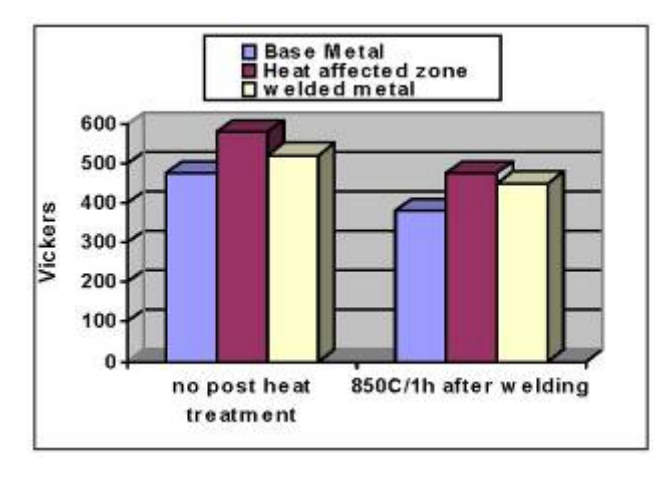


Fig. 1-X-Rays Diffractions of HERAENIUM CE experimental cobalt alloy



The microstructure results of the as cast alloys are shown in Figures 2 (a), consisted of cobalt-rich FCC matrix dendrites, very fine interdendritic eutectic, but high grain sizes. After applying a hreat treatment at 850°C/1 h/ air the carbides may refine, and the grains are equiaxed. Microhardness measurements (figure 3) reveal the increase both of grains sizes and the particles size in the welded metal and in the heat affected zone. DISCUSSION & **CONCLUSIONS:** Optical microscopy observations indicated that of HERAENIUM CE experimental cobalt alloy exhibited interdendritic carbides, solute segregation, relatively large grains; The tensile properties of the heat-treated alloys exhibited significant improvements in ductility and strength when compared with the as-cast counterparts. The main effect of alloy preheating was manifested as a removal of the extensive interdendritic carbide precipitation and appreciable break-up of the dendritic grain structure. This leads to the development of a homogenous equiaxial grained structure and the consequent improvement in mechanical behaviour (by microhardness measurements); By welding with different laser technology, the materials for dental applications may be repair. Cracks may appear either due to casting technology, or to welding by laser.

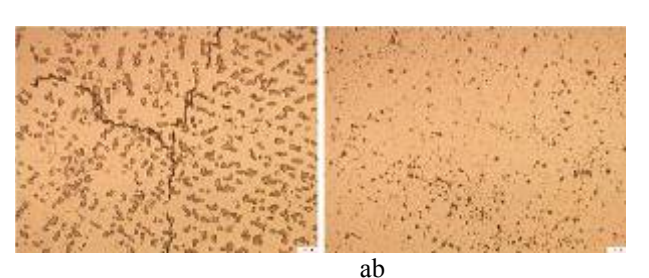


Fig. 2.Microstructural aspects of HERAENIUM CE experimental cobalt alloy

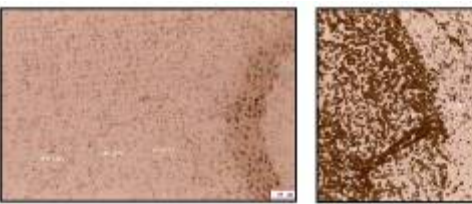




Fig. 3-Microhardness Vickers values of HERAENIUM CE experimental cobalt alloy samples: (a) with no post heat treatments, (b) 850°C/Ih/air after heat treatment

REFERENCES: C. BorŃun, I.Mitelea, L.Miloş, V.Bîrdeanu, L. Sandu (2005) Analysis of laser welded joints on "C" alloy used in removable partial dentures technology, European Cells and Materials vol.10, Suppl. I pg 31, L. Sandu, C. BorNun, L. Ardelean, N. Faur (2005) Finite element analysis of stress distribution induced by thermal variations on cast clasps, European Cells and Materials, vol.9, Suppl.1 pg 3-4.

Adhesion of Oral Streptococci to All-Ceramics Dental Restorative Materials

<u>I. Hauser-Gerspach</u>¹, R. Meier¹, H. Lüthy², J. Meyer¹

¹ Institute of Preventive Dentistry and Oral Microbiology, ² Institute of Dental Materials Science and Technology, Dental School, University of Basel, Switzerland.

INTRODUCTION: In the oral cavity all exposed surfaces, human tooth tissues as well as restorative and reconstructive materials, are rapidly coated with a salivary pellicle, to which early colonizing bacteria, mostly oral streptococci, adhere. These are the first steps in the formation of the oral biofilm, called dental plaque, the major cause of caries, periodontal, and other oral infection-induced diseases.

All-ceramic restorations for medical and dental purposes have gained importance due to their high strength, biocompatibility and excellent aesthetic properties [1]. The present study investigated the adherence of two early colonizers, *Streptococcus sanguinis* and *S. oralis*, and of two caries-associated bacteria, *S. mutans* and *S. sobrinus*, to four different all-ceramic dental materials with experimentally-formed salivary pellicle. In addition, surface roughness and hydrophobicity were determined.

METHODS: Test specimens (Table 1, Fig. 1) were incubated first with saliva, then with a bacterial suspension for one hour in a flow chamber *in vitro* which mimics the environmental conditions in the oral cavity [2]. Numbers of adherent bacteria were determined after staining by fluorescence microscopy (Fig. 1). Roughness (Ra) and water contact angle (CA) were measured [2]. A glass similar to enamel with regard to microbial adhesion *in vitro* served as control [2].

Table 1. Surface roughness Ra (µm) and contact angles CA (degrees) of the dental ceramics (Vita, Bad Säckingen, Germany) and the control glass (Vetter, Ammerbuch, Germany) used.

| Type of material | Ra (µm) | CA (degree) after saliva-coating |
|------------------------|------------|-------------------------------------|
| Glass (Borosilicate) | 0.24 | 43.8 |
| Vita Mark II, MK | 0.26 | 44.3 |
| In-Ceram Aluminia, ICA | 1.33 | 44.1 |
| In-Ceram Zirconia, ICZ | 1.34 | 46.0 |
| In-Ceram, YZ | 0.26 | 44.8 |

RESULTS: On all materials tested, *S. mutans* and *S. sobrinus* adhered approximately ten-fold less than *S. sanguinis* and *S. oralis* (Fig. 2). All salivary-coated specimens showed similar hydrophilic surface properties. Surface roughness of the all-ceramics MK and YZ showed no

difference to glass, while ICA and ICZ yielded 5-fold higher values (Table 1). All bacterial suspensions were hydrophilic as measured by hexadecane partitioning. Surface roughness and hydrophobicity of the materials had no distinctive influence on the adherence.

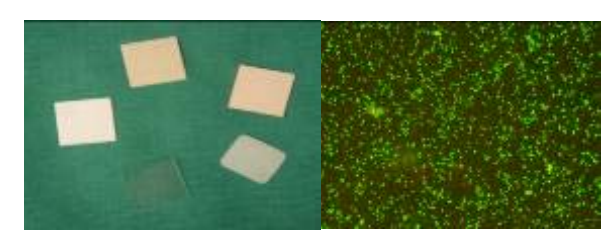


Fig. 1: All-ceramics used MK, ICA, ICZ, YZ (left, counter-clockwise) and glass (transparent). Streptococci adhered to glass (right).

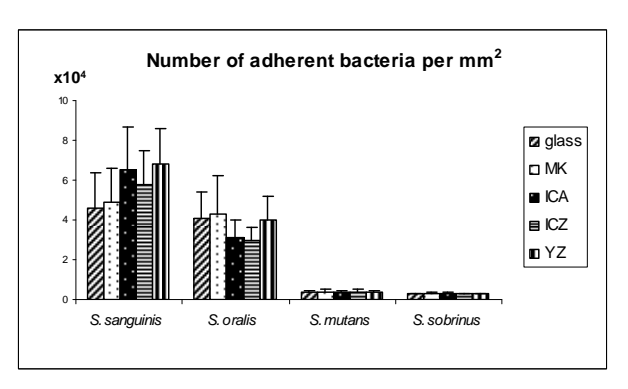


Fig. 2: Adherent streptococci on test materials and control (mean ±SD, n=5).

DISCUSSION & CONCLUSIONS: The results showed that irrespective of the materials tested, *S. sanguinis* and *S. oralis* adhered to much higher degrees than *S. mutans* and *S. sobrinus*. Future investigations should focus on the material-pellicle interactions in order to understand and control the adherence of these important initial colonizers. This *in vitro* model provides a useful tool to study the initial adherence of oral bacteria to new or modified dental materials.

REFERENCES: ¹ H. Lüthy, F. Filser, O. Loeffel, et al. (2005) *Dent Mater* **21**:930-7. ² I. Hauser-Gerspach, E.M. Kulik, R. Weiger, et al. (2007) *Dent Mater J* **26**:361-6.

ACKNOWLEDGEMENTS: Financial support from SSO-Fonds (grant No. 224) and Straumann AG is gratefully acknowledged.

Differential phase contrast – new imaging method for HARWI-II beamline at DESY using hard x-ray grating interferometer

<u>J. Herzen</u>¹, F. Beckmann¹, A. Haibel¹, and A. Schreyer¹ *I GKSS Research Centre, Geesthacht, Germany.*<u>F. Pfeiffer^{2, 3}</u>, T. Donath², and C. David²

INTRODUCTION: Phase contrast imaging is a common technique to visualize soft tissue with much higher contrast than the conventional absorption contrast imaging. Differential phase contrast (DPC), developed at PSI, Switzerland, makes use of a hard x-ray grating interferometer and allows for phase contrast imaging with high brilliance synchrotron sources as well as with conventional x-ray tubes. It is recently reported also to provide dark field information that is very sensitive to micro structures like porosity within the materials¹. Here we present the plans to adopt the DPC technique to the HARWI-II materials science beamline2, operated by GKSS Research Centre, in cooperation with DESY, Hamburg. This will offer an amount of new applications especially in the field of biomaterials like for example studying corrosion of magnesium as implant material. The excellent results obtained at the ESRF³, France demonstrate the potential of DPC for biomedical studies.

METHODS: Figure 1 shows a schematic of the planned DPC setup for the HARWI-II beamline at the 2nd generation synchrotron source DORIS. The setup will consist of three gratings G0, G1 and G2, a specimen, and a detector. The absorbing grating G0 will be placed directly after the monochromator and will serve as a multiplexed source. The phase grating G1 behind the specimen acts as phase mask and produces periodic phase modulations in the xray wave front. Due to the Talbot effect the phase modulation causes a linear periodic fringe pattern in the plane of the second absorbing grating G2 that has the same periodicity as the fringes and acts as analyzer. The grating fabrication process involves photolithography, deep etching into silicon and electroplating of gold.

The grating G1 will be scanned along the transverse direction and for each projection it will yield quantitative images of the specimen's phase shift gradient $d\Phi(x,y)/dx$, the dark field image and the conventional absorption projection.

RESULTS: The DPC setup will be optimized for 28 keV, due to the maximum flux at that energy.

A set of gratings with grating periods $p0 = 55 \mu m$, $p1 = 40 \mu m$, and $p2 = 2 \mu m$ will be produced at PSI in Switzerland. These gratings will be used in the 5th Talbot order with the distances G0 - G1 of 6 m, G1 - G2 of 0.2 m, and 40 m between the source and G0. The spatial resolution of ~15 μm will be achieved in phase contrast images.

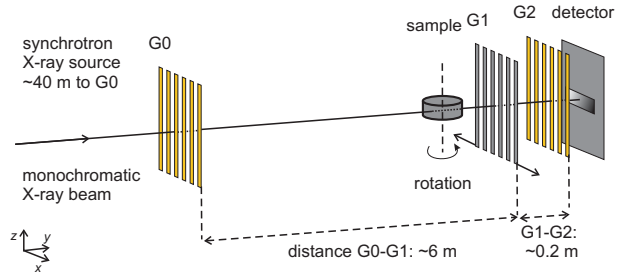


Fig. 1: Schematic of DPC setup for HARWI-II consisting of three gratings G0 (40 m away from source), G1 (6 m from G0.) and G2 (0.2 m from G1), the specimen and the detector.

DISCUSSION & CONCLUSIONS: The reported results on biological samples, the high sensitivity for soft tissue and the stability of the DPC technique using a hard x-ray grating interferometer show its potential for studies in the field of soft tissue.

Adopting this technique for the materials science beamline HARWI-II would expand the range of applications to the field of materials science, especially of biomaterials. The advantages of the synchrotron source with a large field size (70 mm (h) x 10 mm (v)) and monochromatic x-rays will allow for analysing centimetre sized objects.

REFERENCES: ¹F. Pfeiffer et al. (2008) *Hard-X-ray dark-field imaging using a grating interferometer*, Nature Materials **7**, pp. 134-137. ²F. Beckmann et al. (2006) *New developments for synchrotron-radiation based microtomography at DESY*, Proc. of SPIE Vol. 6318, 631810. ³F. Pfeiffer et al. (2007) *High-resolution brain tumor visualization using three-dimensional x-ray phase contrast tomography*, Phys. Med. Biol. **52**, pp. 6923-6930.

² Paul Scherrer Institute, Villigen PSI, Switzerland, ³ EPF Lausanne, Lausanne, Switzerland.

Detection of the Forces and Modulation of Cell-Substrate Interactions

Jochen Köser¹, Jens Gobrecht², Uwe Pieles¹, and Bert Müller³

¹ University of Applied Sciences Muttenz, Switzerland. ² Paul Scherrer Institute Villigen, Switzerland, ³ Biomaterials Science Center, University of Basel, Switzerland

INTRODUCTION: The cell's organization and maintenance of tissues depend on the complex interplay between various cell types and the surrounding extracellular matrix and substrate. It is established by diffusible signalling molecules and direct mechanical interactions linking intracellular cytoskeleton with the extracellular matrix or substrate hence creating a supra-cellular architectural framework. To detect and monitor changes in this framework, several methods have been developed ranging from the labelling of components specific cytoskeletal measurement of forces generated by individual cells. In this paper, we present the concept using nanomechanical cantilever sensors to quantify forces generated from the interplay of cells and cell layers with the supporting micrometer-thick substrate.

METHODS: Nanomechanical cantilever sensors are defined as tiny plate-like structures, which are fixed at the one end to the solid support. Machined from thin, and therefore flexible materials as silicon or polymeric materials they bend in reaction to contractile cell forces acting along their longitudinal axis (Fig. 1). With dimensions of 500 x 100 x 1 um³ forces as small as 0.01 mN/m have been detected via the deflection of a laser beam focused at the apex of the cantilever structure. Furthermore, measurements of mode changes in the resonance frequency of the loaded cantilevers have been monitored that allows determining the stiffness and mass changes on the sensor surface. 1 Such changes upon cellular transformation have recently been demonstrated.²

CONCEPTUAL RESULTS: The successful quantification of cellular forces generated by the cells onto their underlying flexible substrate date back to 1980.³ However, the quantification was rather an rough estimate and the technical complexity prevented the widespread application for the investigation of the implications of cytoskeletal rearrangements on the supra-cellular organization of adherent cells. Nanomechanical cantilever sensors have been successfully applied for the determination of forces created by conformational changes of proteins and nucleic acids as well as the forces created by the expansion of lipid membranes upon the insertion of biomolecules. Varying size and especially

thickness the sensitivity can be adopted. Therefore, micro-plates were used in preliminary experiments to quantify forces of fungi and different cell types including muscle cells. We are going to extend these studies to investigate the interactions of different cells of epithelial and fibroblastic origin with selected substrate materials. The study of contractile cell forces is helpful for the design of support materials and surfaces of medical implants, varying the substrate's morphology and its functionalization even by means of self-assembled nano- and micro-structures. The proposed method works label-free and can monitor architectural changes in real time thus allowing to also detect transient variations and to follow complex cytoskeletal rearrangements e.g. upon cell activation, apoptosis or malignant transformation.

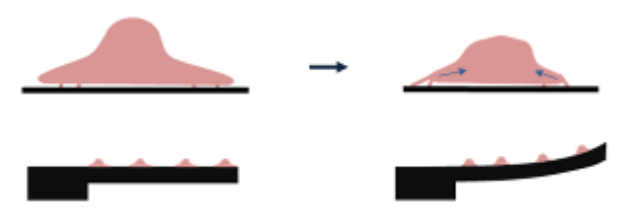


Fig. 1: Principle of real-time monitoring and quantification of contractile forces exerted by cells onto the substrate with cantilever sensors.

DISCUSSION & **CONCLUSIONS:** This communication presents an approach for the quantitative measurement of contractile cell forces on dedicated substrates with tailored morphology and function. It can be used to realize biological or chemical sensors or to improve the surface biocompatibility of medical implants. Consequently it is of fundamental interest and important for different kinds of applications.

REFERENCES: ¹ H.P. Lang, M. Hegner, Ch. Gerber (2005) *Materials Today* **8**(4):30-36. ² S.E. Cross, Y.-S. Jin, J. Rao, J.K. Gimzewski (2007) *Nature Nanotechnology* **2**:780–783. ³ A.K Harris, P. Wild, D. Stopak (1980) *Science* **208**:177-179.

ACKNOWLEDGEMENT: The presented research activities belong to the project 'DICANS', a collaborative initiative between BMC, PSI, FHNW and Concentris GmbH funded by the Swiss Nanoscience Institute.

Vessel staining in tumours by Angiofil®

Sabrina Lang¹, Marco Dominietto², Felix Beckmann³, Julia Herzen³ and Bert Müller¹

¹Biomaterials Science Center, University of Basel, Switzerland. ²Institute for Biomedical Engineering, ETH Zürich, Switzerland. ³GKSS-Research Center Geesthacht, Germany.

INTRODUCTION: In cancer research imaging the blood vessels of tumours plays an important role to investigate the angiogenesis. Microcomputed tomography (μCT) provides the spatial resolution to image the smallest vessels, but not the necessary contrast. Therefore, one has to apply appropriate embedding methods¹ or contrast agents such as barium sulfate.² As the particle sedimentation results in "non-connected" vessels,² alternative contrast agents are desired. The iodine-based contrast agent Angiofil®² belongs to the promising species and is used in the present study.

METHODS: C51 tumour cells were injected in nude mice in strict adherence to the Swiss law for animal protection. Using Magnetic Resonance Imaging (MRI) the tumour was investigated during growth. 200 µl heparin were injected before perfusion. Subsequently, the tumour was filled with the prepared Angiofil® solution via the left ventricle of the heart using the peristaltic pump. Finally, the tumours were extracted, fixed in 4% para-formaldehyde and transferred to the Eppendorf tubes for the imaging. The stained vessels were visualized by means of synchrotron radiationbased micro computed tomography (SRuCT) at the beamline TOMCAT (SLS at PSI, Switzerland) in absorption contrast mode.³ The photon energy was set to 18 keV. A series of 1501 projections with a pixel size of 3.8 µm was recorded.

RESULTS: Fig. 1 shows the 3D representation of the vascular structure within the Angiofil perfused tumour. One clearly recognizes that the stain is concentrated in some vessels. Bifurcations are hardly visible. The vessel tree is only inhomogeneously stained. Nevertheless, it is seen that the centre of the tumour is almost free of connected vessels. The stained vessels have diameters between 8 and 400 μm .

DISCUSSION & CONCLUSIONS: Angiofil can be used to stain vessels including the bigger capillaries in tumour tissue. The procedure, however, has to be improved to obtain the homogeneous distribution of the stain within the vessel tree and the penetration of the smallest capillaries. The analysis of the vessel diameter is required for modelling of the fluid dynamics as well as for the calibration of the in vivo MRI. Therefore, the search for appropriate staining

materials has to be continued, in order to quantify the tumour in reproducible way. The missing stained vessels in the tumour centre are associated with the necrotic part of the tumour. Alternatively, one could apply phase contrast imaging avoiding any staining procedure.⁴

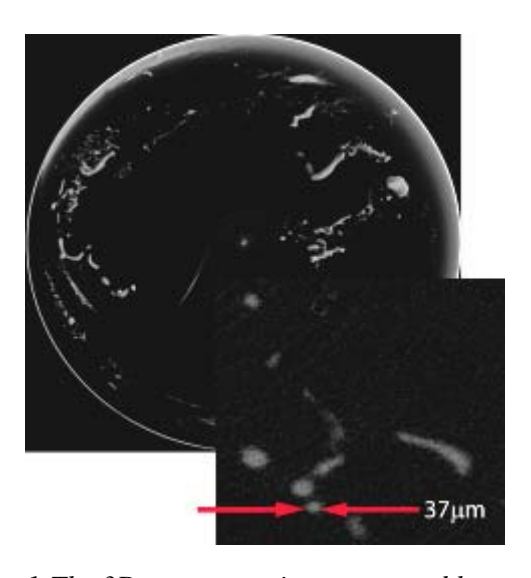


Fig. 1:The 3D representation, generated by VGStudio MAX shows the central part of the tumour (d=7.8 mm), while only at periphery vessel structures appear. The fraction of the virtual slice exhibits different vessels, one 37 μ m thick is highlighted.

REFERENCES: ¹ B. Müller, M. Germann, D. Jeanmonod, A. Morel (2006) *Proc. SPIE* **6318**:631803. ² B. Müller, J. Fischer, U. Diertz, P. Thurner, F. Beckmann (2006) *Nucl. Instrum. Meth.* **B 246**:254-61. ³ M. Stampanoni, P. Wyss, R. Abela, G. Borchert, D. Vermeulen and P. Rüegsegger (2002) *Proc. SPIE* **4503**:178. ⁴ F. Pfeiffer, O. Bunk, C. David, M. Bech, G. Le Duc, A. Bravin, P. Cloetens (2007) *Phys. Med. Biol.* **52**:6923–30.

ACKNOWLEDGEMENTS: The authors acknowledge the valuable support of F. Marone and M. Stampanoni (PSI) during the data acquisition at the beamline. S. Friess (Gloor Instruments AG, Uster, Switzerland) kindly provided the contrast agent Angiofil[®]. The study was financially supported by the SNSF through NCCR Co-Me and SLS/PSI (proposal 20070856).

Effect of polishing of titanium internal fracture fixation plates upon infection resistance.

TF Moriarty, ¹L Debefve, ¹L Boure, ¹ RG Richards^{1,2}

¹AO Research Institute, Davos, Switzerland; ²Cardiff School of Biosciences, Cardiff University, Wales.

Introduction: Polishing the surface of fracture fixation implant materials alters fibroblast¹ & osteoblast² behaviour in vitro and reduces soft tissue adhesion³ & bony overgrowth in vivo⁴. Thus, surface polishing may decrease complications such as, allowing tissues to freely glide over the implant (e.g. tendons in distal radius fractures and muscles in orbital fractures) and easing implant removal. However, surface polishing may also influence the susceptibility of an implant to bacterial colonization. Since infection is still the most important limiting factor of success in internal fracture fixation, the effect of surface polishing on in vivo infection rates needs to be ascertained. In this study, the local infection rate associated with clinically available titanium (Ti) ISO 5832/2 and titanium aluminium niobium (TAN) ISO 5832/11 in their standard microrough form is compared with that of their test polished equivalents and also to clinically available electropolished stainless steel (EPSS) ISO 5832/1.

Materials and methods: Approval to perform this study was granted by the Cantonal animal ethics committee. Standard 4-hole 2.0 mm Synthes® locking compression plates (LCPs) made of standard and polished Ti and TAN in addition to EPSS were used. The surface roughness was evaluated by non contact profilometry and SEM. The surface chemistry and wettability were characterised by XPS and water contact angle. For the in vivo infection study, plates were fixed on the medial tibial diaphysis of healthy, mature, female New Zealand White rabbits using unicortical screws. Immediately after implantation, a human-pathogenic, beta-haemolysing Staplylococcus aureus strain was added at the implantation site. Twenty eight days after implantation surgery, the rabbits were euthanized and evaluated for the presence of bacteria. To use as few animals as possible, we performed consecutive investigative phases. In each phase the bacterial concentration was adjusted towards the intended ID₅₀ (bacterial concentration causing a 50% infection rate) at which the differences in infection rates is most evident⁵.

Results: The mean Ra is shown for each test material in Table 1. Roughness differences were observed between the materials with standard Ti and TAN showing comparable roughness, polished Ti and TAN were smoother and EPSS was the smoothest.

| Implant description | Ra µm | Contact Angle (°) |
|------------------------|-------|----------------------|
| Standard Ti | 0.708 | 91.3 ± 0.37 |
| Polished Ti | 0.322 | 87.9 ± 0.17 |
| Standard TAN | 0.737 | 103.8 ± 0.07 |
| Polished TAN | 0.334 | 100.9 ± 0.24 |
| EPSS | 0.124 | 88.7 ± 0.54 |

Table 1. Surface roughness and contact angle of each LCP

The water contact angle measurements (Table 1) were measured on the slightly curved surface of the LCP and showed no large differences in wettability between standard and polished LCPs of either Ti or TAN. XPS data showed that polishing followed by subsequent anodisation did not affect the final surface chemical properties of the test materials.

After six sequential investigative phases 104 rabbits were included in the study. The inoculum was sequentially adjusted to expose maximum number of animals at the concentrations spanning the ID_{50} . ID_{50} values were determined based on cumulative frequency and were, in rank order from most infection resistant to least; polished TAN (7.1x10 6 CFU), standard TAN (6.3x10 6 CFU), standard Ti (3.9x10 6 CFU), EPSS (3.2x10 6 CFU) and finally polished Ti (2.7 x10 6 CFU) Table 2). The rate of infection for each LCP type is shown in Table 2.

| LCP Type | n (rabbits) | Rate of infection (%) | ID 50 (CFU) |
|----------------------|----------------|-----------------------|-----------------------|
| EPSS | 22 | 54 | 3.2 x 10 ⁶ |
| Polished TAN | 22 | 45 | 7.1 x 10 ⁶ |
| Standard TAN | 21 | 38 | 6.3 x 10 ⁶ |
| Polished Titanium | 20 | 50 | 2.7 x 10 ⁶ |
| Standard Titanium | 19 | 42 | 3.9 x 10 ⁶ |

Table 2. Infection rates of the five implants at the different bacterial challenges.

The differences in infection rate were not significantly different based on analysis with the Chi-squared test with p < 0.05 as level of significance. The Fischer-exact test for the pair wise comparison of the five implants demonstrated no significant differences between the five groups (p < 0.05).

Discussion: Surface polishing of Ti and TAN plates reduced the roughness of the plate surface without change in surface chemistry. The polishing of standard Ti and TAN has been shown to have considerable benefits in relation to reduced bone adhesion and bony overgrowth *in vivo*^{3, 4} and has been shown in the present study not to influence infection rate. Clinical implementation of polished Ti and TAN LCPs is not expected to result in an increased infection rate according to the results of this study.

References:

1. Meredith *et al.*, J Biomed Mater Res A 2005, 73A (1) 541-555. 2. Hayes *et al.*, Trans. 53rd ORS, 2007, 1630. 3. Richards *et al.*, European Orthopaedic Research Society Conference, 2000. Trans. Vol 10 (O-136). 4. Richards, *et al.*, Trans. 53rd ORS, 2007, 1629. 5. Schlegel & Perren, Injury. 2006 37 S2:S67-73.

Acknowledgments: Synthes for kindly providing the LCPs and screws. Urs Schlegel for discussions, Pamela Furlong for her technical support and Dr. V. Frauchiger (Robert Mathys foundation) for XPS.

THE DETECTION OF DENTURE MATERIAL DEFECTS BY A NON-INVASIVE METHOD

M. Negrutiu¹, C. Sinescu¹, L. Goguta², M. Hughes³, A. Bradu³, R Rominu¹, D.Pop¹, S. Cânjău⁴, A. Podoleanu³

¹ Department of Prostheses Technology and Dental Materials, ² Department of Prosthetics, Faculty of Dental Medicine, University of Medicine and Pharmacy "Victor Babeş" Timişoara, Romania

³Applied Optics Group, School of Physical Sciences, University of Kent, Canterbury, UK

INTRODUCTION: When making a denture or removable partial prosthesis, long term preservation of structure and function requires that potential irritating effects are kept at minimum.

In order to avoid the deficiencies of the prostheses made by the classical pressure-pack technique, several alternative procedures were devised, directly related to the material used and also to the manufacturing technology. Thus, at the present time, there are several injecting systems and technologies on the market, that use chemoplastic materials. There are also technologies that plasticise a hard cured material by thermoplastic processing (without any chemical reaction) which is then injected it into a mold.

METHODS: Several complete dentures were made using the conventional pressure-pack procedure, the SR-IVOCAP injecting system, the aspiration-injection system and the thermoplastic molding system.

We also made full dentures with reinforced bases with polymer preimpregnated glass fiber net, polyethelene and glass fiber net - light and heat cured resin and golden metal net.

In this work we used an *en-face* OCT system^{1, 2}, which can deliver B-scans and C-scans from *en-face* (or T-scan) reflectivity profiles. The OCT system operated at 1300 with a low numerical aperture (NA) interface optics which gives a large field of view of 1 cm by 1 cm, but relatively low transverse resolution of 25 µm. Both systems have typical working distances of 2 to 3 cm and depth resolution of 18 to 20 µm (in air).

RESULTS: In all of the investigated prostheses, especially in the dentures made using the conventional pressure-pack procedure we found defects which may cause their fracture. These defects are totally included in the prostheses material and can not be vizualised with any other imaging methods. The polymeric material is very porous. The areas depicted present several small

canals in the base that can be colonized in time with bacteria (Fig. 1).

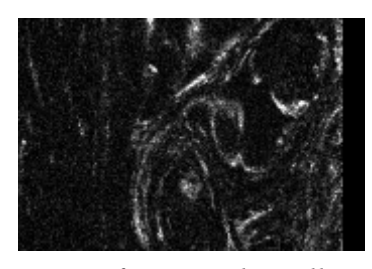


Fig. 1: Detection of areas with small canals in the denture's base produced using the classical method. En_face proximal scanning, 5 mm lateral size, 0.2 mm depth inside.

DISCUSSION & CONCLUSIONS: The defects identified above can lead to fractures of prostheses or/and to bacterial infiltration. Dentures with reinforced base present defects especially at the interface between the reinforcing material and the acrylic denture polymer. In order to avoid future prosthetic failures, it is important to employ a non-invasive imaging method such as OCT as demonstrated here to assess the quality of dental prostheses before ther insertion in the oral cavity. **REFERENCES:** 1. B. T. Amaechi, A. Gh. Podoleanu,

REFERENCES: 1. B. T. Amaechi, A. Gh. Podoleanu, S.M. Higham, D. Jackson, Correlation of Quantitative Light-induced Fluorescence and Optical Coherence Tomography Applied for Detection and Quantification of Early Dental Caries, Journal Biomedical Optics, 8(4); 642-647; 2003.; 2. Amaechi, A. Podoleanu, G. Komarov, J. Rogers, S. Higham, D. Jackson, Application of Optical Coherence Tomography for imaging and assessment of early dental caries lesions, Laser Physics, Special Issue No.2, Laser Methods in Medicine and Biology, 13(5),703-710, May 2003.

ACKNOWLEDGEMENTS: This research was partially supported by the research grant CNCSIS A 1032/2007 of the Romanian National Authority for Scientific Research.

⁴ Student, Faculty of Dental Medicine, University of Medicine and Pharmacy "Victor Babeş"

Timisoara, Romania

Comparison of Computed Tomography and Microradiography for B-TCP Graft Evaluation after mandibular reconstruction.

M.C.Nolff^{1,2}, H. Kokemüller¹, G. Hauschild^{2,3},M. Fehr², A Kampmann¹, K.Rohn², S. Spalthoff¹, J.-H. Bormann¹,M. Rücker¹, N.-C. Gellrich¹

¹ Department of Oro- Maxillofacial Surgery, Hannover Medical School. ² Small Animal Clinic, University of Veterinary Medicine Hannover, Foundation. ³ Department of Orthopedics, University of Münster.

INTRODUCTION: Among the investigated synthetic bone graft substitutes ceramic materials like Hydroxylapatite (HA) or β-Tricalcium-Phosphate (β-TCP) have proved effective¹. Unfortunately, the close chemical and physical proximity to trabecular bone results in a comparable radiodensity. The reliability of non-invasive, radiological in vivo evaluation methods remains questionable². The aim of the study was to assess reliability and accuracy of computed tomography for evaluation of β-TCP grafted bone defects.

METHODS: Twelve adult black-headed sheep underwent segmental resection and reconstruction of the right hemi-mandible. Animals assigned to group I (n=6) were grafted with blood soaked B-TCP cylinders while sheep assigned to group II (n=6) received blood soaked β-TCP composites loaded with autogenous cancellous bone and bone marrow. The sheep were sacrificed twelve weeks after surgery. The cranium of each animal was scanned in a standard CT scanner and mandibular segments were resected and processed for microradiographic evaluation. Microradiographs were aligned, converted into a serial DICOM dataset and fused with the corresponding CT data (Fig. 1) to allow comparison of ceramic area estimates as well as Hounsfield Units of bone and B-TCP. The t-test and chisquare test were used to compare CT and microradiographic area measurements.

RESULTS Two animals developed inflammation of the graft side and graft dislocation that that was visible on CT images. Affected animals were excluded from further evaluation. Grafts in group I presented moderate ceramic degradation (54 \pm 10 %) and incomplete osseointegration. HU estimates for ceramic material (384-1336 HU) and bony callus (436-1269 HU) were comparable. Statistical comparison of area estimates based on CT and microradiography revealed a significant bias (p<0.05, t-test) and a non-significant variance. Group B achieved bony union of the defects and the B-TCP cylinders underwent profound degradation (94 \pm 3 %). New bone and integrated ceramic remnants presented equal HU (ceramic: 231-981 HU; bone: 168-1356 HU). Statistical comparison of area estimates revealed no significant bias and a significant variance (p<0.05, chi-square test).



Fig. 1: Microradiograph (A), CT image (B) and Fusion of both (C).

DISCUSSION & CONCLUSION: Our results indicate that a reliable quantification of ceramic degradation or new bone deposition within a β-TCP graft is not possible with conventional CT. Both, ceramic material and bony callus present a comparable density and the resolution of standard CT images does not allow visualization of the three-dimensional microstructure. Area estimates either showed significant differences of mean values (group I) or significant variance (group II). Ceramic bone graft substitutes are already commonly used for various surgical indications but until today only one comparable study exists³. We need to continue to verify in vivo diagnostic methods for bone graft evaluation to optimize post surgical patient care.

REFERENCES: [1] Blokhuis TJ, Termaat MF, den Boer FC, Patka P, Bakker FC, Haarman HJ. Properties of calcium phosphate ceramics in relation to their in vivo behavior. J Trauma 2000;48(1):179-86. [2] Goldstein SA. Tissue engineering: functional assessment and clinical outcome. Ann N Y Acad Sci 2002;961:183-92. [3] Mankani MH, Kuznetsov SA, Avila NA, Kingman A, Robey PG. Bone formation in transplants of human bone marrow stromal cells and hydroxyapatite-tricalcium phosphate: prediction with quantitative CT in mice. Radiology 2004;230(2):369-76.

ACKNOWLEDGEMENTS: The authors want to thank IVS Solutions providing the needed software and technical assistance.

PMOXA-based dual-functional antimicrobial surfaces

B. Pidhatika, R. Konradi, S. Al-Bataineh, M. Textor

Laboratory for Surface Science and Technology, Department of Materials, ETH Zurich, Switzerland.

INTRODUCTION: Millions of implants are surgically implanted every year with high expectations of biomaterial performance from surgeons and patients. However, bacterial infection presents a serious concern for human implant surgery, which can lead to the need for reoperation. Thus, there is high interest in developing new antimicrobial coatings to fight bacterial infections. Recently, we have published a report where we presented poly(2-methyl-2oxazoline) (PMOXA) as a non-fouling polymer, potential PEG substituent for rendering surfaces resistant to protein adsorption¹ and bacteria adhesion². Our current research aims at developing combined biopassive-bioactive (dual-functional) antimicrobial platforms, where antimicrobial compound (bioactive) will be immobilized on top of inert (biopassive) PMOXA-coated metal oxide surfaces (figure 1).

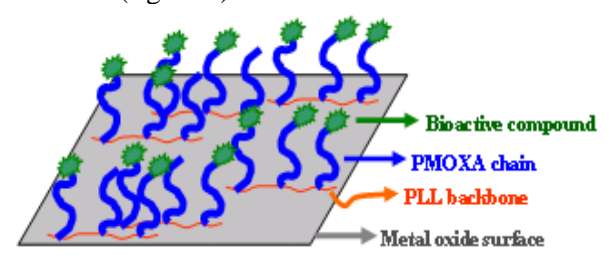


Figure 1. Schematic diagram of PMOXA-based antimicrobial coating

METHODS: PMOXA was synthesized through the living cationic polymerization of 2-methyl-2oxazoline as previously reported¹. This type of chemistry enables the incorporation of functional groups at defined positions along the polymer chain. Alkyne functionality was introduced to the PMOXA chain at α-terminus by initiating the living cationic polymerization of 2-methyl-2oxazoline with a propargylic-initiator. The reaction was terminated with carboxy derivative-terminator; this allows grafting of the polymeric chain from the β-terminus to poly(L-lysine) (PLL) backbone, resulting in graft copolymer, that is alkynyl PLL-g-PMOXA. The chemical structure of the resulted polymers was characterized by NMR and MALDI-"Click" TOF. chemistry is utilized bioconjugation between alkynyl PMOXA and azide-functionalized antimicrobial agent (in our case antimicrobial peptides). Surface modification is based on spontaneous assembly from aqueous buffer solutions. Optical Waveguide Lightmode Spectroscopy (OWLS) was used to *in-situ* monitor polymer adsorption onto metal-oxide coated waveguides and the subsequent exposure to full human serum.

RESULTS: We have synthesized alkynyl PLL-g(3.2)-PMOXA and NMR has confirmed the expected chemical structure. The grafting ratio of 3.2 was chosen based on our previous results¹ (i.e. grafting ratio that gave high adsorbed polymer mass and low protein adsorption). OWLS measurements showed that the polymeric coatings of alkynyl PLL-g(3.2)-PMOXA are protein resistant, where the detected masses were 220 ng/cm² for copolymer and < 2 ng/cm² for protein. Moreover, the results from first trials on developing protocols for bioconjugation by means of "click" reaction on model compounds look promising, as shown by NMR.

CONCLUSIONS: Alkynyl PLL-*g*-PMOXA with grafting ratio of 3.2 was synthesized and the polymer bulk structure was characterized. OWLS confirmed the nonfouling properties of the synthesized alkynyl PLL-*g*-PMOXA polymer.

OUTLOOK: Our efforts are now focused on establishing protocol for "click" reaction on model compounds and then applying it for bioconjugation of antimicrobial peptides and alkynyl PLL-g-PMOXA. Then perform detailed surface characterization on the resulted surfaces before investigating their biopassive and bioactive properties.

REFERENCES:

- ¹ R. Konradi, B. Pidhatika, et al (2008) *Langmuir* **24**(3):613-616.
- ² Pidhatika, B.; Möller, J.; Vogel, V.; Konradi, R. CHIMIA International Journal for Chemistry 2008, in press.

ACKNOWLEDGEMENTS: Financial support from Swiss National science Foundation (SNSF) is gratefully acknowledged.

Suitability of flow composites as adhesives in bonding fiber reinforced composites for orthodontic retention. An in vitro study.

L. Brauchli, S. Pintus, A. Wichelhaus

Clinic for Orthodontics and Pedodontic Dentistry, University of Basel, Switzerland.

INTRODUCTION: Fibre reinforced composites are now becoming available for orthodontic use. However little is known about the bonding properties of available FRC for orthodontic retainers. This study was to investigate the shear bond strengths of an FRC retainer to different flowable composites.

METHODS: EverStick® ORTHO FRC retainer sticks were tested against five different flowable composites (Grandio® Flow, Synergy® Flow, Tetric® Flow, Tetric® Flow Chroma, Unitek Transbond LR®) for their adhesive properties. Each group contained 15 probes. The composite FRC interface had a rectangular surface of 1 x 5mm and the probes underwent 1000 aging cycles between 5 and 55°C. An Instron 4444 was used to measure shear bond values of the FRC stick to composite interface.

RESULTS: Shear forces typically raised to almost 40N (20.4-72.5N) for a 5mm2 contact area between composite and FRC retainer before a fracture occurred. When converted to MPa mean values between 6.5MPa (Tetric Flow) and 8.5MPa (Synergy Flow) were obtained with standard deviations ranging between 1MPa (Tetric Flow) and 2.9MPa (Synergy Flow). Comparing the adhesive properties of the five different groups no significant differences were found (p>0.05).



Fig. 1: Retainer side of the fraction zone (50x magnification). The glass fibres lay bare from surrounding EverStick composite/PMMA matrix.

The fracture zone of all probes is characterized by composite splinters adhering to free glassfibres of the EverStick Ortho retainer (Fig 1). As the huge majority of glassfibres did not break off the retainer, only few glassfibres remained on the sheared off composite block. We could not determine whether the composite splinters were originating from the EverStick composite or from the five tested composite groups.

DISCUSSION & CONCLUSIONS: FRC retainers are a highly esthetic alternative to multistranded wire retainers. High transparency allows for a very incisal placing and might thus enhance gingival health and structural resistancy against acting on forces. Another advantage may be a cost reduction since no technician is involved in the fabrication of the retainer.

Shear forces measured in this study indicate that enough bonding strength can be expected from all combinations of flowable composites and the EverStick® ORTHO FRC. The fracture always occurred within the retainer itself and not at the retainer composite interface. Therefore, the major problem remains the stable integration of glass fibers into the adhesive matrix, even with an industrially silanized retainer.

REFERENCES: ¹M. Diamond (1987) *J Clin Orthod* 21, 182-183. ² J.W. Freudenthaler, G.K. Tischler, C.J. Burstone (2001) *Am J Orthod Dentofacial Orthop* 120(6), 648-653. ³ A. Tezvergil, L.V.J. Lassila, A. Yli-Urpo, P.K. Vallittu (2004) Acta Odontol Scand 62 (1), 51-60. ⁴ M. Geserick, J. Ball, A. Wichelhaus (2004) *J. Clin. Orthod.* 38: 560-562

. **ACKNOWLEDGEMENTS:** We would like to thank those manufacturers who supplied us with materials.

Control of the hydrophilic/hydrophobic interaction balance in the processing of chitosan physical hydrogels for tissue engineering

S. Popa-Nita¹, A. Montembault¹, P. Alcouffe¹, C. Rochas², L. David¹, A. Domard¹

¹Université de Lyon, Université Lyon 1, UMR CNRS 5223 IMP, Laboratoire des Polymères et Biomatériaux, Bât. ISTIL, 15, bd Latarjet, F-69621Villeurbanne Cedex, France

²Université Joseph Fourier de Grenoble, Laboratoire de Spectrométrie Physique, CNRS UMR 5588, B.P. 87, 38402 St. Martin d'Hères, France

INTRODUCTION: Chitosan, natural glycosaminoglycan fully absent in mammals, exhibits the rare property of bioactivity. We developed a new family of biomaterials based on chitosan physical hydrogels for tissue repair and tissue engineering¹ (skin, cartilage, blood vessels, bone..). The polymer network of such hydrogels results only from intermolecular physical crosslinks (hydrogen bonding, hydrophobic interactions, nanocrystallites) without any toxic chemical crosslinking agent. To obtain such hydrogels, a control of the hydrophilic /hydrophobic (H/H) interaction balance in chitosan solutions had to be achieved.

METHODS: The initial chitosan, produced from squid pens, had a low content of N-acetyl-D-glucosamine residues, *i.e.* a degree of acetylation $DA=(1.5\pm0.1)\%$, and a high weight-average degree of polymerisation: $DP_w=3106\pm64$. After a first step of purification, chitosans of different DAs were prepared from the reacetylation under soft conditions of the initial chitosan. Polyelectrolyte chitosan acetate solutions were obtained by stoechiometric protonation of the amine moieties.

RESULTS: The detailed study of the so-called "polyelectrolyte peak", revealed by Small Angle Synchrotron X-Ray Scattering diagrams for aqueous solutions of different concentrations allowed the identification of two organization regimes^{2,3}.

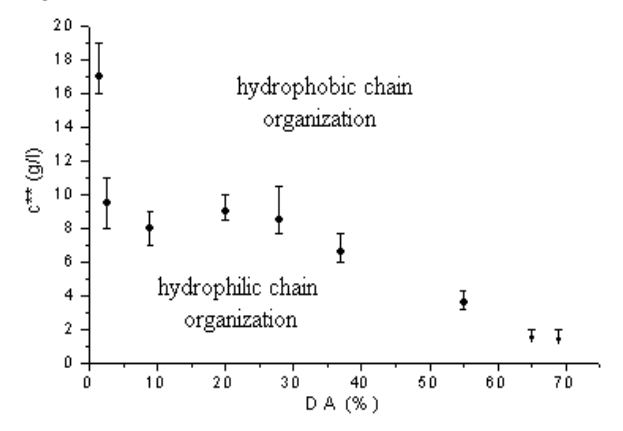


Fig. 1: Law of variation of the crossover concentration c** as a function of DA in chitosan acetate solutions (ESRF D2AM)

In the hydrophilic regime at low polymer concentration, the polymer exhibits conformation of a highly charged polyelectrolyte. In the hydrophobic regime, interchain interactions are favored and then nano-aggregates are present. The crossover concentration (c^{**}) associated to this structural transition is then considered as a way to characterize the H/H interaction balance³. Gelation takes place at a critical value of the H/H interaction balance, either by solvent exchange or by neutralisation of the NH₃⁺ moieties. Therefore, if nano-aggregates are present in the initial solution then, during the gelation stage, they collapse to form a nanostructured gel.

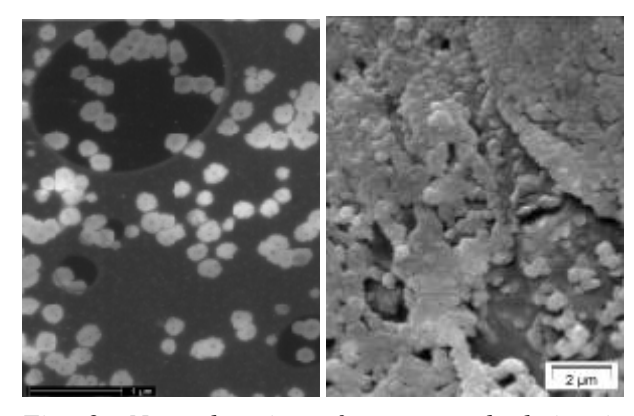


Fig. 2: Nano-domains of aggregated chains in chitosan solutions (left) and hydrogels (right).

DISCUSSION & CONCLUSIONS: The control of the H/H interaction balance in chitosan solutions and during gelation allowed the processing of physical hydrogels with a wide range of mechanical properties, offering promising results in the regeneration of tissue like skin or cartilage³.

REFERENCES: ¹A. Montembault *et al.* (2006), Biochimie **88**: 551-64 ²N. Boucard *et al.* (2007), *Biomacromolecules* **8**: 1209-17. ³S. Popa-Nita *et al.* (2008) *To be published.*

ACKNOWLEDGEMENTS: These studies are part of the NanoBioSaccharides project from the 6th European Framework Program.

The importance of heat treating nickel based alloys used in fixed prostheses technology

S.Porojan, L.Sandu, F.Topală, C.Borțun

"V. Babeş" University of Medicine and Pharmacy, Timişoara, Romania.

Affected

INTRODUCTION: Nickel alloys may be subjected to different types of pre- and post-weld heat treatments, depending on the chemical composition, fabrication requirements intended use. Ni-Cr alloys used in dental technology belong to the precipitation hardened alloys and their mechanical properties are developed by heat treatment to produce a fine distribution of particles in a nickel rich matrix [1-4]. The purpose of the study was to evaluate the effect of heat treatments on microplasma welded Ni-Cr alloys with different composition used in dental technology, by metallographic analyses and microhardness tests.

METHODS: The casting alloys used in this study were Ni-Cr alloys: Wirolloy (Ni 63.2, Cr 23.0, Fe 9.0, Mo 3.0, Si 1.8, C < 1.0, Bego, Bremen, Germany), Wirolloy NB (Ni 67.0, Cr 25.0, Si 15.0, Mo 5.0, Mn, Nb, B, C <1.0, Bego, Bremen, Germany). For the experimental study 16 plates were cast conventionally using an induction melting centrifugal casting machine Orcacast (Π dental, Budapest, Hungary). Half of them were coold slowly at room temperature and half quickly, quenching them in cold water. After casting, the plates were divested, air abraded with 250µm Al2O3 particles, grinded and prepared for welding by polishing and degreasing. The plates were matched and welded using microplasma Welder (Schütz-Dental, Rosbach, Germany). specimen was bilaterally welded in a butt joint configuration, with a spot overlapping of more than 60%, using 0.5 mm in diameter wolfram electrode for joining and 1 mm diameter for surface fining. The pulse delay was maintained at 30 ms and the argon quantity at 5-6 l/min in all cases. The used power step was 8 for joining and 4 for fining. Half of the welded specimens were heat treated using a furnace (Sirio 720S, Sirio Dental, Meldola, Italy), 60 min at 800°C and then cooled uniformly to room temperature. They were analyzed metallographic, and the microhardness was determined in the base metal (BM), weld metal (WM) and heat affected zone (HAZ).

RESULTS: Cracks appear along the joining line and are propagated along the grain boundaries (Fig. 1). The cracks and the modification of the microstructure due to the rapid heating and

solidification process can be a real problem and affect the quality of the weld.

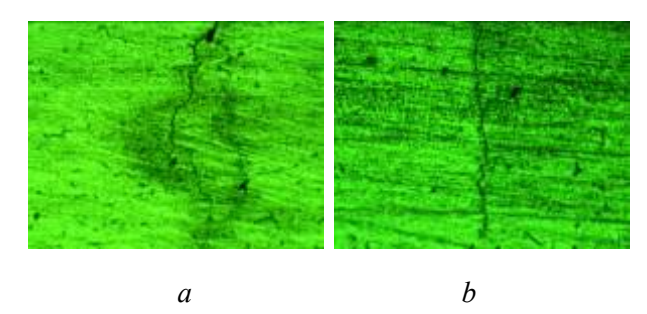


Fig. 1. Metallographic aspect of a crack in the WM for: a. Wirolloy, b. Wirolloy NB.

The dendritic microstructure of the BM became finer especially for Wirolloy (Fig. 2) and the microhardness values decreased after after heat treatments for Wirolloy and increased for Wirolloy NB.

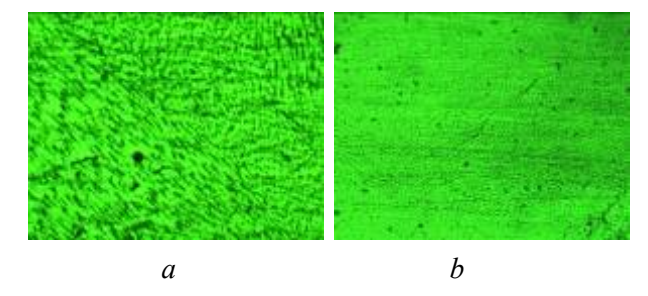


Fig. 4. Metallographic aspect of the WM: a. before heat treatment, b. after heat treatment.

DISCUSSION & CONCLUSIONS: Even the chemical composition of the alloys was similar; their behavior at heat treatment was different. Therefore it is important that the heat treatments procedures be particularized for each alloy type. The microhardness reduction was obtained only for Wirolloy. Regarding the metallographic structure, the most affected by heat treatment was the same alloy.

REFERENCES: ¹ H.J. Burkhardt (2005) *Quintessenz Zahntech* 31(2): 136-42. ² R.S. Funderburk.(1998) *Welding Innovation* XV(2). ³ I.Watanabe, J.Liu, N.Baba, T.Okabe (2004) *Dent Mater* 20(7): 630-4. ⁴ I.Watanabe, A.P. Benson, K.Nguyen (2005) *J Prosthodont* 14(3): 170-4.

European Cells and Materials Vol. 16. Suppl. 1, 2008 (page 46) **ACKNOWLEDGEMENTS:** This study was supported by the Grant CNCSIS_171 from the Ministry of Education and Research, Romania.

ISSN 1473-2262

Surface Modification of PEEK to Aid Primary Human Osteoblast Attachment and Functionality Alexandra H.C. Poulsson¹, R. Geoff Richards^{1,2}

¹AO Research Institute, Davos, CH. ²Cardiff School of Biosciences, Cardiff University, UK.

Introduction: Polyetheretherketone (PEEK) has due to its high strength, good wear and radiolucent properties come into the spotlight as a replacement for metals in devices such as spine cages and craniomaxillofacial (CMF) implants¹. X-ray and MRI evaluation of soft and hard tissue integration to implants can be obscured or distorted by the presence of the metal devices. Several implants have therefore been re-designed in PEEK to allow ease of visualisation. However, cellular attachment to polymers such as PEEK is restricted due to its low surface energy, which can lead to implant loosening, as a result of fibrous encapsulation. To aid cell attachment the surface energy can be increased by plasma surface treatment. The importance of surface oxygen for cell attachment is well established⁴, though the effect of the specific oxygen functional groups such as alcohol/ether(C-OR), carbonyl (C=O) and carboxyl (O-C=O) is less understood and has been shown to vary depending on cell type^{2,3}. The present study aims to investigate the effect of these functional groups on the attachment and functionality of primary human osteoblast-like cells (HOB).

Materials and Methods: Injection moulded PEEK OptimaTM discs (Invibio) with a 13mm diameter were modified by radio frequency (RF) plasma treatment, Thermanox (Nunc) and Ti ISO 5832/2 (Synthes) were used as the control surfaces. Using an EMITECH RF plasma treater, the samples were exposed to varying treatment times. Surface chemical compositions of treated and untreated surfaces were characterised by XPS, wettability by contact angle; topographic changes by AFM and SEM. HOB cells isolated from femoral heads removed during total joint replacement operations were grown to 70-80% confluence in DMEM (10% FCS in 5% CO₂ at 37°C), and plated at 10000 cells/cm². Alpha-MEM (0.1µM dexamethasone and 10mM betaglycerophosphate) was used as mineralisation media over 21 days. Cell functionality was assessed by alkaline phosphatase expression (ALP), mineralisation by Alizarin red S staining of calcium, cell attachment by SEM and cell density through alamar Blue $^{\mbox{\scriptsize TM}}$ assav.

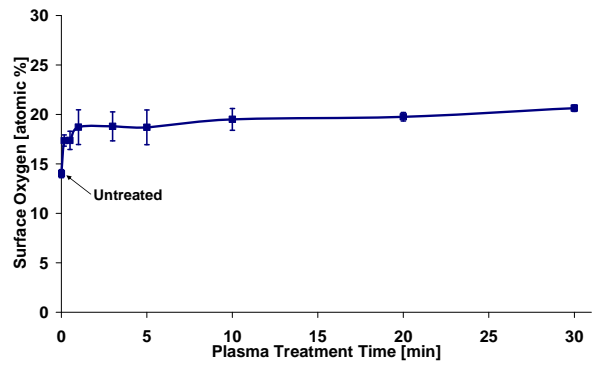


Figure 1: Surface oxygen concentration of PEEK surfaces with increasing plasma treatment time.

Results: XPS analysis of the untreated PEEK showed the presence of 14 atomic% surface oxygen, indicating that these surfaces are relatively hydrophobic in character. The treated PEEK surfaces showed the

surface oxygen concentrations to increase with increasing treatment time up to ~20 atomic%, figure 1. High resolution C1s spectra showed a greater increase in C-OR type functional groups than C=O and O-C=O with increasing treatment time. To study the effects of surface treatment on cell attachment and functionality, the cells were observed after plating on the treated and untreated PEEK, THX and Ti discs. Within 24hrs, the treated surfaces were shown to have higher cell densities than the untreated surfaces. By day 21 the treated surfaces were shown to have similar cell densities to Ti. Initial findings indicate that surfaces with higher C-OR and lower C=O and O-C=O functional group concentrations have higher initial HOB cell attachment and this trend continues to day 21, in contrast to the surfaces with lower C-OR and higher C=O and O-C=O concentrations.

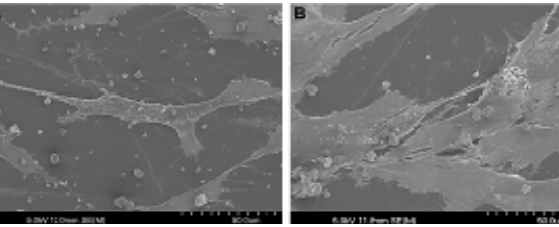


Figure 2: *SE micrographs of cellular attachment after 3 days culture, a) untreated PEEK and b) treated PEEK.*Cells were also observed by SEM to attach more readily to the surfaces with higher concentrations of C-OR functional groups, figure 2, where a) shows the typical attachment to the untreated surfaces and b) shows the typical more flattened attachment on the surfaces with higher CO-R concentrations. ARS staining and ALP expression were observed to be more characteristic on the surfaces with higher concentrations of C-OR functional groups.

Discussion/Conclusions: This study shows that the incorporation of oxygen with plasma treatment can be used to increase the surface energy and thereby aid the adhesion of cells. These findings indicate that the overall influence may be an optimal concentration of C-OR, and the C=O and O-C=O type functional groups are less influential on HOB cell attachment and functionality. Over the 21 day period the HOB cells were shown to behave characteristically on the treated surfaces and by day 21 the ALP expression was higher than on the untreated surfaces and similar to the levels observed on Ti.

References: ¹Kurtz, S.M. and Devine, J.N. Biomat., 28, 4845, 2007. ²Curran, J.M., et al.: Biomat. 27:4783-4793, 2006. ³Mitchell, S.A., et al. Biomat. 25:4079-4086, 2004. ⁴Curtis, A.S. et al.: J.Cell Biol. 97:1500-1506, 1983.

Acknowledgments: Invibio Ltd for partially financing and providing PEEK discs for the study. Synthes for providing Ti discs. P. Furlong and C. Sprecher for help with microscopy and SEM. Dr S. Milz for consultation on histological techniques. Dr N. Gadegaard and the CCE, Glasgow University, for kind use of AFM facilities. RMS, Bettlach for XPS analysis.

Confocal Microscopy and *en-face* C-scan OCT investigations in Class V Composite Restorations

Mihai Romînu¹, Zeno Florița¹, Michael Hughes², George Dobre², Cosmin Sinescu¹, Adrian Bradu², Adrian Gh. Podoleanu²

UMF "Victor Babes" Timisoara, Faculty of Dentistry, Department of Prostheses Technology and Dental Materials, ² Applied Optics Group, University of Kent, Canterbury, UK

INTRODUCTION: There are several methods for evaluating microleakage in class V composite restorations such as bacterial penetration, fluid transport, clarification, radioisotope penetration, electrochemical methods and gas chromatography. Dye penetration tests, however, seem to be the most widely used. The purpose of this study is to evaluate gap formation in class V composite filled cavities using a non-invasive method – optical coherence tomography.

METHODS: The optical configuration uses two single mode directional couplers with a superluminiscent diode as the source at 1300 nm. The scanning procedure is similar to that used in any confocal microscope, where the fast scanning is *en-face* (line rate) and the depth scanning is much slower (at the frame rate) [3]. The *en-face* scans provide an instant comparison to the familiar sight provided by direct view or via a conventional microscope [4].

RESULTS: Gap forming in class V cavities can be evaluated by the OCT technique and with a system resolution of 10 µm we were able to detect gaps as small as 50 µm, but only those of a few micrometers would be experimentally measurable. Imaging gaps narrower than 10 µm requires improvements in our incoherent light source. Furthermore, the use of OCT has the advantage of showing the restored region as well as the gap, if it exists, and precisely localizing its position, as demonstrated here. Exploration of the recent advances in OCT in terms of different excitation wavelengths and wider bandwidths can lead to state-of-the-art imaging systems in conservative denistry enabling imaging of both enamel and dentin. Finally, as demonstrated in the literature, in vivo and real-time OCT images can be obtained. and therefore this method of assessment is potentially useful for clinical diagnostics.

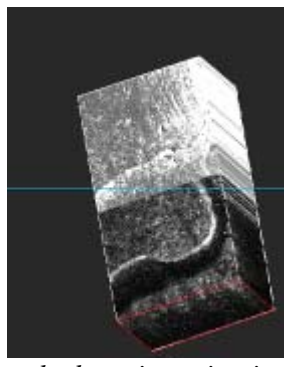


Fig. 2: Microleakage investigation of class V composite restorations: the confocal microscopy investigation (upper image) and the en-face OCT scan (lower image). 3D reconstruction of the gap between the composite filling and the cavity.

DISCUSSION & CONCLUSIONS: OCT has numerous advantages which justify its use in the oral cavity in comparison with conventional dental imaging. OCT can achieve the best depth resolution of all known methods (in principle 1 micron if the source exhibits a sufficiently wide spectrum) and is safe. The role of confocal microscopy is to precisely locate the area on which the OCT system will allow depth image generating in a non-invasive manner.

¹B.T. **REFERENCES:** Amaechi. A.Gh. Podoleanu, S.M. Higham, D. Jackson [2003] Correlation of Quantitative Light Flourescence and Optical Coherence Tomography Applied for Detection and Quantification of Early Dental Caries. Journal Biomedical Optics. ²Tay FR, Pashley DH [2001] Aggressiveness of contemporary selfetching systems I: Depth of penetration beyond dentin smear layers. Dental Materials: 17:296. ³ B R Masters Three-Materials.;17:296. B. R. Masters, Threedimensional confocal microscopy of the human optic nerve in vivo, Opt. Express, 3, 356-359 (1998),

http://epubs.osa.org/oearchive/source/6295.htm. ⁴ J. A. Izatt, M. R. Hee, G. M. Owen, E. A. Swanson, and J. G. Fujimoto, *Optical coherence microscopy in scattering media*, Opt. Lett. 19, 590-593 (1994).

Investigation of the Bond Strength of Aesthetic Brackets on Human Enamel - an Innovative Approach

Roxana Otilia Romînu¹, Cosmin Sinescu¹, Mihai Rominu¹, Meda Negrutiu¹, Mike Hughes², Adrian Bradu², Dorin Dodenciu¹, Philippe Laissue⁴ Sorin Mihali³, Adrian Gh. Podoleanu²

¹ UMF "Victor Babes" Timisoara, Faculty of Dentistry, Department of Prostheses Technology and Dental Materials, ² Applied Optics Group, University of Kent, Canterbury, UK, ³ Kent Institute of Medical and Health Science, Canterbury, UK, ⁴ student, UMF "Victor Babes" Timisoara, Faculty of Dentistry

INTRODUCTION: In orthodontic literature there is very much research published on bonding brackets or other type of attachments since any treatment can fail or be unduly prolongued in spite of good diagnosis and treatment plan if bonding is not done properly. Because of the increase of the mean age of orthodontic patients, a new set of problems have arised, such as bonding brackets to prosthodontic restorations as ceramic crowns or veneers and using aesthetic brackets instead of metal ones. Orthodontic bonding is done primarily with composite resin but can also be performed using glass ionomer or resin cements. The bond strength of the bracket-tooth interface is improved by conditioning of the buccal (or lingual) tooth surface with acids (H₃PO₄ for enamel and HF for ceramics). In our study we investigated and compared the quality of bonding between ceramic polymeric brackets and enamel, brackets, respectively using a combined method - OCT [1,2,3,4] and confocal microscopy.

The aim of out study was to evaluate the resin layer at the brackets base - tooth interface.

METHODS: We used 100 permanent crack- and caries free permanent teeth that were kept in demineralised water at in the refrigerator until the moment of making the samples. All teeth were cleaned with pumice and rotary brushes. In order to maintain constant quality of the samples brushes were changed after every fifth tooth with new ones. After cleaning the teeth acid etched and brackets were bonded conventionally with composite resin.

The bonding protocol was identical for both types of brackets (ceramic and polymer). We bonded ceramic brackets on 50 teeth (group1) and polymer brackets on the rest of teeth (group2).

The two groups were all investigated using OCT at 1300 nm and confocal microscopy (figure 1).

RESULTS AND DISCUSSION: Following the OCT investigation gaps were found in both sample groups. In group1 (ceramic) we found 6 gaps (12%) and in group2 there were detected only 4 (8%). Group 1 presented slightly larger gaps. We

consider that the defects found might have been produced as a consequence of human error.

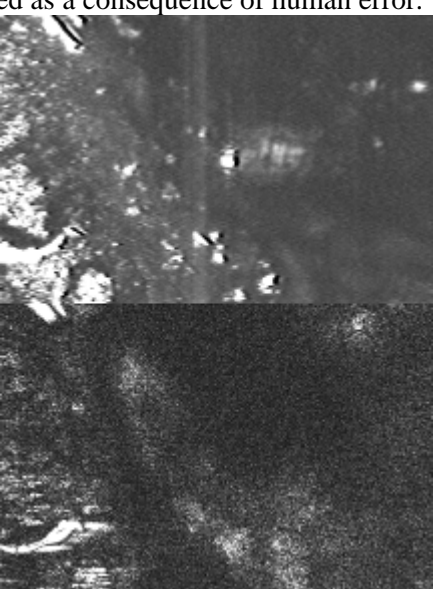


Fig. 1. Defects inside the bonding material investigated with confocal microscopy (upper image and en face OCT scaning (below)

CONCLUSION: Further studies are necessary to determine whether indirect bonding would minimize the error rate.

REFERENCES: ¹B.T. Amaechi, A.Gh. Podoleanu, S.M. Higham, D. Jackson (2003) Correlation of Quantitative Light Induced Flourescence and Optical Coherence Tomography Applied for Detection and Quantification of Early Dental Caries. Journal Biomedical Optics. ²B. T. Amaechi, A.Gh.Podoleanu, G. Komarov, J. Rogers, S. Higham, D. Jackson (2003) Application of Optical Coherence Tomography for Imaging and Assessment of Early Dental Caries Lesions. Laser Physics, Special Issue No.2, Laser Methods in Medicine and Biology, Vol.13, No.5 703-710. ³D. Huang, E.A. Swanson, C.P. Lin, J.S. Schuman et al.(2000) Optical Coherence Tomography, Science 1991 254:1178-11812000. ⁴A. Gh. Podoleanu, J.A. Rogers, D.A.Jackson, S. Dunne Three Dimensional Images from retina and skin. Opt. Express, Vol.7, No.9, p.292-298.

Errors in full dentures casting

L.C. Rusu¹, L. Ardelean¹, C. Bortun¹

¹, Victor Babes" University of Medicine and Pharmacy Timisoara, Romania.

INTRODUCTION: Casting full dentures represents nowadays an alternative to the classical manufacturing of full dentures by barothermopolymerisation, as well as to modern [1,2].injection techniques Acrylic autopolymerisable resins, suitable for casting, have a characteristic casting temperature below 65°C, being prepared in a firmness suitable for casting.

METHODS: The authors used the Vertex casting system, and the specific acrylic resin Castapress (Vertex dental B.V., Zeist, Netherlands). The method includes the classical steps of the manufacturing technology for full dentures, to the final pattern step [3]. A special flask and a reversible hydrocolloid or a silicone material are used in investing the final pattern (fig. 1). After the setting of the impression material, the flask is unwrapped, the model being removed together with the denture base pattern. The wax remains on artificial teeth are cleaned using the special Clean-Tray device (fig. 1).

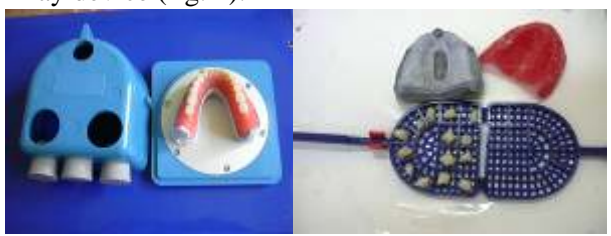


Fig. 1: The final pattern, prepared for wrapping (left), the mold, the denture's base pattern and the artificial teeth in the Clean-Tray device (right).

The teeth are repositioned in the already created investment (fig. 2). The acrylic resin is prepared and poured in the flask through the special orifice, until it is full. Afterwards the polymerisation of the denture is carried out, by immersing it in a special polymerisation pot, filled with water at 50+/-5°C, at a pressure of 2,5 barr, for 30 minutes. Finally, the denture is extracted from the investment, with minimal subsequent adjustments (fig 2.)



Fig. 2: The teeth repositioned in the investment (left), the unwrapped denture (right).

RESULTS: The deficiencies appear mostly when using reversible hydrocolloids (not detected when using a silicone material), because of the air bubbles which develop when pouring the material into the flask (fig. 3). If we try to eliminate these bubbles by pressing the flask, it may result in the melting of the wax pattern (fig.3).



Fig. 3: Bubbles in the reversible hydrocolloid (left), melting of the wax pattern (right).

The deficiences may also develop due to the air incorporation when pouring the acrylic resin into the investment, and they appear as porosities on the mucosal surface of the denture (fig.4). In other cases the dentures appear incomplete, due to the short working time of the resin used and too early setting (fig.4).



Fig. 4: Porosities on the mucosal surface of the denture (left), lack of substance (right).

DISCUSSION & CONCLUSIONS: The system has the following advantages: the reversible hydrocolloid may be reused, reduced polymerisation time, the wide chromatic range of the material (10 colours), minimal adjustments required. The disadvantages are: high cost of the system; in case of retentive fields, problems may occur when unwrapping; possible errors may also occur in teeth positioning. When using a new technology, one has to consider the advantages and disadvantages of the system. We pointed the possible errors which might occur when casting full dentures, using Vertex: porosities on the mucosal surface or lack of substance.

REFERENCES: ¹M.Pilecki, W. Behaeghel, D. Bechaeghel (2006) *Dentis* **2**: 26-29. ²A. Parvizi, T. Lindquist, R. Schneider, et al (2004), *J Prosthodont* **2**: 83-89. ³M. Cordos (2002) *Tehnica Dentara* **2**: 12-13.

3D modeling and stress distribution in cast and combination dental clasps

L.Sandu¹, F.Topală¹, N.Faur², S.Porojan¹, C.Borţun¹

¹ "V. Babeş" University of Medicine and Pharmacy, Timişoara, Romania. ² Politehnica University, Timişoara, Romania.

INTRODUCTION: Cast and combination clasps are widely used in removable partial dentures technology [1-3]. The aim of the study was to achieve 3D models in order to develop applications for basic research use, to design and optimize dental clasps.

METHODS: Enlarged plaster teeth (scale 10:1) were scanned using LPX-1200 Picza Laser Scanner (RolandDG Corporation, Japan). Resulted files were imported in LeiosMesh (Enhanced Geometry Solutions Corporations, Italy), where the point clouds from the teeth surfaces were cleaned and assembled. The collected data were used to construct three dimensional models using Rhinoceros (McNeel North America) NURBS (Nonuniform Rational B-Splines) modeling program. The models were reduced to the natural size in order to obtain a normal size of the teeth and clasps. The resulted solid was tilt in order to obtain functionally effective tooth contours. The height of contour was designed and an adjuvant plane was generated to relieve the surface located +/- 0.25 mm from the height of contour (Fig. 1).

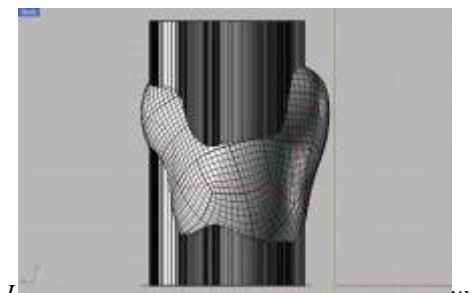


Fig. 1. Height of comour designed on the room surface.

The 3D models were used as a support for clasp modeling (Fig. 2).



Fig. 2. 3D clasp modeling.

Purposely designed experimental three-dimensional models of the clasp arms were constructed on the teeth surface and exported in Ansys finite element analysis software (Ansys Inc., Philadelphia, USA), to be used for structural simulations. All nodes at the base of the clasp retentive arm were restrained in all directions and a concentrated load of 5 N was applied at the inner tip of the clasp arm.

RESULTS: Generated stresses and deformations were calculated numerically and plotted graphically. Results

were displayed as colored stress contour plots to identify regions of different stress concentrations. High stress values were present on the inner surface of the clasp arm, in the part located above the height of contour for the cast arm and near to the base for the wrought wire arm (Fig. 3).

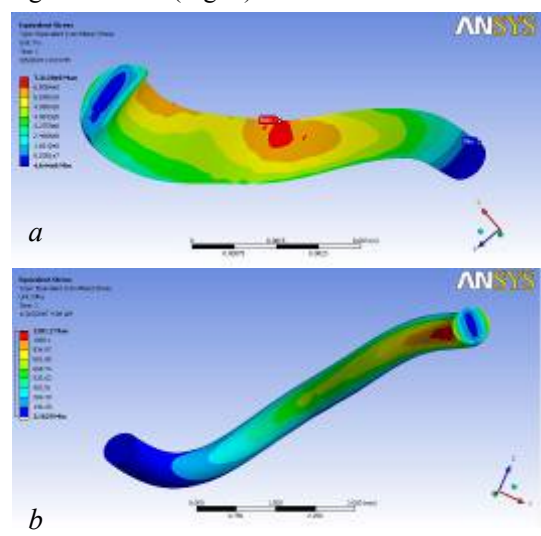


Fig. 3. Stress distribution in the retentive arm of the clasp: a. cast, b. wrought wire.

DISCUSSION & CONCLUSIONS: This in vitro study demonstrated that structural analyses of cast clasps may offer a powerful tool in order to vizualize fracture risk areas. It ensures optimal performance in selection of an adequate clasp design according to each clinical case.

REFERENCES: ¹ A.A. Mahmoud, N. Wakabayashi, H. Takahashi (2007) *Dent Mater* 23(3):317-24. ² R.C.S. Rodrigues, R.F. Ribeiro, M.G. Chiareloo de Mattos, O.L. Bezzon (2002) *J Prosthet Dent* 88:290-296. ³ L.Sandu, C. Borţun, N. Faur, S. Porojan (2006) *Saudi Dental Journal* 18(2):100-4.

ACKNOWLEDGEMENTS: This study was supported by the Grant ID_1264 from the Ministry of Education and Research, Romania.

Corrosion resistance measurements of dental alloys

Fredy Schmidli¹, Markus Büchler², Markus Jungo¹, and Bert Müller¹

¹ Materials Science Institute, Dental School, University of Basel, Switzerland.
² Swiss Society for Corrosion Protection, Zürich, Switzerland.

INTRODUCTION: Metals and metallic alloys still belong to the vital materials in dentistry, as they provide the necessary mechanical stability and elasticity to fabricate designated constructs. Several patients, however, complain of incompatibility owing to corrosion of the applied metals. Consequently, the metallic parts are *in vitro* tested electrochemically to determine their resistance to corrosion. The better approach, however, are in vivo measurements. In vivo studies require the specific set-up accounting for the limited space, accessibility and restricted treatment period. Hence, the ec-pen¹ has recently been developed.

METHODS: The field study is based on the ecpen that consists of two electrodes located in the electrolyte reservoir. Pushing the tip towards the metal part of interest, electrolyte is released to wet the surface. This rather simple and fast procedure allows for electrochemical measurements, as in the present study performed with six dental alloys. The selected alloys are the Ni-based alloy Remanium CS (Dentaurium, Germany), the Co-based alloys Remanium 2000 (Dentaurum, Germany) and Bärlight (Ahlden GmbH, Germany), the Pd-Ag alloy Est. Actual as well as the Au alloys with higher and reduced concentration Est. Royal and Est. Plus (Cendres&Métaux SA, Switzerland).

RESULTS: The ec-pen permits impedance measurements to determine the corrosion potential and the polarization resistances. Table 1 summarizes the results. As expected, Co- and Nibased alloys exhibit low corrosion resistance, while the noble metals show much better values both in buffered saline and natural saliva. Corrosion and polarization resistance data correlates well with the results of crevice corrosion (cp. Table 1).

DISCUSSION & CONCLUSIONS: The electrochemical measurements using the ec-pen are reproducible and allow differentiating between different dental alloys with respect to their corrosion resistance. The obtained data correspond to the ASTM standard test methods for pitting and crevice corrosion resistance.² Consequently, the relatively simple and small ec-pen is a promising tool for patient-relevant impedance measurements to reveal the metal compatibility in vivo.



Fig. 1: Gingival reaction of tooth 12 caused by metal ions.

Table 1. Corrosion resistance measurements of selected dental alloys.

| Dental alloy | Crevice corrosion [µg] | Impedance resistance [Ωcm ⁻² 10 ⁴] |
|--------------|------------------------|---|
| Au high | 0.21 ± 0.10 | 10.5 ± 3.5 |
| Au reduced | 1.20 ± 0.08 | 9.9 ± 2.2 |
| Pd-Ag | 1.8 ± 0.3 | 3.9 ± 1.2 |
| Co-based (1) | 4.4 ± 2.0 | 3.5 ± 2.5 |
| Ni-based | 24 ± 16 | 2.1 ± 2.2 |
| Co-based (2) | 791 ± 30 | 0.15 ± 0.30 |

REFERENCES: ¹ M. Büchler (2004) *GWA. Gas, Wasser, Abwasser* **84**:575-80. ² ASTM Standard Test Methods for Pitting and Crevice Corrosion Resistance. Designation: G48-76 in: Annual book of ASTM standards, vol. 03.02. Philadelphia, PA, USA: American Society for Testing and Materials, 1995.

ACKNOWLEDGEMENTS: The authors thank the suppliers of the dental alloys for providing the materials for free.

Efficient Delivery of Photosensitizer for Rheumatoid Arthritis (RA) Treatment by Photodynamic Therapy (PDT)

<u>C. Schütz¹°</u>, <u>F.Schmitt²°</u>, <u>L.Lagopoulos²°</u>, <u>N. Rossi³</u>, <u>N. Busso²</u>, <u>L. Juillerat-Jeanneret², C. Wandrey¹, P. Käuper^{1,3}*</u>

°The authors participated equally. ¹ EPF Lausanne, Lausanne, Switzerland. ² CHU Vaudois, Lausanne, Switzerland. ³ Medipol SA, Ecublens, Switzerland. *Corresponding author peter.kaeuper@medipol.ch

INTRODUCTION: Rheumatoid arthritis (RA) is an inflammatory disease involving the destruction of the joints by activated macrophages. The treatments presently available for RA are not perfect and new efficient local treatments with

reduced side effects are desirable.

Photodynamic therapy (PDT) is a powerful tool to treat oncological and inflammatory disorders¹. PDT is based on the injection of a photosensitizer, which is activated by light to produce cytotoxic molecules. For successful application in RA, the locally injected photosensitizer must target joint macrophages.

Biomaterial-based nanoparticles are proposed as system for the uptake of photosensitizer by the joint macrophages. Our proposition is therefore to entrap the photosensitizer in a polymeric nanoparticle to both reduce diffusion of the photosensitizer out of the joint and increase its uptake by joint macrophages.

MATERIALS & METHODS: Nanoparticles were based on chitosan and other natural polysaccharides² known for their biocompatibility. The process of nanoparticle formation and photoactive drug incorporation was entirely waterbased. During formulation the surface properties were designed to target activated macrophages. The final formulation was designed to withstand physiological environments and particularly the specific environment in inflamed joints. The size distribution determined by scanning electron microscopy was between 50 and 300 nm (*Fig. 1*).

Entrapment efficiency of the photosensitizers into the nanoparticle was >98% (w/w). Loading capacity was >15% (w/w).

In vitro experiments: These photosensitizer-loaded nanoparticles were assayed on various cell populations, evaluating their uptake and efficacy in PDT protocols to induce cell death. Uptake of the nanoparticles was observed by fluorescence microscopy and fluorimetric reading. Cytotoxicity was assessed by the MTT survival test.

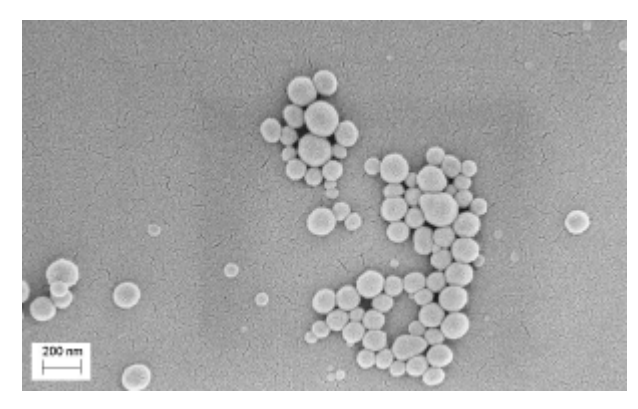


Fig. 1: Electron microscopy (SEM) picture of chitosan based nanoparticles loaded with photosensitizer. Dried from water based dispersion, platinum sputter coated.

In vivo experiments: The albumin-induced arthritis (AIA) model³ was used for *in vivo* test in mice. Inflamed mice knees were injected with the photosensitizer-loaded nanoparticles and exposed to laser light. The level of inflammation of the joints was quantified measuring the serum amyloid A (SAA), an inflammatory acute phase protein.

RESULTS: *In vitro*, optimal uptake of the photosensitizer-loaded nanoparticles was achieved after 3 hr incubation. These nanoparticles did not induce cytotoxicity in the absence of light in the murine RAW 264.7 macrophage cell line, whereas good phototoxic activities were observed in these cells exposed to red laser light.

In vivo, nanoparticles were well tolerated by the mice. Statistical evidence of a decreased status of inflammation after PDT treatment of inflamed mice knees was found using the SAA assay.

REFERENCES: ¹Dolmans, D.E.J.G.J. et *al.*, *Nat. Rev. Cancer*, 2003, 3, 380-387. ²WO2007/031812 (PCT patent). ³Brackertz D. et *al*, *Arthritis and Rheumatism*, 1977, 20, 3, 841-850.

ACKNOWLEDGEMENTS: The research is supported by the CTI, project no. 7985.2 LSPP-LS and the Swiss National Science Foundation, project no 404740-117323/1.

Combined mechanical and corrosion failure mechanism of a tumoral reconstruction hip prosthesis: a case report with SEM evaluation

Sebe Ionela¹, I.Antoniac¹, D.Laptoiu², M Negrusoiu², P.Antoniac¹, R.Istrate³

¹University "Politehnica" of Bucharest, Faculty of Materials Science and Engineering; ² Colentina Clinical Hospital, Department of Orthopedic Surgery and Traumatology, Bucharest, ³Med4Med Group Ltd, Bucharest, Romania

INTRODUCTION: Metallic biomaterials used for total hip replacement surgery are subject to different corrosion and wear mechanisms. The aim of this study is to evaluate the failure causes from the biomechanical and the biomaterials point of view, and study metallurgical changes of some taper junctions of in-vivo loaded modular stems. Modularity is being diversified in total hip prostheses to ameliorate the surgical technique, to optimize implant fixation and adjust hip biomechanics; new reconstructive and minimally invasive techniques require special modular design.

METHODS: One customised implant (DLS®Stryker hip revision stem combined with a retrograde nail for an osteosarcoma resection-reconstruction in a 17 years old patient) was investigated after retrieval following 3 years of invivo use. All contact surfaces of the modular elements were assessed by scanning electron microscopy.



Fig.1: Image of the retrieved customised prosthesis

RESULTS: The retrieved implant showed cracks and a large amount of measured debris; failure patterns were present at the connection area between the two implants. The artisanal morse-type taper junctions failed mechanically, even if corrosion and wear affected all tapers.



Fig.2: Failure zone - macroscopic aspects

Surface analysis and laboratory investigations of previous retrieved hip prosthesis components have proven that the morse taper junctions of the stem are stable and resistant to relevant wear mechanisms. At the connection, the surface displayed typical fatigue fracture patterns; the cause was poor machining with a fatigue crack that yielded to overstress failure under cyclic loading. Periprosthetic bone loss was minimal probably due to short service life of the implant.

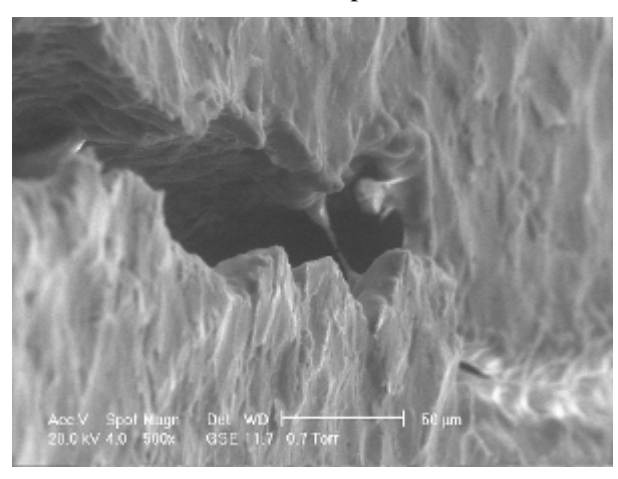


Fig.3: Scanning electron micrographs of the same failure zone (dimpled fractures, a feature of overstress failure)..

DISCUSSION & CONCLUSIONS: If an original taper design is selected, the advantages of modular femoral components in total hip arthroplasty will outweigh the possible risks. Artisanal mechanisms and combinations between implants from different sources are prone to rapid failure due to high mechanical stress and metallic biomaterials with different strenght characteristics. Tumoral reconstruction surgery may require custom made implants, frequently unavailable or too expensive for the current clinical use.

REFERENCES: Pohler OEM failure of metallic orthopedic implants. In Metal Handbook vol 11, Failure Ananlysis and Prevention, 9th Edition Metals Park, OH, ASM, 1987: 670-694

Albumin Adsorption on the Surface of Iron Containing Aluminosilicates

V. Simon¹, S. Cavalu², M. Prinz³, E. Vanea¹, M. Neumann³, S. Simon¹

¹ Babes-Bolyai University, Faculty of Physics & Institute for Interdisciplinary Experimental Research, Cluj-Napoca, Romania. ² University of Oradea, Faculty of Medicine and Pharmacy, Oradea, Romania. ³ University of Osnabrück, Physics Department, Osnabrück, Germany

INTRODUCTION: Aluminosilicate materials present attractive properties for medical application as biomaterials [1]. Among the non-invasive protocols for cancer treatment, hyperthermia received renewed interests [2] and is considered a promising treatment for tumor eradication [3]. Biocompatible ferrimagnetic glass ceramics have been identified as suitable candidates for hysteresis heating [4,5]. The aluminosilicate glass ceramics optimised for hysteresis heating are highly stable in the body. Serum albumin is mainly responsible for the maintenance of blood pH and is associated to the binding and transport of several small molecules such as fatty acids, dyes, metals, amino acids, drugs, as well as several pharmaceutical compounds [6].

This paper reports on proteins uptake on the surface of iron containing aluminosilicate samples tested in simulated body fluids enriched with bovine serum albumin.

Non-crystalline **METHODS:** samples 60SiO₂·20Al₂O₃·20Fe₂O₃ composition obtained by sol-gel method were subjected to partial crystallisation by heat treatment in order to developed proper magnetic crystalline phases. After fine grinding the powder samples were immersed in simulated body fluid (SBF) prepared according to Kokubo composition and in SBF enriched with bovine serum albumin (BSA) in two concentrations obtained by adding 0.1 and 0.2 g lyophilised SBA to 30 ml SBF. The samples immersed were kept under static conditions at 37°C for up to seven days. Fourier transform infrared (FTIR) attenuated total reflectance (ATR) and Xray photoemission spectroscopy (XPS) were used to inspect the albumin adsorption on the sample surface.

RESULTS: The IR results clearly evidence the presence of the protein only on the surface of the sample immersed for 7 days in the 0.67g BSA / 100 ml SBF solution. In the IR spectral region of amide I (1660 cm $^{-1}$) is recorded a new band at 1610 cm $^{-1}$ which is assignable to intermolecular β -sheet structure (or side chains) and indicates the aggregation of the protein. The deconvoluted C 1s and N 1s photoelectron peaks provide more information. From the non-immersed sample only

one single C 1s peak at 285.5 eV is recorded. After one day immersion in SBF the C 1s photoelectron peak is still well fitted with a single line centered at 285.5 eV, but the peak is broadened (2.88 eV) with respect to the non-immersed sample (2.26 eV). The deconvolution of C 1s photoelectron peaks for the samples immersed in SBF solution enriched with BSA leads beside the peak at 285.5 eV to other two components centered at 286.7 and 288.6 eV, but their relative peak areas are notably different (Table 1). The occurrence of nitrogen species is evidenced only after SBF immersion.

Table 1. Percental distribution of differently binded carbons according to C 1s photoelectron peak deconvolution.

| BSA concentration in SBF (g/100 ml) | Binding energy (eV) | | |
|-------------------------------------|-------------------------|-------|-------|
| | 285.5 | 286.7 | 288.6 |
| | Relative peak areas (%) | | |
| 0.33 | 82 | 13 | 7 |
| 0.67 | 51 | 42 | 5 |

DISCUSSION & CONCLUSIONS: X-ray photoelectron spectroscopy appears more sensitive than IR ATR spectroscopy to the changes occurred on the sample surface after immersion in simulated body fluids. The C 1s and N 1s core level XPS spectra show the BSA attachment to the surface of aluminosilicate samples already after one day immersion even in the low BSA enriched SBF.

REFERENCES: ¹ H. Oudadesse, A.C. Derrien, M. Mami et al (2007) *Biomed Mater* **2**:S59-S64. ² H. Gu, K. Xu, Z. Yang et al (2005) *Chem Commun* **34**:4270–72. ³ K.A. Gross, R. Jackson, J.D. Cashion et al (2002) *Eur Cell Mater* **3**S2:114-17. ⁴ M. Kawashita, H. Takaoka, T. Kokubo (2001) *J Ceram Soc Japan* **109**:39-44. ⁵ Y. Ebisawa, F. Miyaji, T. Kokubo et al (1997) *Biomaterials* **18**:1277-84. ⁶ J. Figge, T.H. Rossing, V. Fencl (1991) *J Lab Clin Med* **117**:453-467.

ACKNOWLEDGEMENTS: The present work was supported by the scientific research project CEEX 100/2006 (MATNANTECH) of the Romanian Excellence Research Program.

ESEM Investigation on Osseo Integration of Ti Alloy Implants

M. Tarcolea¹, F. Miculescu¹, S. Ciuca¹, R.M. Piticescu², I. Patrascu³, L.T. Ciocan³

¹ University POLITEHNICA of Bucharest. ² INCDMNR, ³ «Carol Davila » University of Medicine, Romania.

INTRODUCTION: Vanadium free Ti alloy has been developed for biomedical use in orthopedics and dental applications. Interaction of the implant with its biological environment, implant material/osseous interface formation, and long-term success integration in the human body is dependent on surface properties of the implant device. After in vitro tests that allow us to determine the optimum roughness of implant surface and the necessity or not of surface thin-film depositions, we are now in the stage of investigations on implants used for in vivo tests.

METHODS: *In vivo* tests were made with implants of Vanadium free alloy (Ti-Al-Nb). Uncoated samples (50μm roughness) were inserted in rabbit femur for 2 months. Extracted samples were analyzed by environmental scanning electron microscopy (ESEM) and energy-dispersive x-ray (EDX) microanalysis.

RESULTS: The bone–implant interface study revealed a convenient osseous integration. A mineralized extracellular matrix was formed on the implant material, with some fibrous parts in the case of sharp edges.

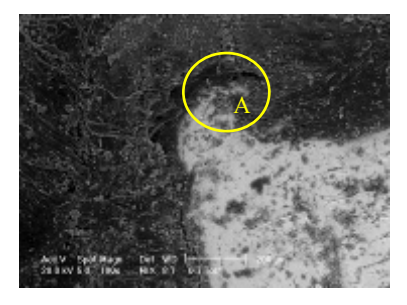


Fig. 1: ESEM observation of tissue/implant interface.

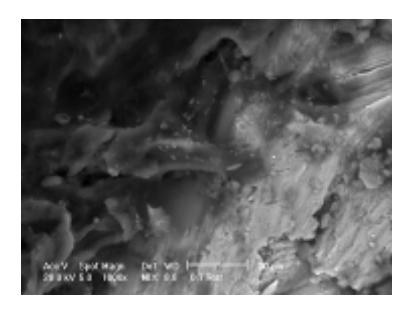


Fig. 2: ESEM observation of tissue/implant interface – detail (A).

Table 1. EDX analysis of elements in implant

| n | Element | Wt % | At % |
|--|---------|-------|-------|
| | AIK | 2.72 | 4.83 |
| | PΚ | 1.89 | 2.92 |
| | NbL | 7.78 | 4.01 |
| - n | CaK | 3.09 | 3.70 |
| M P No Ge Ca 129 229 229 329 329 429 529 529 | TiK | 84.51 | 84.53 |

Table 2. EDX analysis of elements in bone

| | Element | Wt % | At % |
|----------------------------------|---------|-------|-------|
| P | СК | 47.13 | 61.17 |
| | ОК | 29.66 | 28.91 |
| | PΚ | 7.83 | 3.94 |
| BH BM 19 19 2H 2H 2H 2H 1H 1H 1H | CaK | 15.38 | 5.98 |

EDX analysis of the implant revealed the alloy composition: 5%Al, 4%Nb and Ti (balance). The presence of Ca and P can be explained as adherences from cutting. EDX analysis of the bone exposed the absence of any other elements than Ca, C, O and P, proving the biocompatibility of the implant material.

DISCUSSION & CONCLUSIONS: Observation of the interface between the cell layer and substrate revealed the presence of calcium and phosphorous-rich globular deposits associated with collagen fibers on all materials *in vitro* and *in vivo*. No contamination from implant material can be observed.

REFERENCES: ¹ C. Lavos-Valereto, S. Wolynec, M.C.Z. Deboni, B. König Jr. (2001) *Applied Biomaterials* **56**:727-733. ² V. Oliveira, R.R. Chaves, R. Bertazzoli and R. Caram (1998) *Braz. J. Chem. Eng.* **15**:1471-77. ³ C.J. Boehlert K.A. Rider, L.M. Flick (2005) *Mater Trans* **46**:1618-1626.

ACKNOWLEDGEMENTS: The authors express their gratitude to Romanian National Authority for Scientific Research (ANCS) and Managerial Agency for Scientific Research, Innovation and Technological Transfer (AMCSIT-Politehnica), for the funds provided for this research (Research Project CEEX no. 46/2005, RETEβDENT).

Investigations on precipitation phenomena in a SMA (Ni-Ti)

M. Târcolea¹, A.E. Dumitru¹, A.M. Sandu², F. Miculescu¹, C.M. Cotrut¹, N. Miculescu¹

¹ University POLITEHNICA of Bucharest, Romania. ² Toyohashi University of Technology, Japan.

INTRODUCTION: The Ni-Ti alloy (Shape Memory Alloy - SMA) can be used for medical applications if its special property could develop in the range of the common human body temperature. The common control [1] of the heating/cooling transformation temperatures consist in the use of adequate alloy composition with equilibrium structure. A new idea [1, 2], studied in the last period, is to use a Ni rich Ni-Ti alloy and to apply a heat treatment (aging) to obtain the precipitation of specific equilibrium/non-equilibrium Ni_xTi_y compounds. In this manner, the changes of chemical composition of base solid solution (NiTi) allow to modify and control the austenite (A)/martensite (M) transformation temperatures.

MTHODS: The studied alloy was a Ni-Ti one (50.6 Ni, 49.4 Ti). It was delivered as hot and cold rolled sheet (0.5×5.9mm), annealed 1h at 1073K and water cooled, with equilibrium structure (NiTi solid solution). The aging was performed at two different temperatures, 673K and 773K, with four different durations, 3.6ks, 10.8ks, 18ks and 36ks. Antioxidant protection of the samples was solved by means of their encasing in aluminum sheet (0.1mm). Final cooling after treatment was made in water. The samples were investigated by microscopy (SEM and EDX) and micro-hardness. DSC determinations were made on aged samples in comparison with the reference one (in equilibrium state). The heating/cooling rate was 5K/min and the studied temperature range of 263K...343K.

RESULTS: Precipitated compounds identified by EDX were Ti₂Ni, Ti₃Ni₄ and most probably Ti₃Ni.

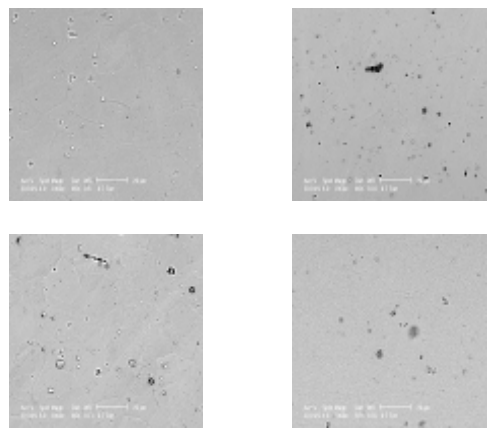


Fig. 1: SEM observations: Effect of aging temperature on precipitation - after 1 h: 673K (up-left), 773K (up-right), after 10 h: 673K (down-left), 773K (down-right).

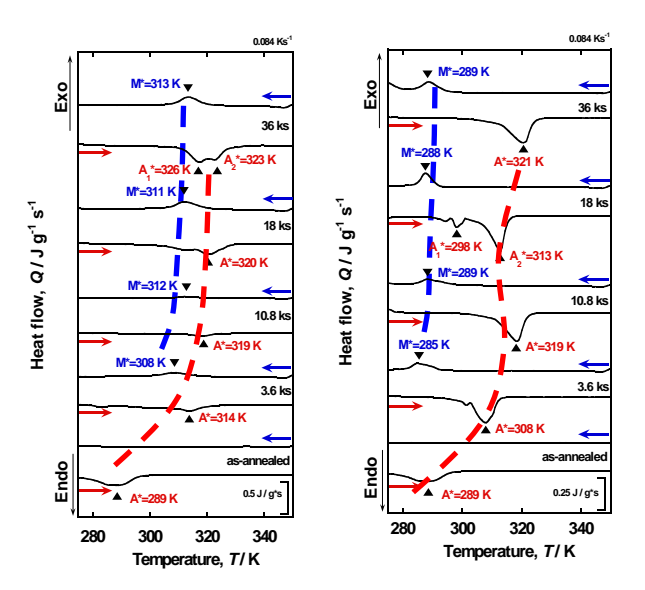


Fig. 3: DSC study on aging temperature and time effects on A and M transformation temperatures.

DISCUSSION & CONCLUSIONS: Increasing aging time, at constant aging temperature, for both treatments, determines systematical displacements transformation start/finish points for both transformations. For the aging at 673K the cooling transformation (M) is happening in the range 300...320K, and for the aging at 773K, it is happening in the range 280...300K. Transformation points at cooling (M) and heating (A) are significant displaced at higher temperatures. The influence is more evident for the transformation at heating (A). It is also visible that aging temperature increasing from 673K to 773K, determines lower transformation points for both transformations (A and M) for all aging durations. It is obvious that this technological procedure allows for a reasonable control of the shape memory effect, related with the direct use of such material for arterial stents, which have to change their shape below the normal temperature body.

REFERENCES: ¹K. Otsuka, X. Ren (2005) *Progress in Materials Science* **50**:511-678. ²D. Tomus, K. Tsuchiya, et al (2004), *Materials Transactions* **45**:219-224.

ACKNOWLEDGEMENTS: Authors express their gratitude to Professor Koichi Tsuchiya, from NIMS (formerly Toyohashi University of Technology), Japan, for his helpful opinions, ideas and, most of all, for metallic material provided, that allow us to develop this research.

Investigation of the preparation design on stresses resulted in ceramic inlays restored premolars

F.Topală¹, L.Sandu¹, N.Faur², S.Porojan¹

¹ "V. Babeş" University of Medicine and Pharmacy, Timişoara, Romania. ² Politehnica University, Timişoara, Romania.

INTRODUCTION: Ceramic inlays can be used on premolars requiring a class II restoration instead posterior composite resins, amalgam or gold inlays and offer a durable and aesthetic alternative. MOD inlays may increase the susceptibility to fracture. Therefore it is important to ensure optimal performance in selection of the adequate preparation design to reduce stresses in teeth structures and also in the restorations [1-3]. The aim of the study was to investigate the effect of preparation design on stress distribution in premolars with different class II and MOD cavity preparations restored with ceramic inlays.

METHODS: The study was performed on an upper first premolar, using a finite element analysis. The geometry of the intact tooth was obtained by 3D scanning using a manufactured device (Fig. 1).



Fig. 1. 3D model of an upper first premolar after laser scaning.

With Rhinoceros modeling program the preparations and the appropriately inlays were designed. These were exported in Ansys finite element analysis software to be used for structural simulations. Twenty-two 3D models of maxillary first premolars, with the following designs of class II and MOD ceramic restorations were generated: eleven class II inlays with butt joint margins, eleven MOD inlays with butt joint margins, both with different tapers (between 0 and 10 degree). The model of the prepared tooth structure for class II was divided into 22568 elements connected at 36935 nodes, and the inlay into 4615 elements connected at 8378 nodes. For the MOD restored tooth, it was divided into 21337 solid elements connected at 35214 nodes, and the inlay into 5990 elements connected at 10809 nodes. Computational simulation of an occlusal load of 200 N was conducted, and stresses occurring in the ceramic restorations, and teeth structures were calculated using Ansys finite element analysis software.

RESULTS: Occlusal load on inlays restored teeth produces stress surrounding the contact areas. In the teeth restored with ceramic class II inlays, the von Mises equivalent stress values were similar to those the intact tooth (Fig. 2). In the teeth restored with ceramic MOD inlays, the von Mises equivalent stress values were higher than in the intact tooth (Fig. 3). For the studied cases, the stress values were not significant influenced by the taper of the preparation.

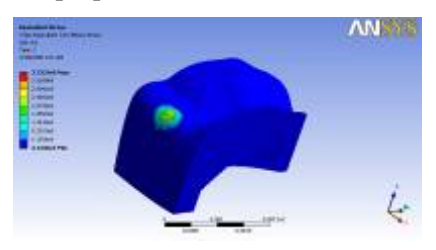


Fig. 2. Stress distribution in a class II inlay for a premolar.

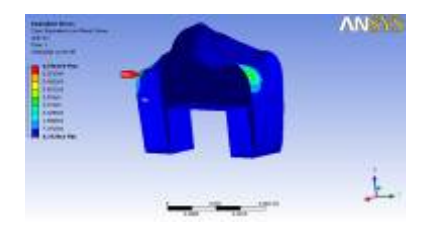


Fig. 3. Stress distribution in a MOD inlay for a premolar.

DISCUSSION & CONCLUSIONS: Within the limitations of the study, it was demonstrated that ceramic inlays on premolars prevent failure and produce a low stress values, even if MOD restorations are used. A taper between 0 and 10 degree of the preparation is not decisive for the stress values.

REFERENCES: ¹ B. Dejak, A. Mlotkowski (2008) *J Prosthet Dent* 99:131-140. ² R.B. Fonseca, A.J.F. Neto, L. C. Sobrinho, C.J. Soares (2007) *J Prosthet Dent* 98:277-284. ³ B. Dejak, A. Mlotkowski, M. Romanowicz (2007) *J Prosthet Dent* 98: 89-100.

ACKNOWLEDGEMENTS: This study was supported by the Grant ID_1264 from the Ministry of Education and Research, Romania.

Biocompatible coatings of TiNiNb shape memory alloys

A..Vladescu¹, V. Braic¹, M. Balaceanu¹, C.M.Cotrut², M.Braic¹

National Institute for Optoelectronics ¹, Romania. University Politehnica of Bucharest, Romania ².

INTRODUCTION: TiNi shape memory alloy (SMA) is extensively used as a material for medical implant devices due to its shape memory effect and biocompatibility. The addition of Nb increases its biocompatibility and conveniently modifies the transition temperatures between austenitic and martensitic phases. However due to its relatively high content in Ni, there are doubts about its use as a biomaterial. Thin film coatings, a transition metal nitride, are widely used for preventing the ions release from the coated substrate, the obtained diffusion barrier films also presenting high protection against corrosion and wear [1], [2].

The paper reports on the results obtained in the corrosion resistance increase of the TiNiNb shape memory alloy (44% at.-Ti, 47% at-Ni, 9% at.-Nb) coated with mono and multilayer films of Ti and Zr nitrides when immersed in an artificial physiological solution (APS).

METHODS: The films (TiN, ZrN, TiN/ZrN) with a thickness of approx. 3.5 μm were prepared by the reactive pulsed magnetron sputtering method [3] and the differential scanning calorimetric tests revealed that the shape memory effect of the alloy were not affected by the coatings. TiN and ZrN monolayer and TiN/ZrN a multilayered structure with 500 layers and a bilayer period of 7 nm were investigated in the present work.

The elemental and phase composition, texture, microhardness and adhesion were investigated by AES, XRD, Vickers micro-hardness and scratch-test. The electro-chemical measurements were carried out at 25° C using coated and uncoated samples, immersed in an APS with a pH=7.4 and the following composition: NaCl - 8.44 g/l, Na HCO₃ - 0.35 g/l, NaH₂PO₄ - 0.06 g/l, Na H₂PO₄· H₂O - 0.06 g/l. The test consisted in the potentiodynamic polarization of the samples (-1000 \div +1500 mV range), using as reference a saturated calomel electrode (SCE). The corrosion current and the critical current for passivation were measured in order to compare the coatings corrosion resistance.

RESULTS: The elemental composition of the coatings, as obtained by AES analysis indicate that the TiN films were slightly overstoichiometric (Ti/N=1.09) and the ZrN films were substoichiometric (Zr/N=0.92). X-ray diffraction

analysis revealed that the TiN and ZrN layers exhibit a strong (111) preferred orientation, as already reported [4]. In the case of the TiN/ZrN multilayers the diffraction patterns present typical diffraction patterns of superlattice coatings with a main (111) Bragg peak (similar to that of the TiZrN monolayer), surrounded by satellite peaks. The highest Vickers microhardness $HV_{0.015}$ [GPa] and critical loads L_c [N] values were measured for the multilayer (32 GPa and 46 N), followed by TiN monolayer (23 GPa and 44 N), and ZrN coating (19.2 GPa and 38 N).

The best corrosion resistance was measured for the multilayered coating (Fig.1). The measured decrease of the corrosion currents indicates that the coatings improved the corrosion resistance over the TiNiNb substrates.

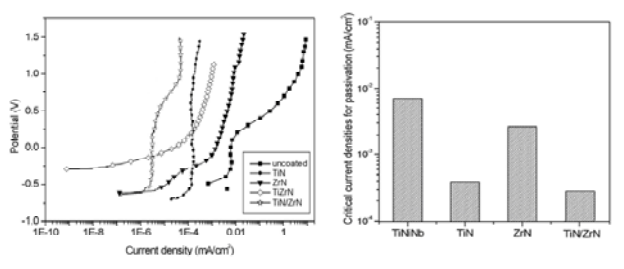


Fig. 1: Current and critical current densities of the coated and uncoated TiNiNb memory shape alloy samples

DISCUSSION & CONCLUSIONS: As compared with the uncoated TiNiNb shape memory alloy samples, all the coated samples exhibited superior corrosion resistance and mechanical characteristics. The TiN/ZrN multilayer coating showed the best corrosion and wear resistance in comparison with the monolayer coatings.

REFERENCES: ¹ Y.Haga, M. Mizushima et al (2005) *Smart Mater. Struct.* **14**: 266-71. ² M. Fenker, M. Balzer and H. Kappl, *Thin Solid Films* (2006) **515**: 27-32. ³ M.Braic, V.Braic, M.Balaceanu et.al. (2007) *Plasma Process. Polym.* 4 (S1): S171–S174. ⁴ N.M.Mustapha, R.P.Howson (2001) *Vacuum* **60**: 361-66.

ACKNOWLEDGEMENTS: The work was supported under the Project ARPA-2-Cex-06-11-15.

Corrosion resistance of the biocompatible Ti and Zr oxynitride thin films

A. Vladescu¹, V.Braic¹, M.Balaceanu¹, M.Braic¹, P.Drob²

¹ National Institute for Optoelectronics, Romania. ² Institute of Physical Chemistry "I.G.Murgulescu", Romania.

INTRODUCTION: In the last few years, thin films of many transition metal oxynitrides such as Ti or Zr oxynitrides have gained increasing importance in various applications due to their excellent combination of high hardness, chemical stability, optical and electrical properties, wear and corrosion resistance [1,2].

The aim of this work is to investigate the microchemical, microstructural, mechanical and anticorrosive characteristics of 316L stainless steel coated with Zr and Ti oxynitride. The choice of these materials for biomedical applications was determined by the fact that they exhibit an optimum combination between the high wear-corrosion resistance of the nitrides and the good biocompatibility of the oxides.

METHODS: The thin films were deposited by pulsed magnetron sputtering [3]. The magnetron cathodes were made of Ti and Zr (both 99.6 % purity) and fed by a pulsed bipolar generator-type ENI RPG5 (positive pulse length 1936 ns, repetition rate 100 kHz). The magnetron current and the negative d.c. substrate bias were of 3 A and 60 V, respectively. The O_2/N_2 mass flow ratios were controlled to be of about 1 and the working pressure was approximately $5x10^{-1}$ Pa. The argon pressure was adjusted in order to keep a constant overall pressure. These parameters were kept constant for the deposition of both layers. The overall thickness of all coatings was ~ 1.2 μm.

The experimental work was focused on the corrosion behavior of the coatings in the Ringer solution. Additional information on the thin films properties was obtained by XPS method, XRD microhardness measurements analysis. The corrosion resistance was adhesion tests. investigated by using a Voltalab 80 apparatus equipped with a saturated calomel electrode (SCE) as the reference electrode. Cyclic potentiodynamic and linear polarisation tests were performed. The following electrochemical parameters determined: $E_{i=0}$ - corrosion potential (like zero current potential), i_p – passive current density, R_p - the polarization resistance, i_{corr} - corrosion current densities and V_{corr} - corrosion rates.

RESULTS: The XPS analysis showed that the coatings consisted of a mixture of metal (Ti or Zr) oxynitrides and oxides, together with adsorbed

oxygen. The oxynitride compounds had relatively high oxygen content, the O/N ratio being of 2.5 and 1.9 for TiON and ZrON films, respectively. The XRD analysis showed that all deposited coatings were amorphous. Hardness values were in the range 14÷16 GPa – TiON and 18÷22 GPa – ZrON. A good adhesion of all the coatings was found (critical loads of 30 - 35 N were obtained), taken into account the data in the literature for transition metal oxides. In Table 1 are summarized the main electrochemical parameters in the Ringer solution, for uncoated and coated samples.

Table 1. Electrochemical parameters of the uncoated and coated samples in Ringer solution.

| Material | $\begin{array}{c} E_{i=0} \\ V \end{array}$ | i_p $\mu A/cm^2$ | R _p kohm.cm ² | i_{cor} $\mu A/cm^2$ | V _{cor} mm/year |
|----------|---|--------------------|-------------------------------------|------------------------|-----------------------------|
| 316L | -0.33 | 15 | 34.7 | 0.75 | 5.79x10 ⁻³ |
| TiON | -0.30 | 8 | 232.3 | 0.10 | 0.78 x10 ⁻³ |
| ZrON | -0.33 | 6 | 246.6 | 0.09 | 0.72 x10 ⁻³ |

DISCUSSION & CONCLUSIONS: TION and ZrON coatings were prepared by pulsed magnetron sputtering on 316L steel. The oxynitride compounds had relatively high oxygen content, the O/N ratio being of 2.5 and 1.9 for TiON and ZrON respectively. ZrON layers exhibited films, hardness values with about 4 GPa higher than that of the TiON films. The experimental results showed the favourable influence of the deposited coatings on the corrosion resistance of the 316L steel in Ringer solution. The main electrochemical parameters were superior to those of the uncoated samples.

REFERENCES: ¹R.W.Y. Poon, J.P.Y. Ho, Xuanyong Liu, C.Y. Chung, P.K.Chu, K.W.K. Yeung, W.W. Lu and K.M.C. Cheung (2005) Thin Solid Films 488: 20-²E.Alves, A.Ramos, N.Barradas, F.Vaz, P.Cerqueira, L.Rebouta and U.Kreissig (2004) Surf. 372-76. ³M.Braic, Technol. **180–181**: Coat. M.Balaceanu, A.Purice, F.Stokker-Cheregi, A.Moldovan, N.Scarisoreanu, G.Dinescu, A.Dauscher, M.Dinescu (2006) Surf. Coat. Technol. 200: 6505-10.

ACKNOWLEDGEMENTS: The work was supported under the Project ARPA-2-Cex-06-11-15.

FGF-2 binding to modified silk fibroin films mimicking the extracellular matrix

E. Wenk¹, A.R. Murphy², L. Uebersax¹, D. L. Kaplan², H.P. Merkle¹, L. Meinel¹

¹Institute of Pharmaceutical Sciences, ETH Zurich, Zurich, Switzerland. ² Department of Biomedical Engineering, Tufts University, Medford MA, USA.

INTRODUCTION: A suitable scaffold for tissue engineering should provide an extracellular matrix (ECM) mimicking environment that is able to support cell interactions and differentiation. The physiological ECM acts as a local depot for growth factors, releases them on demand, prevents their degradation and, in some cases, enhances binding to cell surface receptors. Fibroblast growth factor 2 (FGF-2) specifically interacts with the sulfated glycosaminoglycans heparin and heparan sulfate of the ECM¹.

In the present study, silk fibroin (SF) was modified through diazonium coupling chemistry in order to introduce sulfonic acid functional groups at different ratios. Adsorption of FGF-2 to unmodified and modified SF films and release profiles were analyzed. SF, a fibrous protein biopolymer, is currently explored for several biomedical applications, owing to its unique properties, such as aqueous processability, mechanical strength, biocompatibility and biodegradability². The present study represents the first step towards the development of a ECMmimicking matrix for the storage and controlled delivery of growth factors for tissue repair.

METHODS: SF solution was obtained from cocoons of the silkworm B. mori as previously described³. Diazonium coupling reaction with SF solution was performed as described before³. The molar ratio of diazonium salt to tyrosine in the SF protein was tailored to produce different levels of modification. SF films were prepared and transformed into a β-sheet enriched, water-resistant form by exposing them to water vapor of 96% relative humidity at room temperature (RT) for 12 h. Adsorption of FGF-2 onto SF films was performed at RT and indirectly analyzed by measuring the amount of unbound FGF-2 by ELISA after 1, 2 and 4 h. FGF-2 release experiments were performed in PBS (pH 7.4) at 37°C for 6 d, and the samples analyzed for FGF-2 by ELISA.

RESULTS: Drug adsorption studies showed that after 4 h adsorption of FGF-2 to SF films ranged from 49% (unmodified silk) to 95% (80 sulfo groups per silk molecule) of the initial amount of FGF-2 (Fig. 1A). A linear correlation between sulfonation ratios and FGF-2 adsorption was

detected; higher sulfonation ratios led to increased FGF-2 binding (Fig. 1B). Drug release experiments showed that after 6 days, FGF-2 release from SF films ranged from 0.2% (80 sulfo groups per molecule) to 0.8% (unmodified silk) of the initial loading of FGF-2 (Fig. 1C). Again, a linear correlation between sulfonation ratio and FGF-2 adsorption was observed, with higher sulfonation ratios leading to decreased FGF-2 release (Fig. 1D).

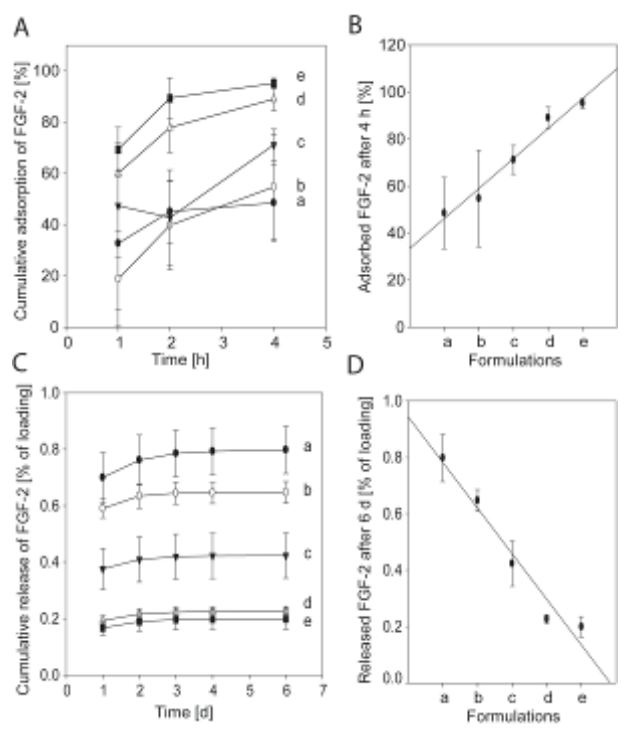


Fig. 1: Cumulative adsorption of FGF-2 to SF films (A), adsorbed FGF-2 after 4 h (B), cumulative release of FGF-2 from SF films (C), and released FGF-2 after 6 d (D); a = unmodified silk, b = 20 sulfo groups per silk molecule, c = 40 sulfo groups per silk molecule, d = 60 sulfo groups per silk molecule, e = 80 sulfo groups per silk molecule.

DISCUSSION & CONCLUSIONS: Modification of SF allowed us to obtain a system with adjustable growth factor binding and delivery. Future work is planned to investigate the impact of the findings on cell growth and differentiation.

REFERENCES: ¹L. Macri et al. (2007) *Adv. Drug Deliv. Rev.* **59**:1366-1381. ²G.H. Altman et al. (2003) *Biomaterials* **24**:401-416. ³A.R. Murphy et al. (2008) *Biomaterials*, in press.

Antifungal Hydrogels

A. Zumbuehl¹, L. Ferreira²³, D. Kuhn⁴, A. Astashkina⁵, L. Long⁶, Y. Yeo⁷, T. Iaconis⁵,

M. Ghannoum⁶, G. R. Fink⁴, R. Langer⁵, and D. S. Kohane⁸

¹University of Geneva, 1211 Geneva, Switzerland; ²Center of Neurosciences and Cell Biology, University of Coimbra, 3004-517 Coimbra, Portugal; ³Biocant-Biotechnology Innovation Center, 3060-197 Cantanhede, Portugal; ⁴Whitehead Institute for Biomedical Research, Cambridge, MA 02142, USA; ⁵Massachusetts Institute of Technology, Cambridge, MA 02139, USA; ⁶Center for Medical Mycology, University Hospitals of Cleveland, Case Western Reserve University, 11100 Euclid Avenue, Cleveland, OH 44106; Purdue University, 575 Stadium Mall Drive G22, West Lafayette, IN 47907-2091; ⁸Laboratory for Biomaterials and Drug Delivery, Department of Anesthesiology, Division of Critical Care Medicine, Children's Hospital, Harvard Medical School, 300 Longwood Avenue, Boston, MA 02115, USA

INTRODUCTION: Fungi are increasingly identified as major pathogens in bloodstream infections, often involving indwelling devices. Materials with antifungal properties may provide an important deterrent to these infections. Here we describe amphogel, a dextran-based hydrogel into which amphotericin B is adsorbed. Amphogel kills fungi within 2 h of contact and can be reused for at least 53 days without losing its effectiveness against Candida albicans. The antifungal material is biocompatible in vivo and does not cause hemolysis in human blood. Amphogel inoculated with C. albicans and implanted in mice prevents fungal infection. Amphogel also mitigates fungal biofilm formation. An antifungal matrix with these properties could be used to coat a variety of medical devices such as catheters as well as industrial surfaces.

METHODS: Dextran-based hydrogels (10-mm diameter and 1-mm thickness, before swelling) were obtained by a photopolymerization reaction of aqueous solutions of dextran acrylate.

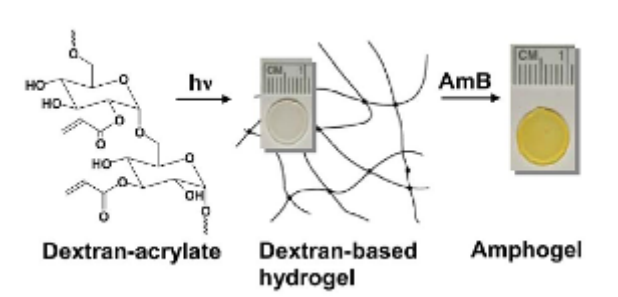


Fig. Dextran-based hydrogels were noncovalently loaded with the antifungal drug amphotericin B.

6 polymer disks were immersed in 16 ml of a solution of DMF: triethylamine (15:1) containing 20 mg of AmB (Sigma-Aldrich, St.Louis, MO) and 5 mg of 4-dimethylaminopyridine. The loading was performed for 12 h, and then the gels were washed with DMF (3 days) followed by PBS (pH 7.2; 3 days).

The polymer disks (1 cm diameter) were placed in the wells of a 24-well tissue culture plate with 1 ml of the *Candida* suspension $(1x10^7 \text{ cells in YNB})$. The disks were incubated for 2 h, at 37°C while shaking at 100 rpm. Then the disks were removed, and the remaining medium was vigorously stirred then diluted to a concentration of 1:1,000. Next, 200 µl of the diluted medium was plated on YEP agar plates. The disks were washed gently in 3 x 1 ml of fresh PBS to remove any nonadherent cells. The disks were crushed and vigorously stirred in 1 ml of PBS, and the suspension was diluted to a concentration of 1:1,000. Then, 200 µl of the diluted suspension was plated on YEP-agar plates. The YEP plates were incubated at 37°C for 24 h, and veast colonies were counted.

RESULTS: Amphogel kills *C. albicans* within 2 h of contact and remains biologically active for at least 53 days. The system was equally active when implanted in an animal model.

DISCUSSION & CONCLUSIONS: We found an unanticipated adsorption of AmB to a specific hydrophilic matrix resulting in a very simple manufacture process, and a marked killing of C. albicans in the absence of detectable release of fungicidal activity. As fungi appear to gain entry into patients via percutaneous devices, the ability to reduce entry through these portals could prevent the introduction of the microorganism and thereby reduce the probability of ensuing disease.

REFERENCES: ¹ A. Zumbuehl, L. Ferreira, D. Kuhn, A. Asthashkina, L. Long, T. Iaconis, M. A. Ghannoum, G. R. Fink, R. Langer, D. S. Kohane (2007) Proc. Natl. Acad. Sci. USA 104: 12994-12998.

ACKNOWLEDGEMENTS: This work was supported by a Swiss National Science Foundation Postdoctoral Fellowship (A.Z.), Fundacao para a Ciencia e a Tecnologia Fellowship SFRH/BPD/ 14502/2003 (L.F.), National Science Foundation Grant BES-0507449, and National Institutes of Health Grants GM035010 (to G.R.F.), NIH DE017846 (to M.G.), NSF BES-0507449 (to R.L. and D.S.K.), and GM073626 (to D.S.K.).